Discovery and Characterization of Genes Involved in Muscle Calcium Handling

APPROVED BY SUPERVISORY COMMITTEE

Committee Chairperson	_____ Thomas M. Wilke, PhD
Committee Member	_____ Joshua T. Mendell, MD, PhD
Committee Member	_____ Eric N. Olson, PhD
Committee Member	_____ James T. Stull, PhD

DEDICATION

For Woody and Louise.

Discovery and Characterization of Genes Involved in Muscle Calcium Handling

by

BENJAMIN RHETT NELSON

DISSERTATION

Presented to the Faculty of the Graduate School of Biomedical Sciences

The University of Texas Southwestern Medical Center at Dallas

In Partial Fulfillment of the Requirements

For the Degree of

DOCTOR OF PHILOSOPHY

The University of Texas Southwestern Medical Center at Dallas

Dallas, Texas

August, 2015

ACKNOWLEDGEMENTS

Completing a doctoral degree is considered by many to be a great personal achievement, accomplished only through great self-sacrifice and –discipline. However, I can say truthfully in my case that it was only achieved through the support of countless others, including family, mentors, and colleagues. First I thank my wife, Melissa, who has supported me day-to-day through the many high and low points of this program – I truly would not have made it this far without her support. I also must thank my mother, Randi, for her instilling in me a desire and expectation of education, as well as my stepfather Trey for his encouragement over the years. My grandparents, Woody and Louise, to whom this dissertation is dedicated, played a pivotal role in developing my curiosity for and engagement of the world – it is one of my greatest honors to dedicate this work in their names. I am grateful for my brother, Clint, with whom I shared many great adventures and misadventures while growing up. I also would like to thank my parents-in-law, Steve and Lynette, for all of their support and encouragement over the past decade.

I am also greatly indebted to the research mentors who have helped light my path. Dr. Shaying Zhao, my first true research mentor took a chance on me as a master's student although I had little research experience, and she invested the time and effort into making me a better scientist. I will always remember fondly the conversations we would have even late into the evening in the lab. I am also immensely grateful for the guidance, encouragement, and occasional prodding of Dr. Eric Olson, without whom the current work would not exist. Even now, I do not think I fully comprehend how my time in his lab has shaped and will continue to shape my philosophy of science. I am also very glad to have worked with Dr. Rhonda Bassel-Duby during my time in the Olson lab – she has been a pillar of support during fruitful and

barren times in my projects. I also would like to thank the time and effort invested by each of my thesis committee members during my training – they are Dr. Thomas Wilke, Dr. Joshua Mendell and Dr. James Stull.

Finally I would like to thank the many colleagues who have supported and honed all my endeavors over the past few years. Specifically I must thank Dr. Douglas Anderson, who has been a friend and constant source of conversation and inspiration during my time in the Olson lab. In one way or another, I feel I owe much of my success to his efforts and creativity. I am also tremendously glad to have worked closely with Dr. Catherine Makarewich during this past year on the DWORF project – she is an ideal colleague who is clearly on a trajectory for great things.

My greatest hope as a future father, mentor, and colleague is that I can make such a positive impression on others as these people have made on me. Thank you all.

DISCOVERY AND CHARACTERIZATION OF GENES INVOLVED IN MUSCLE CALCIUM HANDLING

Publication No. _____

Benjamin Rhett Nelson, Ph.D.

The University of Texas Southwestern Medical Center at Dallas, 2015

Supervising Professor: Eric N. Olson, Ph.D.

Muscle tissue requires continuous cycling of calcium release and clearance to generate and sustain contraction. When the plasma membrane of a muscle fiber becomes electrically excited, a voltage sensor in the membrane, called the dihydropyridine receptor (DHPR), becomes activated and signals to the calcium release channel located in the membrane of the sarcoplasmic reticulum (SR), called the ryanodine receptor (RyR). When the RyR channel is activated, calcium is released into the cytoplasm from the SR, the primary calcium storage compartment of muscle fibers. Calcium then binds to the sarcomere, activating the motor activity of the myosin filaments, and causes the fiber to contract. Following contraction, most of the cytosolic and sarcomeric calcium is recycled back to the SR by the sarco/endoplasmic reticulum ATPase

(SERCA). Although most components of the calcium handling pathway are thought to be already known, the large number muscle-specific genes with unknown functions would suggest that additional components may yet be undiscovered. The first goal of this study was to carry out initial functional characterization of the *Stac3* knockout mouse, in which muscle contraction is severely defective. We found that mice lacking *Stac3*, a gene with skeletal muscle-specific expression, lack muscle contraction because of a defect in excitation-contraction coupling, that is the link between membrane excitation and SR calcium release. The second goal was to identify small peptides that may play a role in muscle function. We examined codon conservation in transcripts annotated as long non-coding RNAs and discovered a transcript that encodes a 34-amino-acid transmembrane peptide with cardiac and slow-twitch muscle expression that we have named Dwarf Open Reading Frame or DWORF. Overexpression of this peptide in cardiac myocytes increases the peak calcium release during contraction while also increasing the rate of calcium clearance. We conclude that DWORF likely serves to increase the apparent enzymatic activity of SERCA. Together the discoveries of *Stac3* and *Dworf* suggest that many important genes in muscle function may be awaiting a closer look or have not yet been discovered at all.

TABLE OF CONTENTS

PRIOR PUBLICATIONS

Anderson, D. M., K. M. Anderson, C. L. Chang, C. A. Makarewich, **B. R. Nelson**, J. R. McAnally, P. Kasaragod, J. M. Shelton, J. Liou, R. Bassel-Duby and E. N. Olson (2015). "A micropeptide encoded by a putative long noncoding RNA regulates muscle performance." Cell 160(4): 595-606.

Garg, A., J. O'Rourke, C. Long, J. Doering, G. Ravenscroft, S. Bezprozvannaya, **B. R. Nelson**, N. Beetz, L. Li, S. Chen, N. G. Laing, R. W. Grange, R. Bassel-Duby and E. N. Olson (2014). "KLHL40 deficiency destabilizes thin filament proteins and promotes nemaline myopathy." J Clin Invest 124(8): 3529-3539.

Liu, N., **B. R. Nelson**, S. Bezprozvannaya, J. M. Shelton, J. A. Richardson, R. Bassel-Duby and E. N. Olson (2014). "Requirement of MEF2A, C, and D for skeletal muscle regeneration." Proc Natl Acad Sci U S A 111(11): 4109-4114.

Nelson, B. R., D. M. Anderson and E. N. Olson (2014). "Small open reading frames pack a big punch in cardiac calcium regulation." Circ Res 114(1): 18-20.

Nelson, B. R., F. Wu, Y. Liu, D. M. Anderson, J. McAnally, W. Lin, S. C. Cannon, R. Bassel-Duby and E. N. Olson (2013). "Skeletal muscle-specific T-tubule protein STAC3 mediates voltage-induced Ca^{2+} release and contractility." Proc Natl Acad Sci U S A 110(29): 11881-11886.

TABLE OF FIGURES

TABLE OF TABLES

LIST OF ABBREVIATIONS

4-CMC	4-chloro-*m*-cresol
aa	amino acid
AAV	adeno-associated virus
ACh	acetylcholine
AChR	acetylcholine receptor
ANP	atrial natriuretic peptide
ARVD2	arrhythmogenic right ventricular dysplasia, type 2
ATP	adenosine triphosphate
ATPase	adenosine triphosphate hydrolase
AV node	atrioventricular node
bp	base pair
Ca^{2+}	ionic calcium
cAMP	cyclic adenosine monophosphate
cDNA	complementary deoxyribonucleic acid
CPVT	catecholaminergic polymorphic ventricular tachycardia
CRISPR	clustered regularly interspersed short palindromic repeats
dCTP	deoxycytidine triphosphate
DHPR	dihydropyridine receptor
DMD	Duchenne muscular dystrophy
DNA	deoxyribonucleic acid
ECC	excitation-contraction coupling
ECF	extracellular fluid
ER	endoplasmic reticulum
FDB	flexor digitorum brevis
FPKM	fragments per kilobase per million
GFP	green fluorescent protein
gRNA	guide ribonucleic acid
H&E	hemtoxylin and eosin
hGH	human growth hormone
HRP	horseradish peroxidase
Hz	SI unit, hertz
IBFQ	Iowa black fluorescent quencher
ICF	intracellular fluid
K^+	ionic potassium
kDa	SI unit, kilodalton
KO	knockout
LacZ	β-galactosidase
lncRNA	long non-coding RNA
MCU	mitochondrial calcium uniporter
MDa	SI unit, megadalton
mg	SI unit, milligram
MGB	minor groove binder
MICU1	mitochondrial calcium uptake 1
mL	SI unit, milliliter

mM	SI unit, millimolar
mM	SI unit, millimolar
mRNA	messenger ribonucleic acid
ms	SI unit, millisecond
Na^+	ionic sodium
Na^+/K^+-ATPase	sodium/potassium adenosine triphosphate hydrolase
NCBI	National Center for Biotechnology Information
NCX	sodium-calcium exchanger
NFAT	nuclear factor of activated T-cells
NFQ	non-fluorescent quencher
nM	SI unit, nanomolar
nm	SI unit, nanometers
NMD	nonsense-mediated decay
NMJ	neuromuscular junction
ORF	open reading frame
PCR	polymerase chain reaction
PKA	protein kinase A
PLN	Phospholamban
PMCA	plasma membrane calcium adenosine triphosphate hydrolase
qPCR	quantitative polymerase chain reaction
RNA	ribonucleic acid
RPKM	reads per kilobase per million
rRNA	ribosomal ribonucleic acid
RyR	ryanodine receptor
SA node	sinoatrial node
SERCA	sarco/endoplasmic reticulum adenosine triphosphate hydrolase
SH3	src-homology 3
SNP	single-nucleotide polymorphism
SR	sarcoplasmic reticulum
T-tubules	transverse tubules
TAC	thoracic aortic constriction
TRIC	trimeric intracellular cation channel
UCSC	University of California Santa Cruz
UTR	untranslated region
WT	wild-type
αMHC	alpha myosin heavy chain
μM	SI unit, micromolar

CHAPTER 1. INTRODUCTION

Cardiac, skeletal, and smooth muscle are specialized contractile tissues that are responsible for generating all mechanical forces in vertebrates, both involuntary and voluntary. Although the mechanisms of excitation and contraction vary greatly among these different forms of muscle, they all share a common dependence upon calcium-mediated signaling to convert excitatory signals to downstream shortening of actomyosin filaments and thus contraction. Excitation of striated muscle fibers (cardiac and skeletal) results in release of calcium from the sarcoplasmic reticulum (SR) that then stimulates activation of the actomyosin filaments, causing the muscle to contract. During the relaxation phase, calcium is removed from the cytosol primarily by re-sequestration to the SR and to a lesser extent by moving calcium outside of the cell. This dissertation will focus on identification and characterization of two novel proteins involved in the release and re-sequestration of calcium in cardiac and skeletal muscles.

1.1 SCOPE OF STUDY

Most congenital muscle diseases arise from monogenic mutations that obstruct either development or function of the muscle tissue [1, 2]. Although whole genome sequencing is becoming routine, it is often impossible to evaluate the relevance of potential disease-causing mutations in humans due to the large number of non-deleterious genetic variation in the human population. Identification of disease-causing mutations is also limited by the fact that the biological functions of most genes have not been rigorously evaluated.

I set out to characterize the molecular functions of genes with muscle-specific expression for which there was no published functional information. Simply put, we hypothesized that, when mutated, genes with muscle-specific expression should cause muscle-specific disease

phenotypes that we could then exploit to understand the function of the mutated gene. I evaluated a number of uncharacterized candidate genes for muscle-specific expression and ultimately became interested in the gene SH3 and cysteine rich domain 3 or STAC3. The goal of this portion of the project, therefore, was to understand the role of STAC3 in muscle function. We used knockout mice to determine that STAC3 is required for excitation-contraction coupling (ECC) in skeletal muscle. The importance of STAC3 in ECC is demonstrated by the fact that muscles of homozygous knockouts are completely incapable of contraction. Identification of STAC3 as a required factor for skeletal muscle ECC was unexpected at the outset of the project since other components of ECC were identified decades ago and ECC is one of the most dogmatic models in muscle physiology.

Soon after starting my work on STAC3, others in the Olson Lab and I became interested in the functions of several of the muscle-specific long non-coding RNA (lncRNA) genes. We came to realize that some of these lncRNAs may encode small proteins. My interest in lncRNAs then shifted to identification of small open reading frames (ORFs) within these putatively non-coding transcripts. This interest spurred me to search for conserved small ORFs within the RNA-seq data generated by others in our lab. This search led to identification of a novel cardiac RNA transcript that encodes a small transmembrane peptide, which I named Dwarf Open Reading Frame or simply DWORF. While the function of DWORF is less apparent at present than that of STAC3, it appears that DWORF may positively regulate SR calcium uptake by SERCA. Future investigation of DWORF will be necessary to define its molecular and physiologic roles further.

1.2 REVIEW OF LITERATURE

1.2.1 Historical Context

The physical underpinnings of biological animation has fascinated and perplexed scientists for centuries. The earliest postulation focused on metaphysical etiologies such as "animal spirits" and mystical fluids [3]. It was not until Luigi Galvani's description of "animal electricity" in 1791 that a physical mechanism, electricity, was shown to evoke animation in otherwise "dead" animals. Galvani discovered that muscle contraction is elicited by simultaneously applying ends of a metal rod to muscles and lumbar nerves in frog leg preparations. Based on countless iterations and permutations of these experiments, he concluded that animals maintained an electrical disequilibrium that could be triggered for release by an electrical stimulus.

The idea that animal systems bear intrinsic electrical capacity was highly controversial at the time, and Galvani's theory garnered much criticism, most notably from the famed contemporary physicist Alessandro Volta [3]. Volta insisted that Galvani's muscle preparations contracted by the action of extrinsically applied "metal electricity", not intrinsic "animal electricity." Volta viewed the frog preparations merely as a sort of "biological oscilloscope" for studying metal electricity (which he considered to be the only true source of electricity), since the muscle/nerve preparations were far more sensitive than any physical apparatus of the time. For many years, the scientific community considered Volta's interpretation to be the correct one, despite numerous experimental findings that were inconsistent with his hypothesis. More than thirty years after Galvani's original postulation, however, Leopoldo Nobili directly measured biological electricity using physical instrumentation, although at the time he did not consider the results to support Galvani's hypothesis. Finally in 1838 Carlo Matteucci repeated and expanded

these experiments and concluded that Galvani was correct and that animal muscles and nerves do have intrinsic electrical potential. Despite his strife-filled career, many now consider Galvani to be the father of electrophysiology.

Despite final acceptance of the theory of biological electricity, it nevertheless took more than a century before the modern, quantitative understanding of electrical propagation and signaling was established by Hodgkins and Huxley through their work on squid giant axons [4]. This work was later extended to describe the excitatory phase of skeletal and cardiac muscle. The equations and techniques pioneered by Hodgkins and Huxley during their collaboration formed the foundation of modern electrophysiology and are regarded as one of the greatest contributions to biophysics in the 20th century.

While the electrical nature of muscle contraction was first appreciated in the 1790s, understanding the biochemical signaling events downstream of excitation did not begin until the 1880s when Sydney Ringer defined the ionic requirements of the cardiac contraction and quite importantly showed the necessity of calcium in this process [5]. The latter discovery occurred serendipitously when Ringer observed that a frog heart would contract when perfused with ‘saline’ made mistakenly by his technician with London tap water, but not when distilled water was used, as Ringer had intended. He went on to determine that the tap water contained physiologic levels of calcium, which happened to be absent in the distilled water. These findings paved the way for *ex vivo* experimentation in multiple fields of study, since Ringer’s solution (as it came to be known) is a near ideal physiologic solution for multiple organ systems. Even today, a modified recipe known as Lactated Ringer’s solution, is a ubiquitous treatment for blood or fluid loss in the medical field.

Despite the early appreciation of calcium's importance by Ringer, it took many years still to determine the exact molecular role of calcium in ECC. However, by 1952 it was clear to some that calcium may be the physiologic link in excitation-contraction coupling since it is released during muscle stimulation and is a potent activator of actomyosin ATPase activity [6]. The role of calcium began to unravel in 1951 when Marsh demonstrated that *in vitro* muscle contraction could be reversed by a soluble muscle protein [7]. This finding was also confirmed in 1952 using intact glycerinated muscle by Bendall [8]. This relaxation factor was henceforth known as the Marsh-Bendall factor [9]. In 1955 the Marsh-Bendall factor was shown to be identical to Kielley-Meyerhof ATPase granules [10, 11]. In the early 1960s two groups, Hasselbach/Makinose and Ebashi/Lipmann, showed that this relaxing ATPase fraction was actually fragmented SR vesicles and that it caused relaxation by stripping calcium from the actomyosin complex [9, 12]. In the early 1970s, MacLennan isolated the protein ATPase of the SR, now known as the sarco/endoplasmic reticulum calcium ATPase or SERCA [13-15]. MacLennan was also the first to clone genes encoding SERCA proteins [16, 17].

While experiments on muscle relaxation solidified the mechanistic importance of calcium in ECC, still little was known about how calcium is released following an action potential. The voltage sensor of the T-tubule was the first ECC calcium channel identified by the observation that a small "charge movement" was measured in the T-tubule just prior to onset of the slow calcium current [18]. The necessity of the slow calcium (L-type) channel was demonstrated by Beam in 1986 using the *dysgenic* mouse strain, which completely lacks ECC [19]. This channel was also found to be sensitive to inhibition by dihydropyridines and was thenceforth called the dihydropyridine receptor or DHPR [20]. The final connection was made later to show that the *dysgenic* phenotype results from loss of the skeletal muscle DHPR channel [21].

Identification of the SR calcium release channel by the Fleischer lab proceeded in parallel to discovery of the DHPR voltage sensor [22]. Using ATP-dependent calcium uptake assays of fractionated SR, it was found that the terminal SR contains a calcium release channel that is sensitive to ruthenium red and the plant alkaloid ryanodine – hence these channels are called ryanodine receptors or RyRs [23]. Using tritium-labeled ryanodine as a probe, the channel was localized to the cuboidal feet structures in the triad that had been observed by electron microscopy [24]. This radiolabeled-probe strategy was also used to isolate the RyR and demonstrate that it is indeed a calcium channel [25]. The cDNA encoding the skeletal muscle ryanodine receptor was first cloned in 1989 [26] and the cardiac cDNA in 1990 [27]. In 1994 the gene encoding the skeletal muscle RyR was knocked out, and the mice completely lacked ECC as predicted, confirming the essential role of the RyR in muscle contraction. These mice were called *dyspedic* to denote the similarity of the phenotype to *dysgenic* mice and because they lacked the SR "feet" structures.

With the identification of calcium as the key regulator of muscle contraction and its three critical handlers, the DHPR, the RyR, and the SERCA, the current model of ECC was defined. This model satisfactorily explains the basis of muscle contraction in skeletal muscle and the heart. Additional proteins have been identified which modulate components of this pathway, including phospholamban, sarcolipin, FKBP 12.6, calmodulin, and a number of others, however, none of these are considered to be essential components of ECC. In this regard, the current model is expected to be complete in its essential components, however, it is worth noting that skeletal-type ECC cannot be functionally reconstituted in non-myocytes by expression of these factors, indicating that there may be additional components [28].

1.2.2 Excitatory Mechanisms in Striated Muscles

1.2.2.1 The Action Potential

In muscle and neuron physiology, excitation refers to the electrical signaling events in the plasma membrane that ultimately lead to calcium release. This process depends on highly polarized, differential gradients of ions across the plasma membrane. Extracellular fluid is high in sodium (~150 mM) and low in potassium (~5 mM) [29]. Inside the cell, however, the balance of sodium and potassium is inverted such that potassium is high and sodium is low. This unequal distribution is established and maintained by the sodium/potassium ATPase (Na^+/K^+-ATPase), which simultaneously transports three sodium (Na^+) ions outward and two potassium (K^+) ions inward, against their respective concentration gradients (Figure 1-1). Differential distribution of sodium and potassium species across the membrane stores potential energy in the form of a diffusion gradient. Membrane electrical potential arises from differential permeability of membranes to charged ions, which is achieved primarily by passive transport of potassium out of the cell (down its concentration gradient) while sodium channels remain closed. This electrochemical gradient is the mechanistic basis for rapid transmission of information in nerve and striated muscle membranes.

1.2.2.2 Excitation in Skeletal Muscle

In skeletal muscle, the process of excitation begins at the site where a motor neuron axon forms a specialized chemical synapse with the muscle fiber, known as a neuromuscular junction (NMJ) (Figure 1-2) [29, 30]. Upon electrical depolarization of the motor neuron's synaptic button by an action potential, voltage-gated calcium channels open allowing external calcium to flow inward. Transient increase in cytosolic calcium concentration causes internal acetylcholine-filled vesicles to fuse with the plasma membrane, thereby releasing acetylcholine (ACh) into the

synaptic cleft. ACh then rapidly diffuses across the synaptic cleft and binds to and activates acetylcholine receptors (AChRs) on the muscle plasma membrane before being degraded by the enzyme acetylcholinesterase.

The AChR is a ligand-gated non-specific cation channel that opens in response to binding of its neurotransmitter ligand, ACh. Opening of the AChR allows extracellular positively charged ions (primarily sodium) to enter the cell at the motor-end plate generating a graded depolarization that is proportional to the number of activated AChRs. If local depolarization by AChRs is of sufficient magnitude, voltage-gated sodium channels adjacent to the motor-end plate become activated and begin to propagate an action potential along the plasma membrane of the muscle fiber, known as the sarcolemma. This action potential rapidly spreads electrical depolarization along the sarcolemma and into specialized invaginations of the sarcolemma known as transverse tubules or T-tubules where the electrochemical coupling phase, known as excitation-contraction coupling (ECC) takes place.

1.2.2.3 Excitation in Cardiac Muscle

While excitation of skeletal myocytes requires direct synaptic innervation, cardiac excitation is regulated primarily by intrinsic mechanisms. The cardiac conduction system begins at a bundle of specialized pacemaker cells known as the sinoatrial node (SA node) that reside in the anterolateral wall of the right atrium near the superior vena cava (Figure 1-3) [29-31]. The SA node undergoes rhythmic electrical depolarization that governs the pace of the entire heart. Therefore, the SA node acts as a gatekeeper to the pacemaker function of the heart, and as such it is the site of autonomic innervation which either slows (parasympathetic innervation from the vagus nerve) or speeds (sympathetic innervation from sympathetic ganglia) the frequency of depolarization (i.e. heart rate).

Electrical activity at the SA node rapidly propagates throughout the atria as a wave of depolarization using gap junctions of the intercalated disks, which separate the cytosolic compartments of adjacent myocytes but allow permeation of small, electrically active ions. Depolarization of the atria causes the chambers to contract, reducing their volume and forcing the blood within them into the ventricular chambers. Because the atrial myocytes are electrically isolated from those of the ventricle, the wave of depolarization cannot pass directly to the ventricle. Instead it must pass through another gatekeeper node known as the atrioventricular node (AV node), which lies in the anteromedial border of the right atrium near the junction of the interatrial and interventricular septa. Upon reaching the AV node, there is a brief delay in propagation to allow the atria to complete emptying of their contents.

Once the AV node fires, it sets off a second wave of depolarization in the ventricles that begins at the bundle of His, but quickly diverges into the left and right bundle branches. These bundles are composed of myocytes that are specialized for conduction and allow the excitatory signal to propagate rapidly through the interventricular septum where it induces contraction of the adjacent myocardium. Excitatory signals from the bundle branches then spread further to the Purkinje cells, which further disseminate the depolarization to the remaining myocardium. As the depolarizing wave is spread from one myocyte to the next through the gap junctions, the plasma membrane of each myocyte propagates the signal as an action potential in a fashion similar to neurons and skeletal myocytes. Like skeletal myocytes, most cardiac myocytes contain T-tubules, which are the primary site of excitation-contraction coupling in cardiomyocytes.

1.2.3 Excitation-Contraction Coupling

1.2.3.1 Overview

Although the source of excitation differs in skeletal and cardiac muscle, both myocyte types require propagation of an action potential along the plasma membrane that is then converted to an intracellular signal to trigger the contractile machinery [29, 30]. Because the surface area-to-volume ratio of striated myocytes is rather small, the interior portion of the myocyte would be very slow to contract if it were dependent on diffusion from the plasma membrane, since diffusion is very slow at distances more than a few nanometers. Therefore, in order to allow near simultaneous contraction of the central and peripheral regions of the cell, striated myocytes contain internal extensions of the plasma membrane, known as T-tubules, which reach deep into the interior of the cell (Figure 1-4A).

In addition to vastly decreasing the average distance between the cell surface and the contractile machinery, the T-tubules are further specialized with molecular machinery that initiates the downstream process of contraction (Figure 1-5). Closely apposed to the T-tubule lie specialized portions of the SR known as junctional SR. These highly specialized junctions of external and internal membranes are called triads (Figure 1-4B) in skeletal muscle and dyads in cardiac muscle, owing the different names to the respective organization of the structure that is different in each tissue. These two membrane systems, while entirely separate, are maintained in close proximity by cross-bridging proteins, which include junctophilin, triadin and junctin [32].

Signaling between plasma membrane and junctional SR begins when a depolarizing action potential reaches the dihydropyridine receptor (DHPR; also known as the L-type calcium channel and $Ca_V1.1$/$Ca_V1.2$), which is a voltage-sensitive calcium channel that resides within the

T-tubule (Figure 1-5). Upon stimulation by an action potential, the DHPR channel opens allowing calcium ions to flow into the cell. In cardiac muscle, this initial influx of calcium then binds to the ryanodine receptor (RyR), the primary calcium release channel of the SR, causing calcium to be then released from the internal SR calcium store. This coupling mechanism is known as calcium-induced calcium release. In skeletal muscle, the coupling mechanism between the DHPR and the RyR is considerably more complex and does not rely upon calcium as a second messenger [33]. Instead, activation of the DHPR results in a conformational change in the protein structure that is rapidly relayed to the RyR using a physical coupling mechanism, which is poorly understood at present. In both muscle types, however, it is the SR calcium store that is largely responsible for contraction of the sarcomere.

1.2.3.2 Microanatomy of the Excitation-contraction Coupling Junction

ECC occurs at specialized points of apposition between the T-tubule and the SR. Although the arrangement of these two membranous systems is generally similar in skeletal and cardiac muscle, there are a number of differences that delineate each muscle type.

T-tubules are deep extensions of the plasma membrane that vastly increase the surface area-to-volume ratio of the cell, and as such they decrease the diffusion distance from calcium release sites to the sarcomeres. They are found in nearly all mammalian striated muscle fibers, with the exception of neonatal myocytes and adult atrial myocytes in some small mammalian species [34-38]. They are major sites of transmembrane exchange and signaling, and as such contain many important protein complexes including the DHPR [39, 40]. In skeletal muscle, T-tubules primarily develop postnatally (except for the diaphragm and intercostal muscles) and are arranged at regular intervals corresponding to the intersection of A- and I-bands of the sarcomere (Figure 1-4A) [41]. At the microscopic level, this arrangement results in a doublet pair of T-

tubules which appear to flank the Z-line of the sarcomere [42]. The T-tubules of cardiac myocytes, however, directly co-localize with the sarcomere Z-line, resulting in a single T-tubule per sarcomere [36].

The architecture of the SR is also analogous but different in skeletal and cardiac muscle. In both muscle types, the SR forms a membranous network throughout the myocyte that can be divided into at least two substructures, longitudinal and junctional SR. The longitudinal SR is enriched in the calcium pump SERCA, while the junctional SR contains the calcium release channel RyR and the calcium buffering protein calsequestrin [43]. In skeletal muscle, the junctional SR forms node-like structures called terminal cisternae that store large reserves of calcium. Each of these SR nodes is closely associated with one half of a T-tubule, and they are often arranged such that either side of a T-tubule is associated with junctional SR in a pattern known as a triad, which is vaguely reminiscent of a cartoon butterfly [44] (Figure 1-4B). In cardiac myocytes instead of forming discrete synapse-like structures, the junctional SR wraps around a portion of the T-tubule in a structure called a dyad [45].

Because ECC is dependent upon physical coupling in skeletal muscle and calcium diffusion in the heart, the distance between the T-tubule and the junctional SR is strictly maintained at about 15 nm in cardiac myocytes and 10 nm in skeletal myocytes [44, 45]. A number of proteins have been implicated in the formation and maintenance of these junctions, including junctophilin, junctin, and triadin [45, 46]. The DHPR and RyR channels, although important components of the triad, do not directly contribute to triad formation or maintenance as evidenced by the fact that triads are present even when DHPR, RyR or both have been genetically eliminated [47, 48].

1.2.3.3 The Dihydropyridine Receptor

The dihydropyridine receptor (also known as the L-type calcium channel) is a voltage-dependent calcium channel that is composed of four subunits α_1, α_2/δ, β, and γ in equivalent ratios (Figure 1-7) [49, 50]. The α_1 subunit is the largest of the four and forms the transmembrane calcium pore. There are four isoforms of the α_1 subunit that exhibit different tissue expression patterns, with α_{1S} (CACNA1S) being the skeletal muscle isoform and α_{1C} (CACNA1C) the cardiac isoform [51]. The α_1 subunit is required for ECC, but calcium permeability of the skeletal muscle isoform, α_{1S}, is not essential for coupling since the skeletal-type mechanism does not use calcium as a second messenger between the DHPR and RyR [52, 53]. The β subunit is an intracellular component that is required for ECC and is necessary for proper voltage sensitivity and calcium permeation [54-56]. The β subunit has four isoforms, β_1 being the skeletal muscle isoform and β_2 and β_4 being expressed in the heart [51, 57]. The α_2/δ subunit is a heavily glycosylated membrane-associated protein that is the disulfide bonded cleavage product of the CACNA2D1 gene [50]. The α_2 portion of this subunit is extracellular and is anchored by a disulfide bond to the δ subunit, which is a single-pass transmembrane protein. The γ subunit is a heavily glycosylated four-pass transmembrane protein. The α_2/δ and γ subunits are not required for ECC, but may exert subtle effects on channel function or expression [58].

The DHPR α_{1S} subunit was the first gene known to be required for ECC. Work in the 1960s on the recessive muscular dysgenesis (*mdg*) phenotype revealed that although these mice had histologically apparent muscle tissue, they were completely paralyzed and suffered from a number of developmental abnormalities [59-61]. These abnormalities were later shown to result

from a defect in ECC caused by loss of the dihydropyridine-sensitive calcium channel, CACNA1S [21, 62-65]. Later the β_1 subunit was also demonstrated to be necessary for proper charge displacement and gating of the DHPR and by extension ECC [54-56, 66].

Mice lacking α_{1S} or β_1 subunits of the DHPR are born in expected Mendelian ratios, but die very soon after birth due to asphyxiation [59, 60]. The most obvious feature of the affected mouse pups is complete lack of skeletal muscle contraction while cardiac muscle is spared from paralysis. In histological sections, the muscle mass of these mice is clearly affected in all muscle groups, and there is abnormal clustering of nuclei within the spindly myofibers. These ECC null mice also have a number of non-muscle developmental defects that are presumed to be secondary to absence of muscle contraction *in utero*. The body posture of ECC null mice is limp and rounded with edema noted in some fetuses. There are a number of skeletal abnormalities in these mice, particularly involving the development of the rib cage and costal cartilages [59, 60]. The bony tubercles at muscle insertion sites of long bones are also dramatically reduced [67, 68]. Muscle innervation is also aberrant in these mice as demonstrated by increased branching of the phrenic nerve of the diaphragm muscle and an increased number of miniature endplate potentials [69-72].

1.2.3.4 The Ryanodine Receptor

Muscle contraction is triggered when calcium ions stored in the SR lumen escape through ryanodine receptors located in the junctional SR (Figure 1-8) [73]. Ryanodine receptors are named for their sensitivity the plant alkaloid ryanodine, which at low concentrations locks the channels in an open subconductance state and blocks it at high concentrations [23, 74]. There are three isoforms of ryanodine receptors in mammals with differential tissue distributions: skeletal muscle (RYR1), cardiac muscle (RYR2), and neuronal tissue (as well as many others) (RYR3)

[27, 75]. Ryanodine receptors form homotetramer complexes with masses in excess of 2 MDa, each subunit weighing about 550 kDa [24, 25, 76-78]. Because of the massive size of the complex, RyRs can be readily seen by electron microscopy in the cleft between T-tubules and the junctional SR where they are called 'feet' (mice lacking RyR1 are called *dyspedic*) (Figure 1-4) [79, 80]. Loss of either RyR1 or RyR2 abolishes contraction in the respective muscle type with phenotypes highly similar to loss of the DHPR pore subunit [80, 81]. RyRs are directly activated by a number of substrates, notably DHPR (in the case of skeletal muscle), polylysine [82], calcium ions [83], adenosine [84], high concentrations of caffeine [85], the scorpion toxin maurocalcine [86], and 4-choro-*m*-cresol (4-CMC) [87]. In addition to ryanodine, RyRs are also inhibited by magnesium ions and ruthenium red [76, 85]. Gating properties of RyRs are modulated by post-translational modifications including phosphorylation, nitrosylation, and oxidation as well as by binding of proteins such as FK506-binding proteins 12 and 12.6, calmodulin, and the calsequestrin/triadin/junctin complex [73].

1.2.3.5 The Skeletal-type Coupling Mechanism

The skeletal muscle DHPR signals to the downstream RyR calcium channel via a physical coupling mechanism (Figure 1-6). This coupling mechanism is unique to the skeletal muscle form of the channel and requires no entry of external calcium into the cell. In contrast, the cardiac DHPR uses calcium as a second messenger and is dependent upon extracellular calcium entry through the channel pore. Although a satisfactory molecular explanation for the physical coupling of the skeletal-type DHPR/RyR has not been described, a number of observations support that the channels are indeed physically linked. First, external calcium is not required for skeletal ECC, ruling out that external calcium acts as a second messenger. Second, either calcium channel immunoprecipitates with the other [88]. Third, DHPR and RyR arrange

into tetrad formations (four DHPR complexes associated with four corresponding RyRs tetramers) observable by freeze-fracture electron microscopy, and binding of ryanodine to the RyR causes alteration of DHPR conformation in the tetrads [65, 89-91]. Fourth, the conductance and expression of the DHPR is enhanced by the expression of RyR, known as retrograde signaling [92-94]. Fifth, treatment of *dyspedic* myotubes expressing RYR1 with nifedipine, a DHPR blocker, reduces sensitivity of the RyR to caffeine, but this does not occur when the cardiac RyR is expressed instead [95].

A considerable number of studies have attempted to define how the DHPR physically links to the RyR to give rise to bidirectional coupling [96]. Since skeletal myocytes lacking the DHPR or RyR are not rescued by expression of the respective cardiac channel, several groups have investigated activity of chimeric clones by incorporating portions of the skeletal muscle channels into otherwise inactive cardiac channels to identify the critical regions for the skeletal muscle coupling mechanism. The chimeric studies of DHPR revealed that the intracellular loop between transmembrane helices two and three (known as the II-III loop) from skeletal muscle confers full functionality to the cardiac DHPR with respect to both orthograde (DHPR→RyR) and retrograde (RyR→DHPR) signaling and that disruption of this sequence abrogates signaling [97-100].

Many early studies attempted to define the critical sub-regions of the II-III loop with *in vitro* assays using synthetic small peptides from this region to activate RyR1. These studies showed that small regions of the skeletal II-III loop could activate RyR, however, it was also shown that corresponding peptides derived from the cardiac II-III loop had similar activity [82]. The activity-bearing region was further characterized into two distinct sequences, one that included a phosphorylation site [101] and another that was eventually reduced to just ten basic

(positively charged) amino acids, called *peptide A-10* [102-105]. Other basic (positively charged) peptides including polylysine [82] and the scorpion toxin maurocalcine [86, 106-110] have also been shown to activate calcium release from RyR, indicating that electrostatic interactions could play a role in ECC.

Other attempts to define the critical residues *in vivo* used the skeletal DHPR as a backbone and then substituted the II-III loop with the corresponding, but highly dissimilar sequence from the house fly, *Musca domestica*, which resulted in a mostly skeletal DHPR that lacked orthograde and retrograde signaling (Figure 1-9) [96, 100, 111]. Short sequences from the skeletal II-III loop were then systematically added back to the foreign II-III loop to determine the minimal sequences. These sequences were permutated to determine precisely which amino acid residues contribute to the coupling mechanism. It was determined from these experiments that four residues are critical for orthograde signaling (A739, F741, P742, and D744) and two of those (A739 and F741) were also required for retrograde signaling.

Unfortunately, the peptide-based assay and the chimeric construct experiments yielded incongruent conclusions. Further study of the *peptide A-10* sequence *in vivo* demonstrated that the DHPR retained full activity even when the *peptide A-10* sequence had been scrambled [112]. Collectively the DHPR chimera studies have quenched the idea that the *peptide A-10* region mediates the skeletal-type ECC mechanism, though the evidence remains that it is an activator of RyR, at least in isolation.

The skeletal-type ECC mechanism also depends upon specialization of the skeletal muscle ryanodine receptor, as neither the cardiac or brain isoforms are functionally equivalent [113]. Therefore, studies expressing chimeric molecules of the skeletal muscle (RyR1), cardiac

(RyR2), and brain (RyR3) ryanodine receptors in *dyspedic* myotubes (lacking RyR1) have attempted to elucidate the regions of RyR1 that mediate the skeletal-type ECC [114]. These studies have been less conclusive than those with DHPR in determining the critical regions, but have demonstrated that the D2 region is likely important and that multiple regions may individually contribute to skeletal-type properties of tetrad formation, orthograde signaling, and retrograde signaling [93, 115-117].

In vitro binding assays have demonstrated that RyR1 can also interact with fragments of the DHPR III-IV loop [118, 119]. This information suggests that the DHPR III-IV loop also participates in coupling of the two channels, which was also supported by the fact that a mutation (R1086H) of the DHPR III-IV loop relieves inhibition of RyR1 and causes malignant hyperthermia in humans [120, 121]. Further studies, however, showed that the III-IV loop non-specifically influences DHPR gating since substitution of the region with that of a distantly related channel restores inhibition [122]. These studies do not exclude a role for the III-IV loop in skeletal-type ECC, but they do indicate that the role is not isoform dependent.

1.2.3.6 Diseases of the Excitation-contraction Coupling Machinery

Heritable diseases involving the skeletal muscle ECC machinery are quite rare and most commonly involve muscle weakness and/or unrestricted release of calcium from the SR in response to succinylcholine or volatile anesthetic agents during surgical procedures [123-125]. (Summarized in Table 1-1) The rapid and unregulated release of calcium from the SR results in systemic contracture of skeletal muscle and a massive increase in oxidative metabolism. This increased metabolic rate rapidly ramps up internal body temperature resulting in a condition called malignant hyperthermia, which can be fatal without immediate intervention including cessation of anesthesia and administration of the RYR1 inhibitor dantrolene [126]. In humans

genetic lesions that cause malignant hyperthermia are primarily located in the gene encoding the skeletal muscle isoform of the ryanodine receptor (RYR1) [73, 127, 128], but a rare malignant hyperthermia-causing mutation in the DHPR pore-forming subunit has also been identified [120, 121]. Mutations in RYR1 also cause multiminicore disease and central core disease (also called central core myopathy), both of which are hypotonic muscle diseases that may also increase susceptibility to malignant hyperthermia [128-131]. Exertional rhabdomyolysis has been linked to a number of ECC components including RYR, DHPR, and calsequestrin [132]. A mutation in the DHPR pore forming subunit is known to cause hypokalemic periodic paralysis [133, 134].

Mutations in ECC components also are responsible for a number of monogenic cardiovascular diseases as well as being functionally altered in many idiopathic and chronic forms of heart disease. Mutations in the cardiac RYR (RYR2) cause an autosomal dominant form of stress-induced tachycardia called catecholaminergic polymorphic ventricular tachycardia (CPVT) by increasing sensitivity of the channel to β-adrenergic stimulation and increasing the open probability at low calcium concentrations [135-137]. Manifestation of CPVT is typically initiated by exercise or severe emotional stress and can result in a ventricular arrhythmia that is often fatal. Mutations in cardiac calsequestrin (CASQ2), a calcium buffering protein of the SR, are also known to cause an autosomal recessive form of CPVT [138-140]. Mutations in the junctional protein triadin (TRDN) and the calcium binding protein calmodulin (CALM1) have been implicated as rare causes of CPVT [141, 142]. A mutation in RYR2 also causes arrhythmogenic right ventricular dysplasia, type 2, a disease characterized by fatty infiltration of the right ventricular myocardium that results in electrical conduction disturbances and can lead to cardiac arrest [143, 144].

Brugada syndrome is a genetic heart disease characterized by electrical abnormalities, including ST-segment elevation and short QT interval, that can result in arrhythmogenic electrical activity and ventricular fibrillation [145, 146]. It is a major cause of sudden unexplained death in adults with structurally normal hearts, especially in young men of Southeast Asian and Japanese descent [147, 148]. The most common gene causing Brugada syndrome is the cardiac sodium channel, but reports have also stated that mutations in the DHPR pore-forming α_{1C} subunit (CACNA1C) and the β_2 subunit (CACNB2) can cause this disease [149-151].

Timothy syndrome is another cardiac arrhythmic disorder resulting from mutation of the DHPR pore-forming α_{1C} subunit (CACNA1C) [150-154]. Unlike Brugada syndrome, which presents with short QT intervals on ECG and normal heart morphology, Timothy syndrome is characterized by a prolonged QT interval and severe heart malformation [155, 156]. Another unique and rather surprising feature of Timothy syndrome is the involvement of multiple developmental systems that are not usually thought to depend upon the cardiac-type DHPR. These features most often include syndactyly, facial and dental deformities, and autism in about 80% of patients who survive long enough for assessment as the disease is often fatal in early years.

1.2.4 Mechanisms of Calcium Clearance

1.2.4.1 Overview

Striated muscle fibers rely on rapid cycling of calcium into and out of the cytosolic compartment in order to sustain repeated contraction and relaxation. When triggered by an upstream action potential, calcium rapidly enters the cytosol where it binds to troponin C and

exposes the actin filament to the myosin motor protein to generate muscle contraction [157]. In order for the myofiber to return to a relaxed state, calcium must be stripped from the cytosol. The excess calcium is shuttled to the SR, into mitochondria, or to the extracellular space (Figure 1-5). In the mouse heart, this process fully cycles at the phenomenal rate of about eight times per second.

Because calcium concentration is very high in the SR and extracellular space, transporting calcium out of the cytoplasm is an energy intensive process. Calcium is exported to the extracellular space by the sodium-calcium exchanger (NCX), which utilizes the sodium diffusion gradient (maintained by the sodium-potassium ATPase) to move three sodium ions into the cell and one calcium ion out. Direct pumping of calcium to the extracellular space is accomplished by the plasma membrane calcium ATPase (PMCA) pump, but this process is very slow and accounts for a minor fraction of excreted calcium. Although an appreciable percentage of calcium is excreted following contraction, the majority of it is transported to the SR by the SERCA pump which directly hydrolyzes ATP in the transport process and has a very high affinity for cytosolic calcium allowing near complete removal. Like PMCA, the SERCA enzymatic cycle is rather slow, but its low throughput is greatly outweighed by extremely high SERCA abundance in the SR membrane.

Although SR pumping is the predominant removal mechanism in all species, the relative amount going to the SR, extracellular space, and mitochondria varies by species and pacing conditions [158]. In rabbits, removal to the SR accounts for 70%, extracellular removal by NCX 28%, and 2% by PMCA and mitochondria. These proportions are comparable for other large mammals including human, cat, dog, guinea-pig, and ferret [157]. Rats and mice have a greater utilization of SERCA with the SR accounting for 92%, NCX 7%, and PMCA/mitochondria 1%.

1.2.4.2 Extracellular Calcium Clearance

Calcium concentration is maintained at ten-thousand fold higher in the extracellular compartment compared to resting cytosolic levels. Because of this high relative ratio, transport of calcium into extracellular space is an energy-dependent process. A small percentage of calcium is exported via PMCA, a ubiquitously expressed calcium pump that hydrolyzes ATP as an energy source; however, the contribution of PMCA to total calcium export is minor compared to the large throughput of the sodium-calcium exchange protein which is expressed at high levels in the sarcolemma and T-tubules [158-160]. Therefore, the remainder of this discussion will focus on the NCX.

The NCX is a ten-pass integral membrane protein of the plasmalemma that antiports sodium and calcium by secondary active transport, meaning that NCX uses diffusion potential of one ion species down its concentration gradient to transport another against its concentration gradient [160-165]. NCX utilizes potential energy stored in the sodium gradient generated by the Na^+/K^+-ATPase [166, 167]. NCX proteins are encoded by three distinct genes, each also having multiple isoforms: NCX1 (encoded by SLC8A1; cardiac and skeletal muscle isoform: NCX1.1), NCX2 (SLC8A2), and NCX3 (SLC8A3) [168-171].

When operating in the 'forward' direction, NCX exchanges extracellular sodium ions for intracellular calcium [159]. Conversely the 'reverse' direction moves calcium into the cell and sodium out. The sodium to calcium exchange ratio is generally considered to be 3:1, making the transporter electrogenic since sodium bears one positive charge and calcium two [163, 166]. The direction and magnitude of NCX fluxes are proportional to the relative intracellular and extracellular concentrations of sodium and calcium. Because concentrations of both of these ion species (calcium especially) vary greatly in temporal and spatial dimensions, the apparent

function of NCX is highly dynamic. In addition to dynamic regulation by substrate availability, NCX may also be regulated allosterically by sodium and calcium ions, pH, and protein phosphorylation [159].

Because of its dynamic, bi-directional transport properties, NCX is thought to contribute to multiple stages of the contractile mechanism [157, 159, 172]. During an action potential, voltage-gated sodium channels open and intracellular sodium concentration rises rapidly, especially near the plasma membrane. This shift in local sodium concentration causes NCX to function in the reverse direction, moving sodium out of the cell and calcium in. By this mechanism, NCX has been shown to contribute to calcium-induced calcium release by priming the dyadic cleft with calcium so that calcium entering through DHPR reaches the RyR release threshold faster [173-175]. Upon release of calcium by the RyR, the dyadic calcium concentration increases, and NCX intrinsically shifts to forward flux to remove calcium from the cell. Because forward flux causes sodium to enter the cell, NCX may also provide depolarizing current that prolongs the repolarization phase of the action potential. Similar mechanisms may be at play in skeletal muscle, however, calcium entry through DHPR is not essential to ECC and the role for NCX is generally not well understood.

The NCX has been proposed to contribute to the pathology of heart failure by several mechanisms. Heart failure is known to involve a number of perturbations in ion concentrations [176]. Concentrations of both calcium and sodium are known to be increased in the context of heart disease. When cytoplasmic calcium concentration is high, NCX could contribute to after-depolarization by moving too much sodium into the cell. In the case of high intracellular sodium, NCX may help to repolarize the cell following an action potential [177]. Conversely in the case of cellular acidosis caused by ischemia-reperfusion injury, the sodium-hydrogen antiporter

exchanges intracellular protons for sodium. This high-sodium scenario can cause a large influx of calcium through the NCX which must then be removed by the calcium ATPase pumps, further stressing the metabolic machinery.

Whether protein levels of NCX are altered in heart disease has been the subject of much debate, but the ratio of NCX to SERCA has been proposed as an important determinant of SR calcium load and contractility [176]. The balance of NCX to SERCA activity may have a direct effect on how much calcium is stored in the SR. When NCX activity is low and SERCA's is high, more calcium will be stored in the SR, which in turn will affect contractility by increasing the rate of calcium release by the RyR. Conversely when NCX activity is higher, it could deplete the SR of calcium and cause decreased contractility.

1.2.4.3 Calcium Uptake by Mitochondria

Mitochondria are sub-cellular organelles that specialize in breaking down and producing metabolic substrates for the cell. Since mitochondria occupy as much as one-third of the volume of a cardiac myocyte and are interspersed among the myofilaments and SR, it has been proposed that they may also function as a site of intracellular calcium storage. Calcium and other small solutes diffuse freely across the outer mitochondrial membrane, but transfer across the inner membrane requires facilitated diffusion by transporter proteins. The mitochondrial calcium uniporter (MCU) and its regulatory protein, mitochondrial calcium uptake 1 (MICU1), were only recently identified [178-180]. The MCU is a nuclear-encoded protein that forms a multimerized pore complex in the inner mitochondrial membrane [181].

Although total mitochondrial calcium storage capacity is rather high, most estimates suggest that mitochondria are responsible for clearing less than 1% of calcium during muscle

relaxation [158, 182]. This conclusion means that mitochondrial calcium storage is practically negligible on a beat-to-beat basis. Despite the dispensability of the MCU in muscle relaxation, MCU knockout (KO) mice reveal that mitochondrial calcium influx may be an important mechanism for regulation of mitochondrial function [183]. MCU KO mice have normal basal metabolism, however, the skeletal muscle of these mice is weak and has decreased pyruvate dehydrogenase activity. Therefore, mitochondrial calcium influx may help to synchronize energy production with energy consumption during muscle activity, but this calcium flux is negligible for contraction.

1.2.4.4 Calcium Re-sequestration to the Sarcoplasmic Reticulum

Striated muscle cells contain an extensive membrane network called the sarcoplasmic reticulum. The SR network allows muscle cells to store a very large amount of calcium that can be released rapidly to cause contraction and was first isolated by Kielley and Meyerhof in 1948 [15, 184]. In 1951 Marsh demonstrated the first factor allowing relaxation of actomyosin filaments [7, 185], and in 1958 Setsuro Ebashi demonstrated that the relaxation factor was imparted by ATPase activity in the SR fraction [10]. It was later shown by several groups that the mass migration of calcium back to the SR is accomplished by a single dedicated pump, the sarco/endoplasmic reticulum calcium ATPase (SERCA). The SERCA pump is a single transmembrane polypeptide of about 102 kDa [13, 186]. SERCA pumps calcium back into the SR against its concentration gradient by hydrolyzing ATP [12]. The pumping cycle of SERCA results in transport of two calcium ions into the SR and release of ADP, P_i, and H^+ [187-189].

SERCA is a member of the P-type ATPase family that also includes other notable membrane transporters including the PMCA, the Na^+/K^+-ATPase, the H^+/K^+-ATPase, the H^+-ATPase, and the copper-transporting ATPase [190]. P-type ATPases are comprised of four

primary domains, the phosphorylation domain (P-domain), the actuator domain (A-domain), the nucleotide domain (N-domain), and the membrane domain (M-domain) (Figure 1-11). The P-domain is the catalytic core of the protein and as such contains the highest number of invariant residues across all family members. The P-domain hydrolyzes ATP to ADP, transferring the gamma phosphate of ATP to an aspartic acid in the DKTGTLT motif. The N-domain is linked to the P-domain by a hinge structure and orients the ATP molecule to interact with the catalytic aspartic acid residue. The A-domain is the smallest of the cytosolic domains and is the second most conserved. During the catalytic cycle, the TGE motif of the A-domain contacts the catalytic site. The M-domain is largely responsible for ion specificity and pumping function. As such, it is the most evolutionarily variable region and is also the most mobile during the catalytic cycle.

The SERCA pump family is encoded by three distinct loci, SERCA1 (ATP2A1), SERCA2 (ATP2A2), and SERCA3 (ATP2A3) [191]. Each of these genes produces multiple isoforms through alternative splicing of the mRNA transcripts. These isoforms each have distinct expression patterns with regard to their tissue distribution. SERCA1 encodes two isoforms that are only found in fast-twitch skeletal muscle with differential developmental expression patterns, SERCA1a being the adult isoform and SERCA1b, fetal. SERCA2 also encodes two isoforms: SERCA2a, which is highly expressed in adult cardiac and slow-twitch skeletal muscle and fetal and smooth muscles to a lesser extent, and SERCA2b, which is expressed ubiquitously. SERCA3 encodes at least six isoforms, all of which are expressed in non-muscle tissues.

SERCA activity is regulated by multiple mechanisms, including post-translational modification and protein-protein interactions. SERCA2a is modified by post-translational conjugation of the small ubiquitin-like peptide SUMO1 to two lysine residues in the N-domain [192]. SUMO modification increases the ATPase activity of the protein and also appears to

affect its stability. Notably, SUMOylation of SERCA2a appears to be deregulated in the context of heart failure, and supplementation of SUMO1 expression by adeno-associated viruses (AAV) seems to prevent heart failure resulting from thoracic aortic constriction in mice and ischemic injury in swine [192, 193]. Recently pharmacologic intervention with a small molecule called N106 was shown to increase SUMOylation of SERCA2a *in vivo* and restore cardiac function in a mouse model of heart failure [194]. Allosteric activation of SERCA though serine phosphorylation by calmodulin-dependent kinase II (CaMKII) was suggested by one group [195], but a functional role form this modification was later dismissed by other groups [196]. SERCA activity is also modulated by stoichiometric interaction with multiple small transmembrane proteins, including phospholamban (PLN), sarcolipin (SLN), and most recently discovered myoregulin (MRLN) [197]. Activity of all SERCA isoforms is inhibited by thapsigargin [198].

1.2.4.5 Small Transmembrane Inhibitors of SERCA

Early investigations into the dynamic regulation of cardiac contractility indicated that β-adrenergic signaling by epinephrine leads to positive effects on cardiac contraction (inotropy) and relaxation (lusitropy) and that this pathway is a major determinant of cardiac contractility *in vivo* [199, 200]. Many years later, it was demonstrated that these effects were due to a rise in cytosolic cyclic AMP (cAMP) which increases the activity of the cAMP-dependent protein kinase A (PKA). Since most investigations at the time focused on actomyosin dynamics, at first it was suggested that PKA may directly increase the sensitivity of cardiac troponin for calcium; however, this possibility was later eliminated [201].

Multiple groups in the mid-1970s reported that PKA could phosphorylate the cardiac SR, suggesting that an SR-dependent (i.e. calcium-dependent) mechanism could explain the effects of PKA, but none of these reports identified a satisfactory molecular mechanism [202]. They did

show, however, that PKA generates a phosphoester serine-phosphate bond that was distinct from the acyl phosphate intermediate of SERCA [202, 203]. Around this time Arnold Katz's lab was investigating PKA phosphorylation of the SR. They discovered that addition of cAMP and PKA had rapid synergistic effects on SR calcium uptake and was correlated with phosphorylation of a 22 kDa protein [204-206]. This phosphoprotein was named phospholamban by contraction of the word *phosphate* with the Greek word *λαμβανειν* ("lambanein"), meaning "to take." Discovery of phospholamban and its regulation by phosphorylation established a direct link from catecholamine-dependent increases in contractility and relaxation to the underlying molecular mechanism of calcium handling[1].

Further study of phospholamban has revealed a number of important findings. For one, it was found that the 22 kDa protein is actually a pentameric form that can be reduced to monomers of about 6 kDa by boiling the sample before electrophoresis [207-209]. Additionally, it was shown that phospholamban is the phosphorylation target of PKA at serine-16 ($pSer^{16}$) and CaMKII at threonine-17 ($pThr^{17}$) [210, 211]. Phosphorylation of phospholamban at either of these sites relieves its inhibition on SERCA and increases the rate of cytosolic calcium removal (relaxation) and the total SR calcium store (contractility) [212]. Molecular cloning of the phospholamban complementary DNA (cDNA) revealed that the protein is 52 amino acids in length and can be divided into three structural domains, Ia, Ib, and II [210, 211, 213]. The first twenty amino acids form an alpha helical structure to make up domain Ia. Domain Ib is comprised of the next ten amino acids and sits at the membrane interface where it is connected to

[1] Notably many groups failed to reproduce this effect in rabbit fast-twitch skeletal muscle preparations, as it was later discovered that phospholamban is specific to cardiac and slow-twitch muscle.

domain Ia by a small loop region [214]. Finally domain II is the rigid transmembrane helix that anchors the protein in the membrane and binds to the M-domain of SERCA. Domain II forms functional interactions with transmembrane helix M6 of SERCA, while Domain Ib is also important for functional modulation of SERCA [215, 216]. Although phospholamban can inhibit the activity of all muscle SERCA isoforms, it is only coexpressed with the SERCA2a isoform [191].

Sarcolipin is a very small protein that was initially described simply as a low-molecular-weight proteolipid in SR fractions of rabbit skeletal muscle. Molecular cloning revealed that the peptide is composed of 31 amino acids and encodes a C-terminal transmembrane helix and a small cytosolic N-terminal region [217]. Sarcolipin immunoprecipitates with SERCA1, but is not necessary for the activity of the pump. In contrast to phospholamban, which is expressed in the cardiac ventricle and slow skeletal muscle, in rodents sarcolipin is only appreciably expressed in the cardiac atria [197, 218]. In the atria, sarcolipin is thought to inhibit the calcium uptake rate of SERCA by binding the same groove as phospholamban; however, the regulatory mechanism may be slightly different. Unlike phospholamban, sarcolipin is not known to be phosphorylated *in vivo*[2] [219-221]. Sarcolipin has been reported to inhibit SERCA by uncoupling ATP hydrolysis from calcium pumping, thus generating a futile ATPase and producing heat as a byproduct [222, 223]. A recent study used sarcolipin KO mice to demonstrate that the sarcolipin futile cycle is essential for non-shivering thermogenesis in adult mice [224]. This is quite a

[2] It has been reported that CaMKII can phosphorylate sarcolipin on threonine-5 *in vitro* and that this may affect the inhibitory action on SERCA; however, evidence of a role *in vivo* is weak at present.

surprising conclusion given that expression of sarcolipin is limited to slow twitch muscle fibers[3] and the cardiac atria in adult mice [197]. Therefore, the significance of this mechanism in non-shivering thermogenesis requires evaluation by other groups, ideally with an independent mouse line to rule out a co-segregating phenotype of the sarcolipin KO haplotype.

A distant homolog of sarcolipin and phospholamban, coined "sarcolamban," was recently described in *Drosophila melanogaster* which greatly expanded the evolutionary scope of regulation of SERCA by small proteins [225]. We hypothesized that additional members of this family could exist in mammal which are encoded in putatively non-coding transcripts [226]. Our lab recently described, in Anderson et al., a novel family member in mammals which was named "myoregulin" [197]. Like other members of the family, myoregulin is a small protein encoding a C-terminal transmembrane domain that inhibits SERCA activity and shares the functional L-F-X-X-F motif with other family members (Figure 1-12). Notably however myoregulin expression is restricted to skeletal muscle and overlaps very little with expression of phospholamban or sarcolipin.

A crystal structure of SERCA was first solved in 2000, but only recently were crystals obtained with sarcolipin bound to the pump [188]. This complex was discovered somewhat serendipitously while attempting to crystalize SERCA1a with magnesium in the absence of calcium [227, 228]. Sarcolipin binds in a groove composed of the M2, M6, and M9 transmembrane helices and stabilizes the enzyme in the magnesium-bound E1 state. These crystallographic studies agree with previous studies that sarcolipin and phospholamban share the

[3] In mice, slow twitch fibers are found primarily in the soleus, a relatively small postural muscle group of the hindlimb. In humans, slow fibers are more abundant and are found in most muscle groups.

same binding site, demonstrated by the fact that they can both be cross-linked to M2. However, they do not agree entirely with several prior studies regarding the enzymatic state of SERCA that phospholamban/sarcolipin bind – most studies have suggested that sarcolipin binds to an E2 state [224, 229-233]. Although sarcolipin and SERCA have not been crystalized in an E2 state (suggesting it is not thermodynamically stable), Winther et al. note that the binding groove is still accessible in the [H_n]E2 state, but that this groove is occluded or disrupted upon transition to the [Ca_2]E1P conformation [228]. As such, the exact mechanism by which sarcolipin and phospholamban inhibit SERCA remains a controversial topic.

SERCA is a member of the P-type ATPase family that includes several other well-studied enzyme pumps, such as the Na^+/K^+-ATPase, but also includes many proteins with unknown function. Regulation of P-type ATPases by small transmembrane peptides appears to be a common theme. As discussed above, SERCA isoforms are modulated by no fewer than three transmembrane peptides, phospholamban, myoregulin, and sarcolipin [191, 197]. In muscle the small transmembrane protein, phospholemman (also known as FXYD2), regulates the Na^+/K^+-ATPase of the plasma membrane, and other members of the FXYD family also regulate this pump in non-muscle tissues [234-237]. When unphosphorylated, phospholemman inhibits Na^+/K^+-ATPase, but when phosphorylated it activates the pump [238]. In yeast, two small transmembrane proteins, PMP1 and PMP2, increase the activity of the H^+-ATPase [239, 240]. Taken together these examples suggest that regulation of P-type ATPases by small transmembrane proteins may be generalizable to other family members. The examples of the FXYD and PMP proteins also suggest that the function of these proteins in regulating pumps may be quite versatile and nuanced.

1.2.4.6 Countercurrent Ion Exchange

The SR is a specialized compartment for the storage and rapid release of calcium. Because calcium is an ionic species, bearing a 2+ charge, movement of calcium across membranes generates electric potential that must be balanced for optimal release kinetics [241]. In order for calcium to move down its concentration gradient (SR lumen → sarcoplasm) unimpeded, the SR membrane potential must be kept neutral (i.e. 0 mV) or at least lower than the equilibrium potential for the RyR so that opposing electrical force is negligible. Although SR countercurrent was described in the 1980s, this phenomenon is still poorly understood with respect to both the relevant ion species and the protein facilitators.

The SERCA pump is the only known ATPase of the SR, therefore, all counter balances are equilibrated by either passive or secondary active transport by use of electrochemical gradients. Potassium, with a 1+ charge, is considered to be the most important counter ion during SR calcium release, but others such as hydronium, with a 1+ charge, also seem to play a minor role. The role of anion balance (primarily chloride, with a 1- charge) is documented, but not very well understood [241]. Understanding the role of chloride transport in muscle contraction is confounded by the fact that there are many types of channels in the SR membrane that are capable of chloride conductance and the gating properties of these channel types are not uniform.

Trimeric intracellular cation channels (TRIC), TRIC-A and TRIC-B, are very important in balancing potassium ions during calcium flux. These channels each have distinct roles as revealed by the different phenotypes in KO mice of the individual channels, but they also appear to play redundant roles in cardiac calcium release. Double KO of these genes results in early embryonic death and near complete blockage of calcium release in cardiomyocytes, revealing the very important role of SR potassium flux [242]. A recent study on isolated SR vesicles

demonstrated that TRIC channels are actually not required during calcium release, per se, since RyR seems to carry its own counter current, but that TRIC channels allow potassium to escape as calcium re-enters the SR during diastole [243]. Small conductance calcium-activated potassium channels and the H^+/K^+ exchanger have also been suggested to play a role in potassium balance during calcium re-sequestration [244].

1.2.4.7 Pathologic and Physiologic Consequences of Impaired Calcium Clearance

In the heart, clearance of calcium during diastole is essential for relaxation and storage of calcium for successive contractions. As such, elevated end-diastolic calcium concentration leads to decreased cardiac performance and is a common feature in most forms of diastolic heart failure [245]. Changes in expression of critical proteins and sub-cellular structure are thought to underlie defects in diastolic calcium clearance. Loss of T-tubules (a process also known as detubulation) is a documented phenomenon in advanced heart failure [246-249]. Detubulation leads to orphaned RyRs that can become asynchronous with the cardiac action potential because of the increased distance from DHPRs. Loss of the dyadic micro-domain also causes alteration of calcium uptake kinetics by SERCA [250]. A number of changes in calcium handling genes have also been shown to be perturbed in the setting of heart failure, including SERCA, phospholamban, and NCX [251]. Increases in the ratio of phospholamban to SERCA reduce the cell's ability to re-sequester calcium in the SR, which increases tension of the resting fiber and reduces contractile strength in subsequent contractions. Aberration of SERCA activity may lead to a greater reliance on NCX for calcium removal, but increased intracellular sodium, which also may occur in heart failure, diminishes the ability of NCX to remove calcium the cell.

Accumulation of calcium has also been implicated in some skeletal muscle diseases, namely muscular dystrophies. It is hypothesized that loss of dystophin[4] or other components of the dystrophin-glycoprotein complex results in chronic microscopic shredding of the sarcolemma or hyperactivity of stretch-activated channels. These events may allow calcium to leak into the cell and accumulate by overwhelming the calcium clearance machinery [252]. It is thought that accumulation of calcium contributes significantly to dystrophic disease progression by promoting myofiber necrosis [253]. This hypothesis is supported by the fact that overexpression of stretch-activated calcium channels in skeletal muscle results in a dystrophic phenotype [254]. Recently deregulation of calcium by way of increased intracellular sodium and NCX over-activity were also shown to play a role in muscular dystrophy [255].

Alterations in calcium clearance have also been suggested as a contributing mechanism in physiologic fatigue of skeletal muscles, although this is among many other hypothesized causes [256]. Recent work by Anderson et al. in which the skeletal muscle inhibitor of SERCA, myoregulin, was knocked out showed an increase in running endurance in the KO mice [197]. This work contributes further evidence that calcium handling plays a crucial role in the physiology of muscle fatigue.

Because of the involvement of SERCA in muscle diseases, it was hypothesized that increasing activity of SERCA, either by pharmacologic or gene-based therapy, might be an effective strategy. In mice, overexpression of SERCA1a using a transgene or adeno-associated virus in the muscles of dystrophic mice improved the severity of the disease [257]. Similarly, overexpression of SERCA2a in failing hearts of rodents, pigs, and sheep has been shown to

[4] Patients with Duchenne muscular dystrophy, lack the costameric protein dystrophin in sufficient quantity or quality.

improve heart function [258-265]. Based on these encouraging results, human clinical trials were undertaken to evaluate the safety and efficacy of SERCA2a gene therapy using AAV [266]. These trials initially yielded positive effects on the study end points [267-269]. However, a recent press release from Celladon states that AAV-delivered SERCA2a (known commercially as “mydicar”) failed to meet the study end points in phase II [270]. The reason for this outcome is currently unknown, but since success was achieved in a number of animal models, viral delivery, dosing, or other trial-related factors may be the cause [271]. These disappointing results indicate that although calcium re-uptake is a promising therapeutic target, successful modulation of this pathway *in vivo* may require new strategies.

1.3 FIGURES

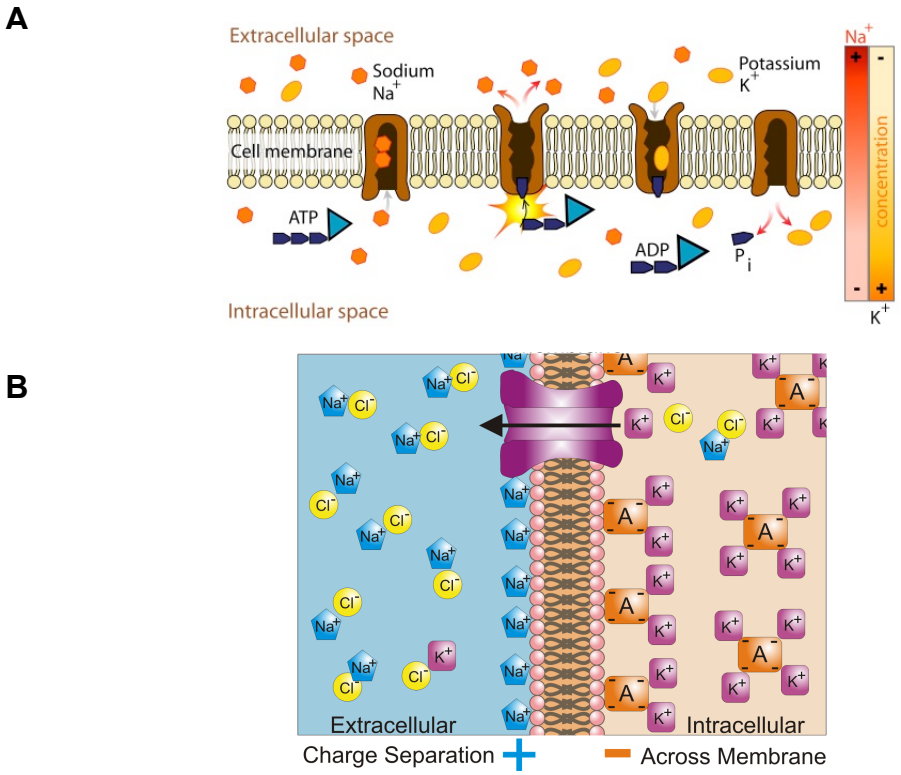

Figure 1-1. The Na^+/K^+-ATPase and the basis of membrane potential.

(*A*) The Na^+/K^+-ATPase (shown in brown) uses energy from ATP to transport three sodium ions out of the cell and two potassium ions into the cell, both against their concentration gradients. Continual pumping generates an electrochemical disequilibrium across the plasma membrane that maintains the interior of the cell in a negatively charged state. (*B*) Within the cell, potassium negates the charge of anionic species, including proteins and metabolites. Potassium leak channels selectively and continuously allow potassium to diffuse out of the cell. As potassium leaks from the cell, the interior becomes more negatively charged since anionic species are unable to follow across the membrane. Potassium flows from the cell until the negative electrostatic forces holding potassium in the cell are equilibrated with the diffusion force. This phenomenon is known as the potassium reversal potential or E_K. Membrane potential is derived from the electrochemical balancing of all electrically active solutes.

(*A*) was created by Wikipedia user LadyofHats. (*B*) was created by Wikipedia user Synaptidude. Both used under the Creative Commons License 3.0 [272].

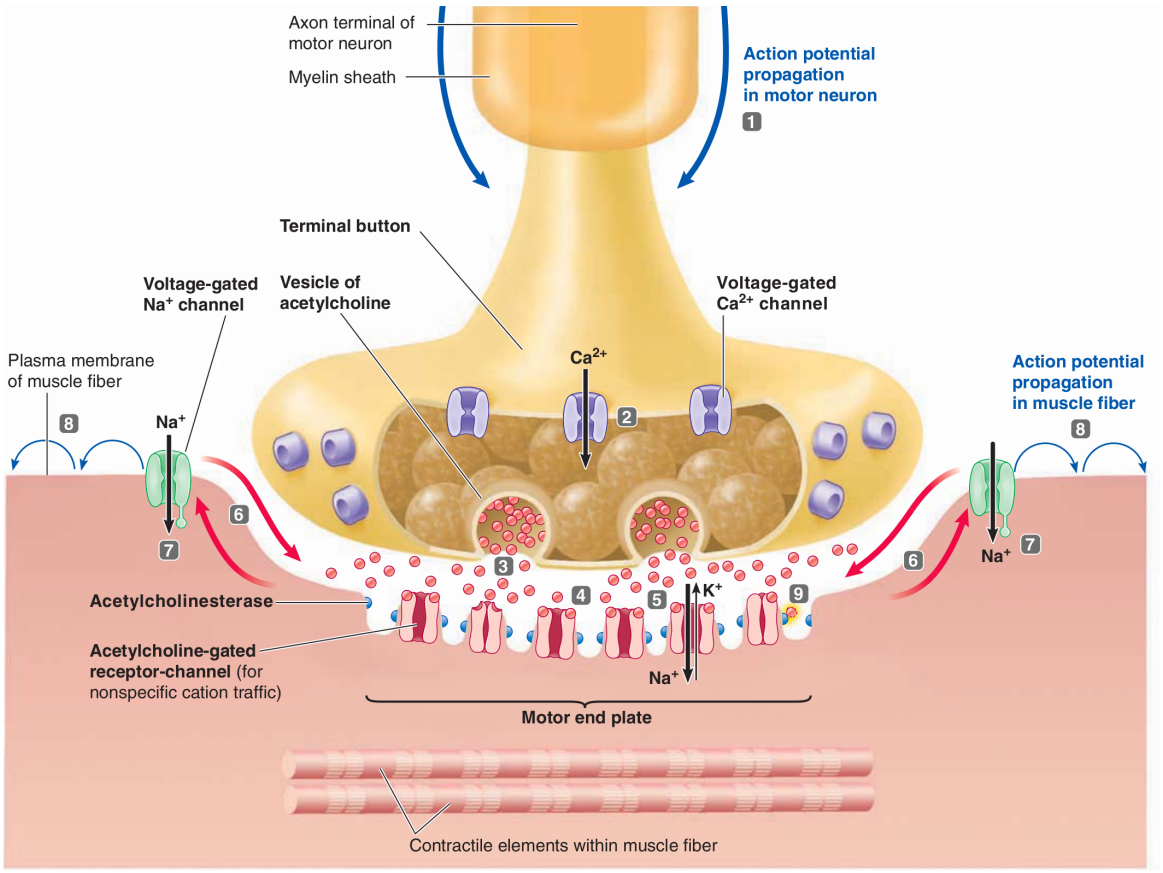

Figure 1-2. The neuromuscular junction.

The sequence of events leading to a muscle action potential proceeds as follows: (*1*) An action potential travels down the axon of a motor neuron, finally reaching the terminal synaptic button. (*2*) Voltage-gated calcium channels of the terminal button open, allowing extracellular calcium to enter the neuron. (*3*) Calcium entry induces acetylcholine-filled vesicles to fuse with the plasma membrane, releasing acetylcholine (ACh) into the synaptic cleft. (*4*) Acetylcholine diffuses across the cleft and binds to the acetylcholine receptor (AChR) of the muscle plasma membrane. (*5*) The AChR opens, allowing cations to flow freely across the membrane and generating a graded electrical depolarization. (*6*) When the region around the cleft becomes sufficiently depolarized, adjacent voltage-gated sodium channels open. (*7* & *8*) Sodium flows into the cell initiating an action potential that propagates along the plasma membrane of the muscle fiber. (*9*) ACh is degraded in the cleft by acetylcholinesterase, and AChRs begin to close.

Reprinted from [30] with publisher's permission.

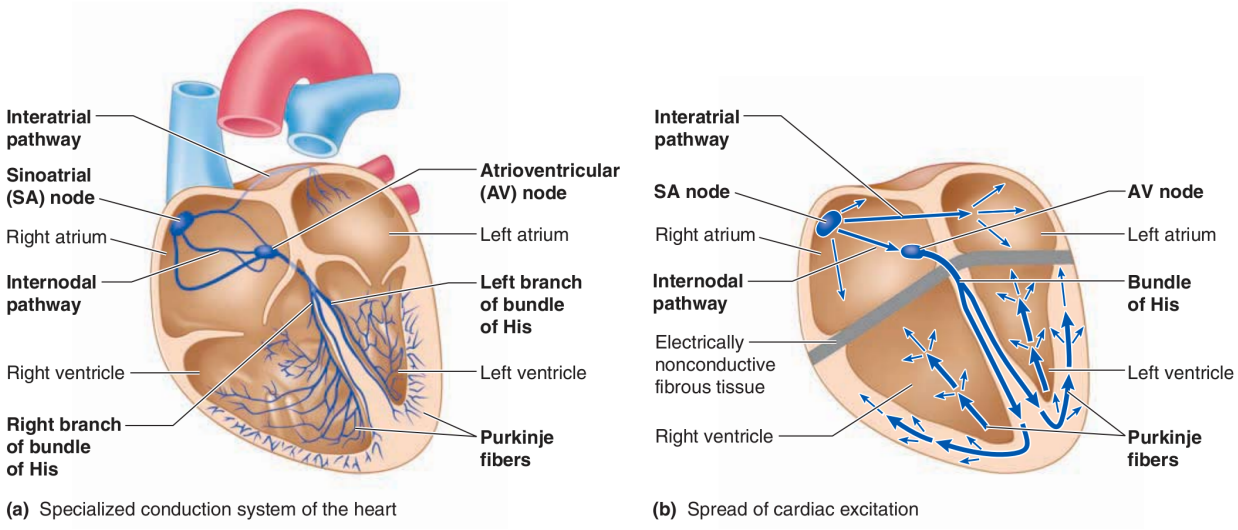

Figure 1-3. The cardiac conduction system.

Cardiac conduction begins at the SA node, the biological pacemaker of the heart, and spreads throughout the atria. The AV node is the only electrical path to the ventricle, since the atria are electrically isolated by a non-conductive fibrous wall. The AV node connects to the Bundle of His, which branches into the right and left bundle branches. The bundle branches give way to the Purkinje fibers which rapidly spread the wave of depolarization throughout the remaining myocardium. Components of the conduction system are bolded.

Reprinted from [30] with publisher's permission.

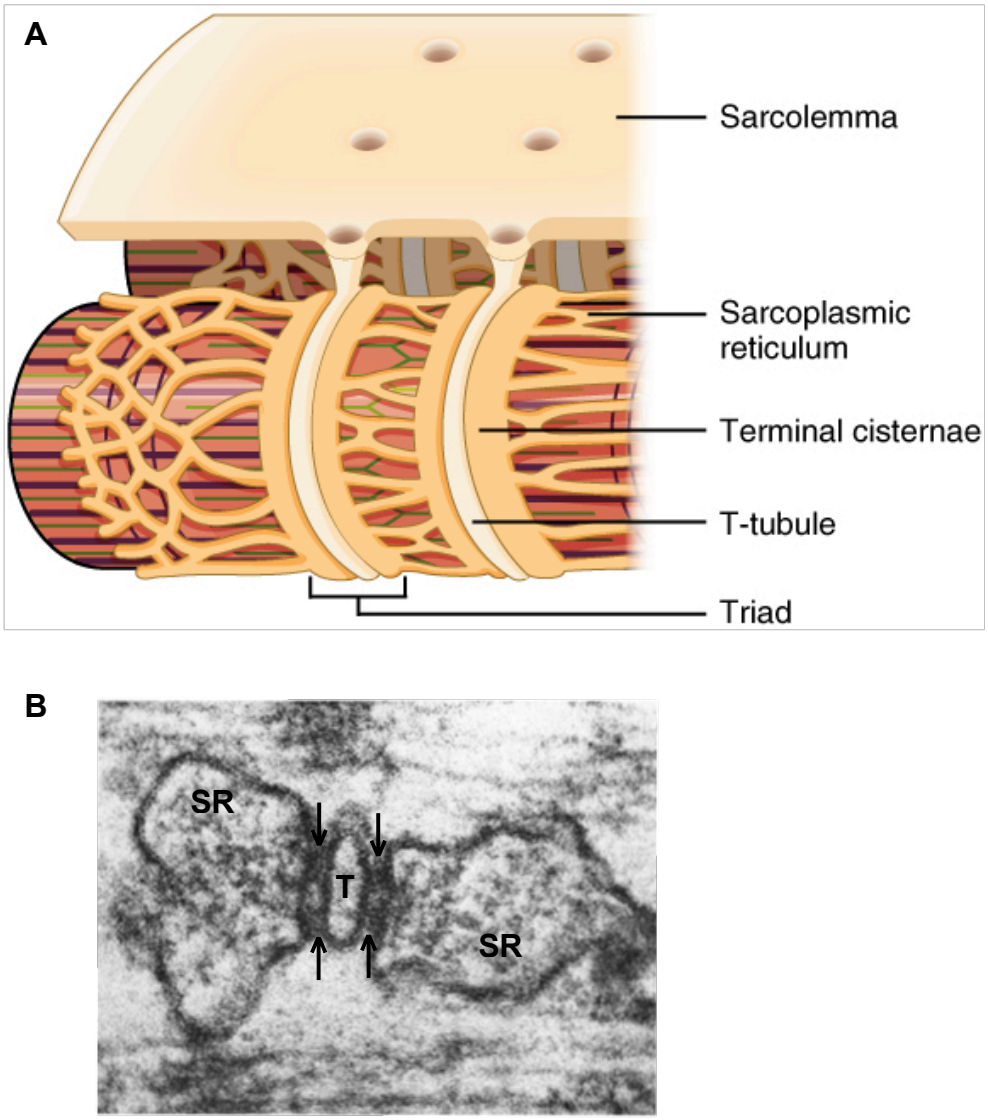

Figure 1-4. Ultrastructure of the skeletal muscle triad.

(*A*) The sarcolemma reaches deep into the muscle interior through invaginations called T-tubules. The terminal cisternae of the sarcoplasmic reticulum meet the T-tubule in synapse-like structures called triads. Triads are found at the intersection on the A- and I-bands, flanking the Z-lines. (*B*) Electron micrograph showing a triad. Calsequestrin can be seen inside the terminal cisternae (SR). Arrows indicate ryanodine receptor "feet" structures. T = T-tubules. (*A*) was created by OpenStax College and used under Creative Commons license agreement 3.0 [272, 273]. (*B*) is reprinted from [79].

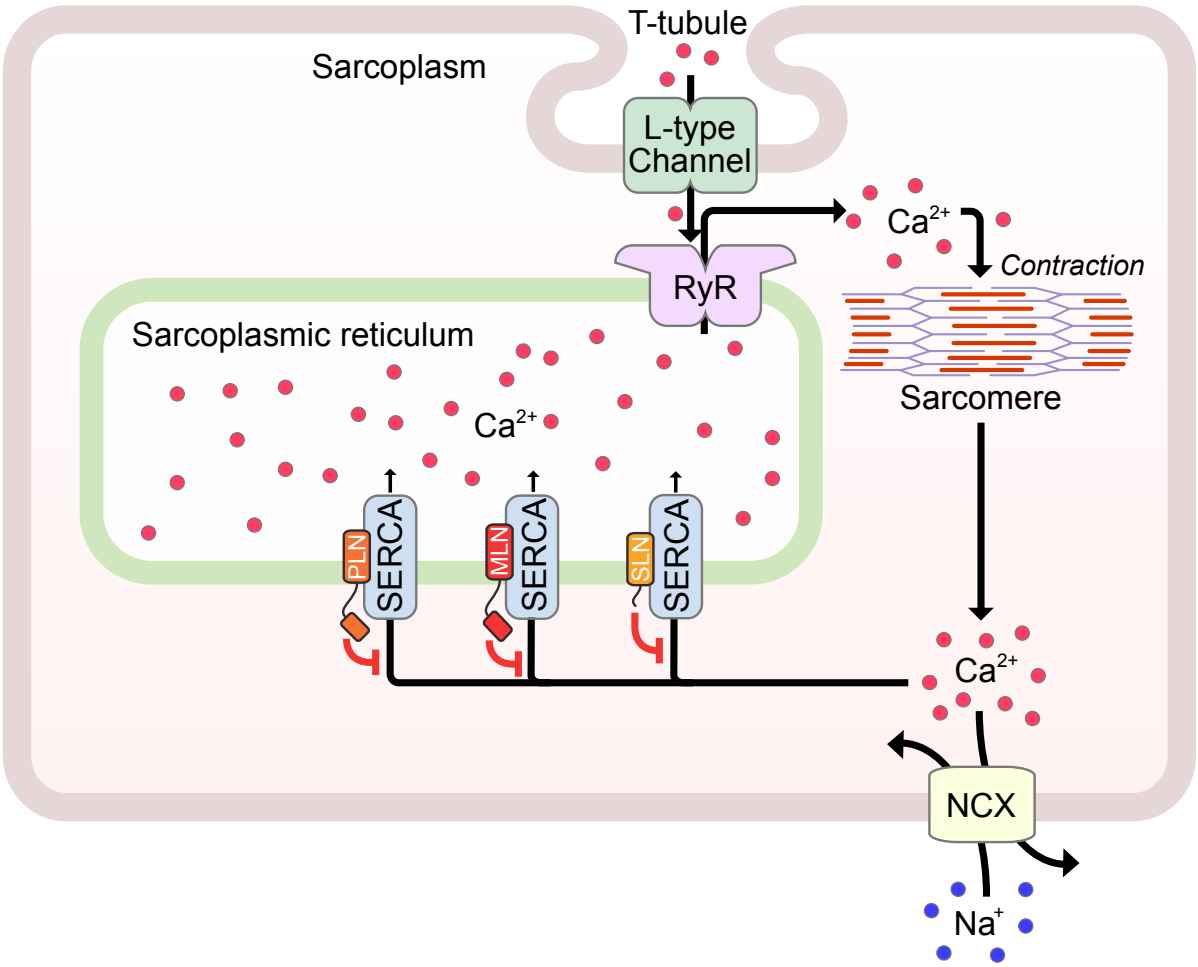

Figure 1-5. Overview of myocyte calcium fluxes.

Excitation of a muscle fiber by an action potential causes extracellular calcium to enter through the L-type channel (also known as the DHPR), which triggers opening of the RyR (in skeletal myocytes, the DHPR/RyR interaction is direct, not calcium mediated). The RyR releases calcium stored in the sarcoplasmic reticulum, causing the sarcomere to contract. Following contraction, calcium is transported into the sarcoplasmic reticulum by SERCA or extruded from the cell by NCX using energy stored in the sodium diffusion gradient.

Original artwork created by José Cabrera; modified by Benjamin Nelson.

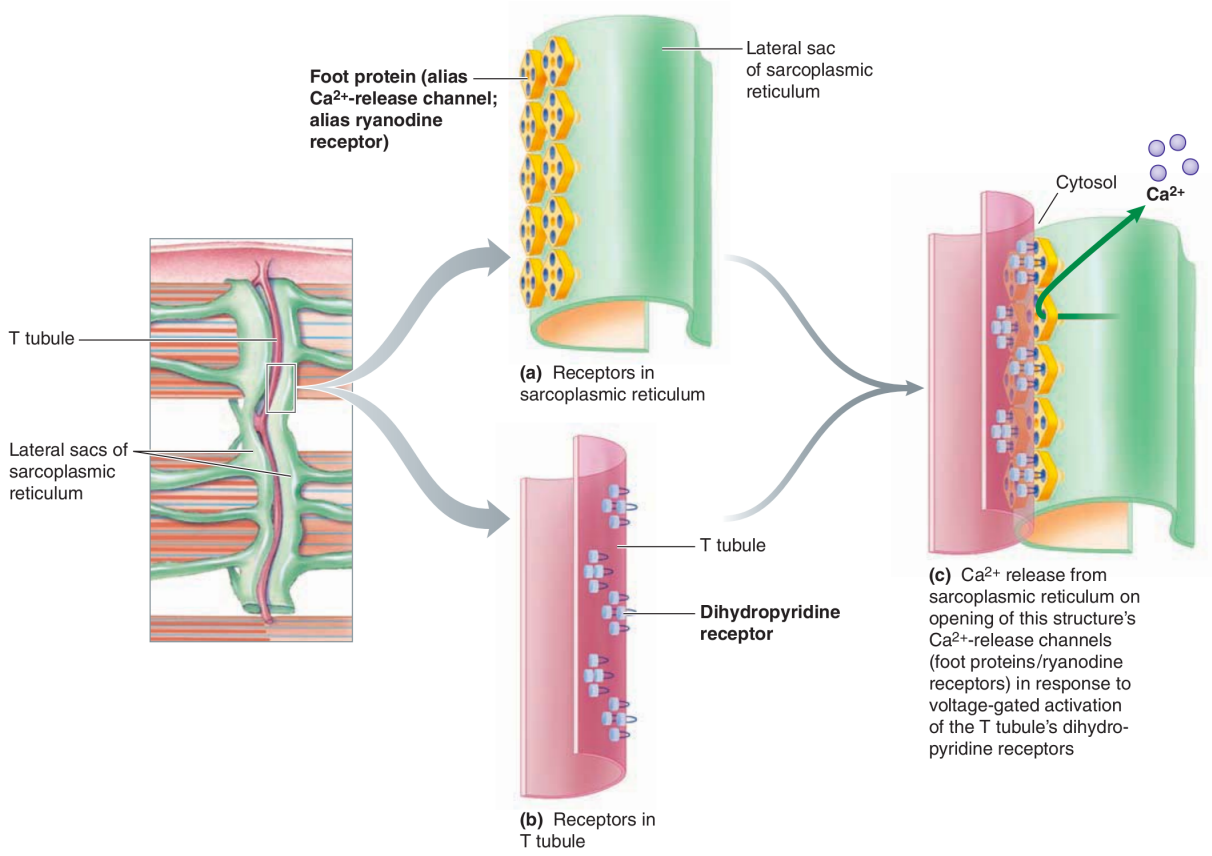

Figure 1-6. Physical linkage of the skeletal muscle triad.

The triad is made up of a pair of closely apposed membranes, the T-tubule and the junctional SR. (*a*) RyRs form homotetrameric calcium release units on the face of the junctional SR. (*b*) DHPRs form "tetrad" structures in the T-tubule. The II-III loop is noted on the individual DHPRs (see section 1.2.3.5 on page 1-15 for the significance of this region). (*c*) The close apposition of the two membranes, brings the DHPR voltage sensors into direct or very nearly direct contact with the RyRs. This arrangement allows for very rapid signaling from the T-tubule and SR.

Reprinted from [30] with publisher's permission.

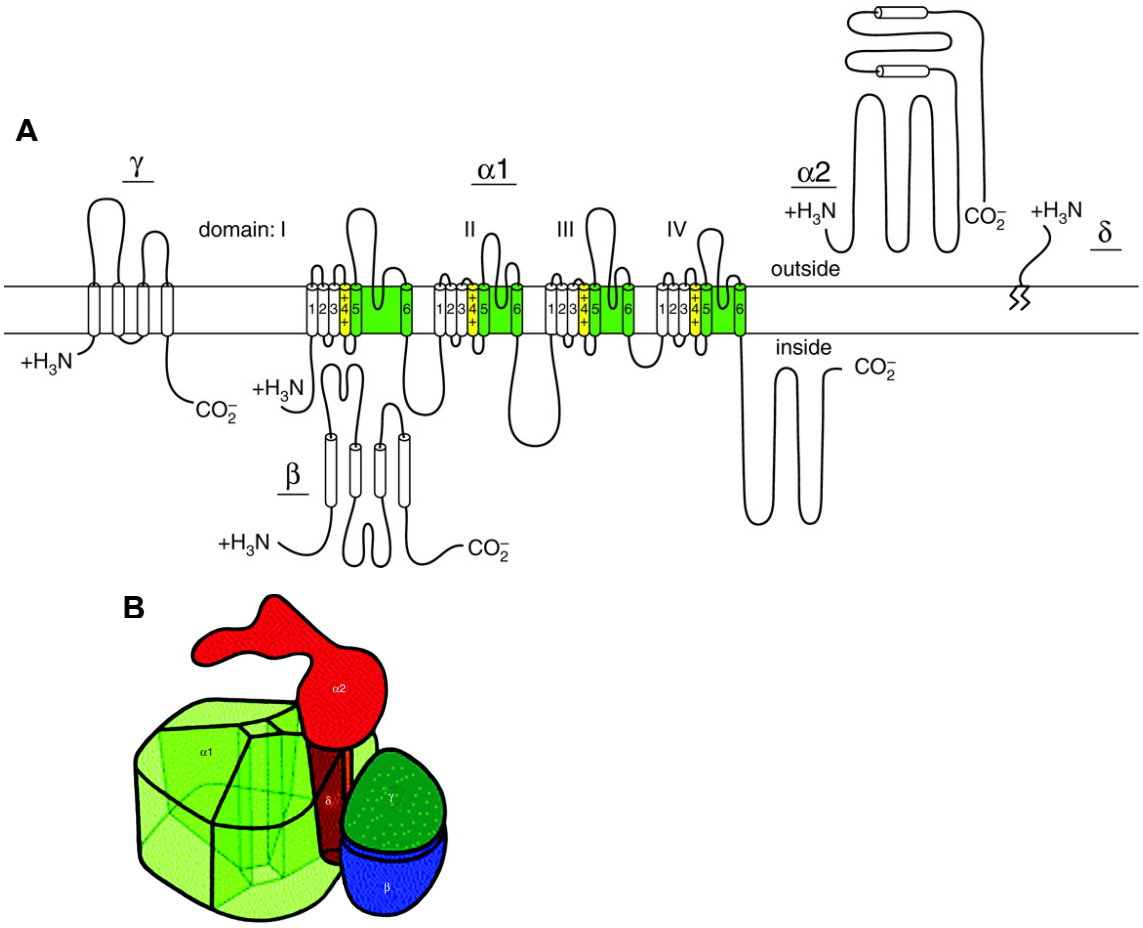

Figure 1-7. Structural topology of the DHPR subunits.

The DHPR is made up of five distinct subunits, α_1, β, γ, α_2, and δ. (*A*) In the α_1 subunit, the fourth transmembrane helix (yellow) in each domain serves as the voltage sensor of the channel. The calcium conducting pore is formed by the coordination of helix five and six (green). The cytosolic loop between transmembrane domains II and III of the skeletal muscle α_{1S} is thought to play a critical role in the skeletal-type ECC mechanism. The α_2 and δ subunits are encoded by the same gene, but are cleaved to produce the two fragments remain linked by a disulfide bond. (*B*) Three-dimensional representation of the DHPR calcium channel. The α_1 subunit forms a calcium selective pore. The β subunit is cytoplasmic and required for ECC. The remaining subunits are not required components for ECC.

Reprinted from [274] with publisher's permission.

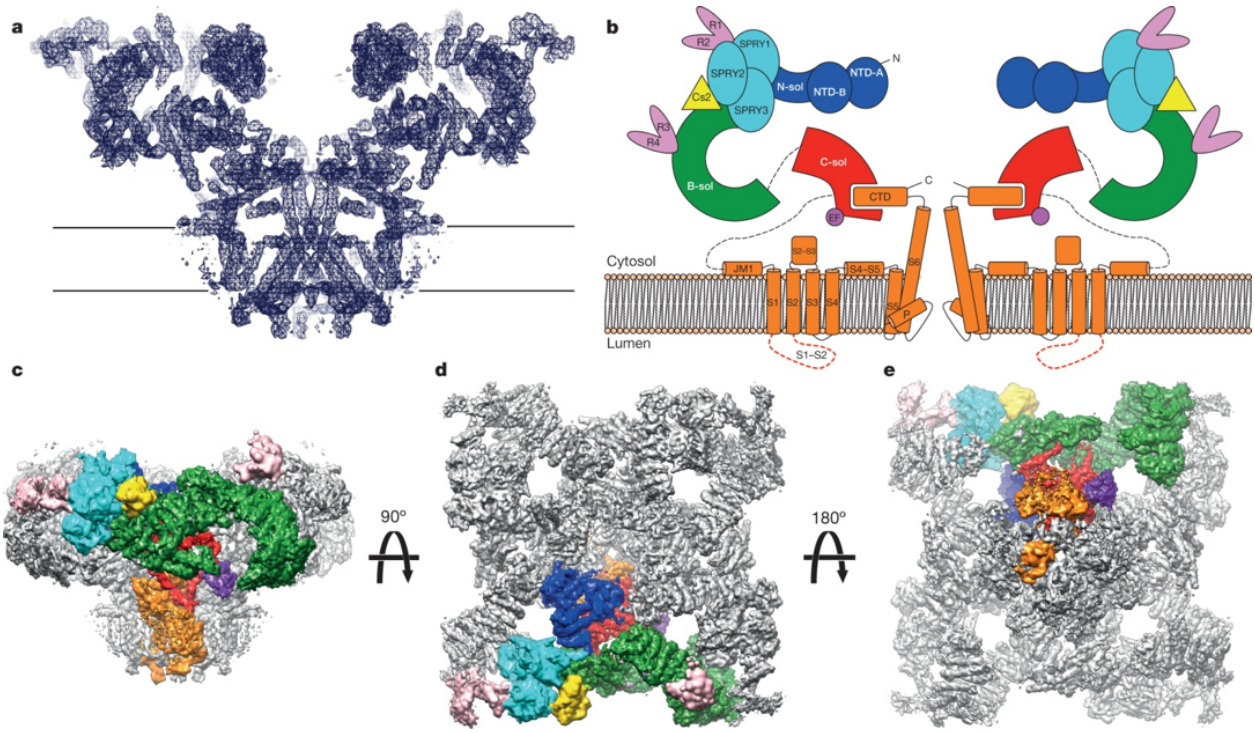

Figure 1-8. Structural organization of the ryanodine receptor.

(*a*) Slice of the electron density of the rabbit skeletal muscle RyR situated in a simulated SR membrane. Cytosol is above, SR lumen is below. (*b*) Color-coded schematic rendering of defined RyR domains; two protomers shown. Color-coding is continued in panels *c*, *d*, and *e*. (*c*) View from the side. (*d*) View from cytosol. (*e*) View from SR lumen.

Reprinted from [275] with publisher's permission.

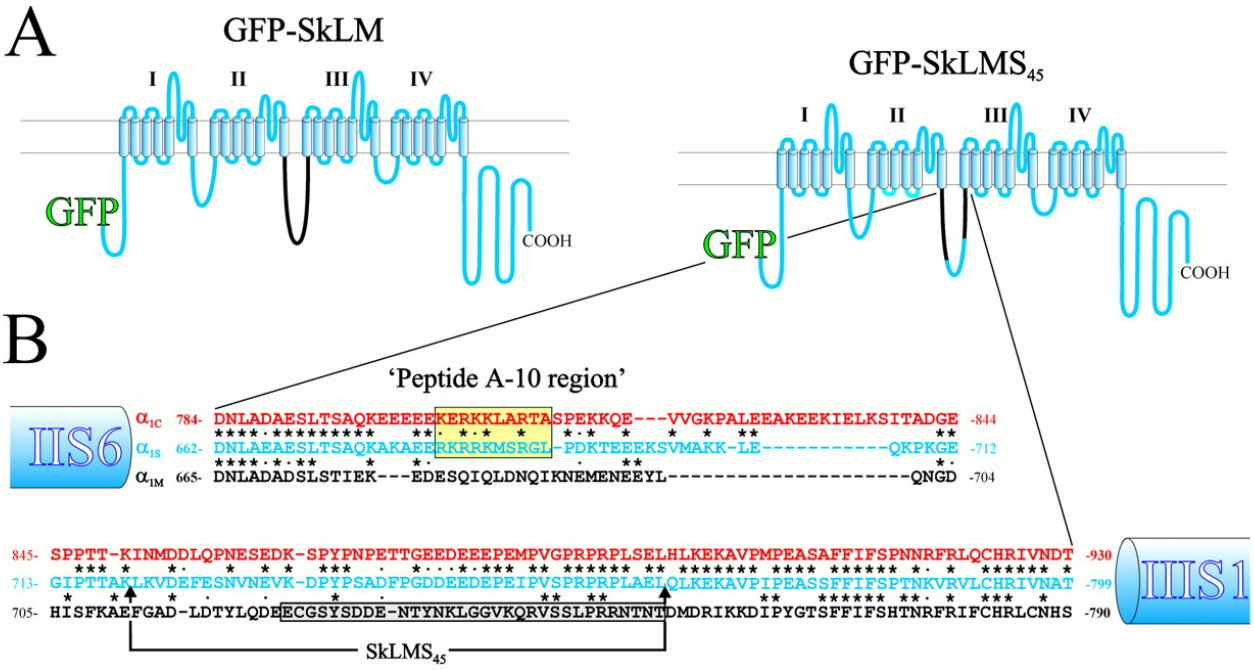

Figure 1-9. Chimeric constructs of the skeletal muscle DHPR α_{1S} subunit.

(*A*) The II-III loop of a GFP fusion protein of the rabbit DHPR α_{1S} subunit was replaced with the II-III loop of a distantly related α_1 subunit (shown in black, also labeled α_{1M}) from *Musca domestica* (house fly). The GFP-SkLM protein does not permit skeletal-type ECC, but insertion of 45 amino acids from the wildtype α_{1S} loop restores coupling. (*B*) Expansion of the II-III loop sequence. The region of α_{1M} boxed in grey was replaced with the sequence of α_{1S} between the arrowheads. Notably, this region does not include the *peptide A-10* region.

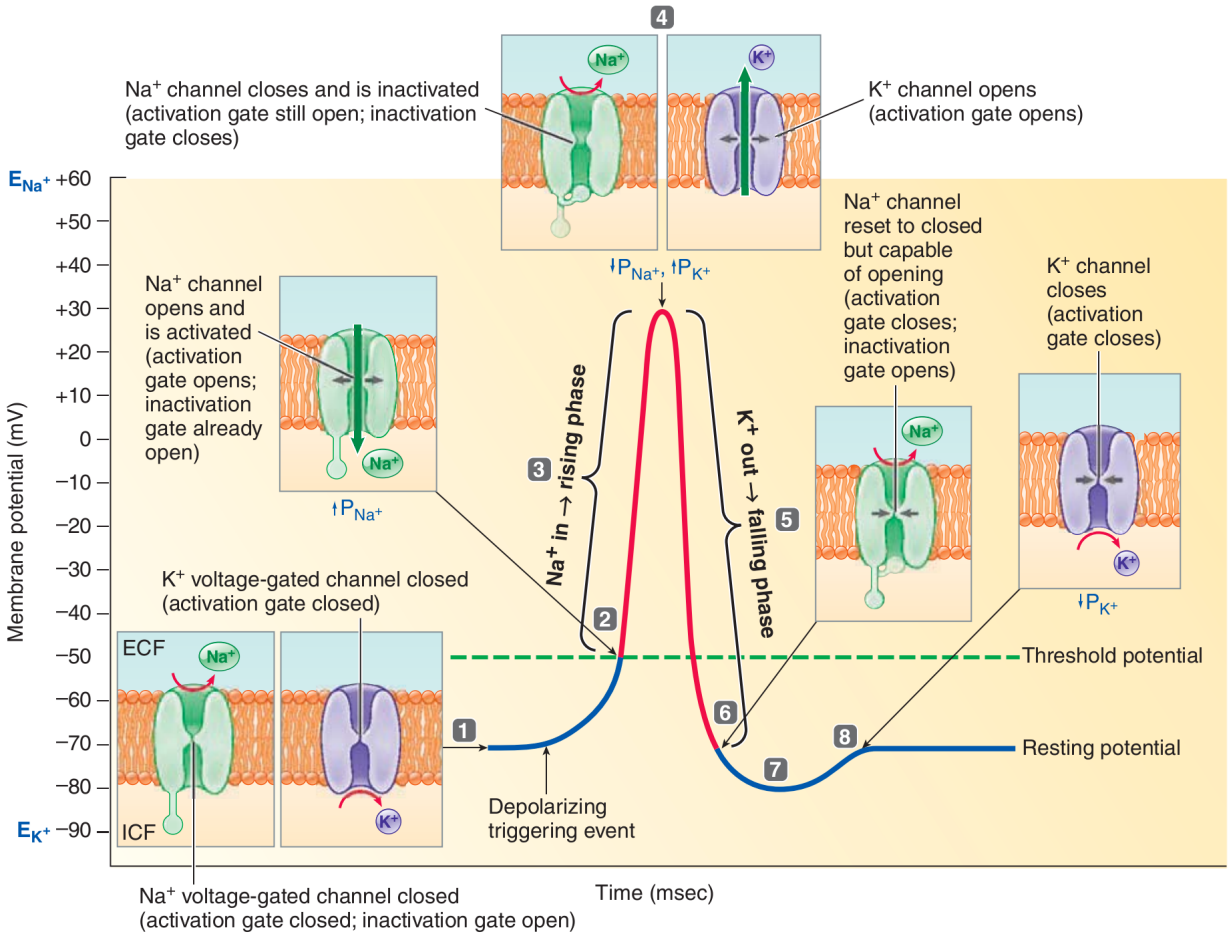

Figure 1-10. Action potential propagation.

Sequence of events during an action potential: (*1*) A depolarizing stimulus raises the local membrane potential. (*2*) When the membrane potential reaches the gating threshold of the voltage-gated sodium channel, the channel opens allowing sodium to flow rapidly into the cell. (*3*) Sodium continues to enter the cell, creating a positive membrane potential. (*4*) Sodium channels are inactivated and close; voltage-gated potassium channels open. (*5*) Potassium escapes from the cell. (*6*) Sodium channels are reset and capable of activation. (*7*) Potassium continues to exit the cell, resulting in hyperpolarization. (*8*) Potassium channels close and are reset. The membrane potential returns to resting state. During a propagating action potential, these steps proceed as a chain reaction down the length of the membrane. ECF = Extracellular Fluid; ICF = Intracellular Fluid.

Reprinted from [30] with publisher's permission.

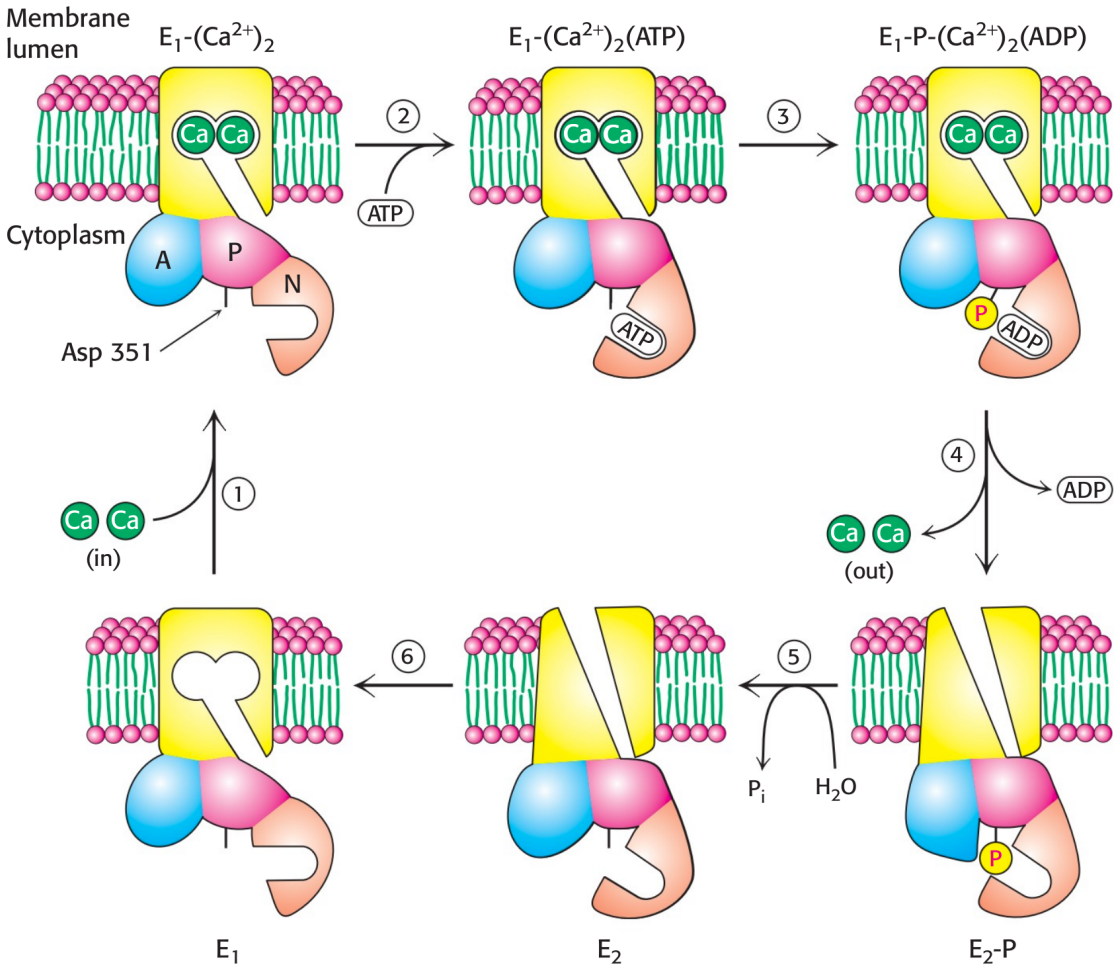

Figure 1-11. SERCA domain architecture and pumping cycle.

The SERCA protein is composed of four domains: actuator (A), phosphorylation (P), nucleotide-binding (N), and membrane (shown in yellow). The pumping action proceeds as follows: (*1*) two calcium ions bind the M domain. (*2*) ATP is bound by the N domain. (*3*) ATP is used to phosphorylate the catalytic aspartic acid residue of the P domain. (*4*) A major conformational shift occurs and ADP is released into the cytosol while the calcium ions are released into the SR lumen. (*5*) The A domain assists in hydrolysis of the phosphorylated aspartate residue and inorganic phosphate is liberated. (*6*) A conformational change occurs to regenerate the high affinity calcium binding sites of the E1 state.

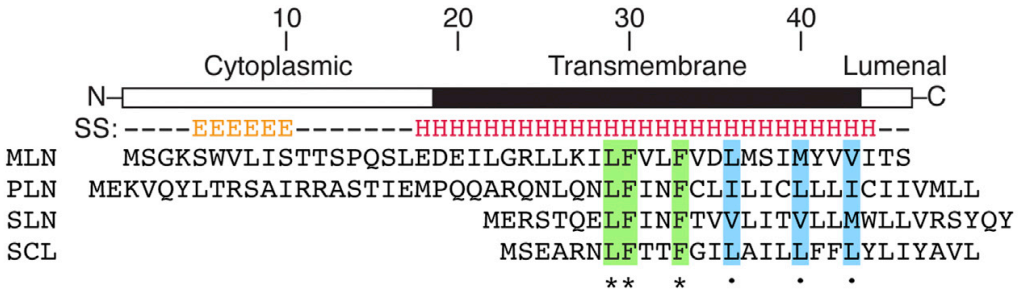

Figure 1-12. Sequence alignment of SERCA inhibitory peptides.

Physiologic inhibitors of SERCA are small transmembrane proteins of the SR. Myoregulin (MLN), phospholamban (PLN), and sarcolipin (SLN) inhibit SERCA in mammals. Recently a distant homolog of these proteins was identified in *Drosophila melanogaster* and named sarcolamban (SCL). All members of this family share the conserved L-F-X-X-F motif.

Reprinted from [197] with publisher's permission.

1.4 TABLES

Table 1-1. Diseases associated with the excitation-contraction coupling machinery.

Disease	Gene(s)	Symptoms	References
Malignant hyperthermia	RYR1 CACNA1S	Muscle contracture and hyperthermia in response to anesthesia.	[73, 127, 128]
Exertional rhabdomyolysis	RYR1 CACNA1S CASQ1	Breakdown of muscle tissue upon exertion, releasing myoglobin and other muscle proteins into the bloodstream.	[132]
Hypokalemic periodic paralysis	CACNA1S	Reversible muscle paralysis with exercise; resolves with rest.	[133, 134]
Catecholaminergic polymorphic ventricular tachycardia	RYR2 CASQ2 TRDN CALM1	Cardiac arrhythmia and possible arrest caused by adrenergic distress.	[135-142]
Arrhythmogenic right ventricular dysplasia, type 2	RYR2	Fatty infiltration of the heart which can lead to arrhythmia and cardiac arrest.	[143, 144]
Brugada syndrome	SCN5A CACNA1C CACNB2 GPD1L KCNE3	Electrical abnormalities including ST-segment elevation and short QT interval, that can result in arrhythmogenic electrical activity and ventricular fibrillation.	[149-151]
Timothy syndrome	CACNA1C	Prolonged QT interval and severe heart malformation. Also notable for non-muscle deformities.	[150-154]

1.5 REFERENCES

1. Abath Neto, O., et al., *Integrative data mining highlights candidate genes for monogenic myopathies.* PLoS One, 2014. **9**(10): p. e110888.

2. Kaplan, J.C. and D. Hamroun, *The 2015 version of the gene table of monogenic neuromuscular disorders (nuclear genome).* Neuromuscul Disord, 2014. **24**(12): p. 1123-53.

3. Piccolino, M., *Animal electricity and the birth of electrophysiology: the legacy of Luigi Galvani.* Brain Res Bull, 1998. **46**(5): p. 381-407.

4. Schwiening, C.J., *A brief historical perspective: Hodgkin and Huxley.* J Physiol, 2012. **590**(Pt 11): p. 2571-5.

5. Miller, D.J., *Sydney Ringer; physiological saline, calcium and the contraction of the heart.* J Physiol, 2004. **555**(Pt 3): p. 585-7.

6. Sandow, A., *Excitation-contraction coupling in muscular response.* Yale J Biol Med, 1952. **25**(3): p. 176-201.

7. Marsh, B.B., *A factor modifying muscle fibre synaeresis.* Nature, 1951. **167**(4261): p. 1065-6.

8. Bendall, J.R., *Effect of the marsh factor on the shortening of muscle fibre models in the presence of adenosine triphosphate.* Nature, 1952. **170**(4338): p. 1058-60.

9. Szent-Gyorgyi, A.G., *The early history of the biochemistry of muscle contraction.* J Gen Physiol, 2004. **123**(6): p. 631-41.

10. Ebashi, S., *A granule-bound relaxation factor in skeletal muscle.* Arch Biochem Biophys, 1958. **76**(2): p. 410-23.

11. Kumagai, H., S. Ebashi, and F. Takeda, *Essential relaxing factor in muscle other than myokinase and creatine phosphokinase.* Nature, 1955. **176**(4473): p. 166.

12. Ebashi, S. and F. Lipmann, *Adenosine Triphosphate-Linked Concentration of Calcium Ions in a Particulate Fraction of Rabbit Muscle.* J Cell Biol, 1962. **14**(3): p. 389-400.

13. MacLennan, D.H., et al., *Membrane formation by the adenosine triphosphatase of sarcoplasmic reticulum.* J Biol Chem, 1971. **246**(8): p. 2702-10.

14. MacLennan, D.H., *Isolation of proteins of the sarcoplasmic reticulum.* Methods Enzymol, 1974. **32**: p. 291-302.

15. MacLennan, D.H. and P.C. Holland, *Calcium transport in sarcoplasmic reticulum.* Annu Rev Biophys Bioeng, 1975. **4**(00): p. 377-404.

16. MacLennan, D.H., et al., *Amino-acid sequence of a Ca2+ + Mg2+-dependent ATPase from rabbit muscle sarcoplasmic reticulum, deduced from its complementary DNA sequence.* Nature, 1985. **316**(6030): p. 696-700.

17. Brandl, C.J., et al., *Two Ca2+ ATPase genes: homologies and mechanistic implications of deduced amino acid sequences.* Cell, 1986. **44**(4): p. 597-607.

18. Schneider, M.F. and W.K. Chandler, *Voltage dependent charge movement of skeletal muscle: a possible step in excitation-contraction coupling.* Nature, 1973. **242**(5395): p. 244-6.

19. Beam, K.G., C.M. Knudson, and J.A. Powell, *A lethal mutation in mice eliminates the slow calcium current in skeletal muscle cells.* Nature, 1986. **320**(6058): p. 168-70.

20. Rios, E. and G. Brum, *Involvement of dihydropyridine receptors in excitation-contraction coupling in skeletal muscle.* Nature, 1987. **325**(6106): p. 717-20.

21. Tanabe, T., et al., *Restoration of excitation-contraction coupling and slow calcium current in dysgenic muscle by dihydropyridine receptor complementary DNA.* Nature, 1988. **336**(6195): p. 134-9.

22. Fleischer, S., *Personal recollections on the discovery of the ryanodine receptors of muscle.* Biochem Biophys Res Commun, 2008. **369**(1): p. 195-207.

23. Fleischer, S., et al., *Localization of Ca2+ release channels with ryanodine in junctional terminal cisternae of sarcoplasmic reticulum of fast skeletal muscle.* Proc Natl Acad Sci U S A, 1985. **82**(21): p. 7256-9.

24. Inui, M., A. Saito, and S. Fleischer, *Purification of the ryanodine receptor and identity with feet structures of junctional terminal cisternae of sarcoplasmic reticulum from fast skeletal muscle.* J Biol Chem, 1987. **262**(4): p. 1740-7.

25. Hymel, L., et al., *Purified ryanodine receptor of skeletal muscle sarcoplasmic reticulum forms Ca2+-activated oligomeric Ca2+ channels in planar bilayers.* Proc Natl Acad Sci U S A, 1988. **85**(2): p. 441-5.

26. Takeshima, H., et al., *Primary structure and expression from complementary DNA of skeletal muscle ryanodine receptor.* Nature, 1989. **339**(6224): p. 439-45.

27. Otsu, K., et al., *Molecular cloning of cDNA encoding the Ca2+ release channel (ryanodine receptor) of rabbit cardiac muscle sarcoplasmic reticulum.* J Biol Chem, 1990. **265**(23): p. 13472-83.

28. Suda, N., et al., *Ca2+-induced Ca2+ release in Chinese hamster ovary (CHO) cells co-expressing dihydropyridine and ryanodine receptors.* J Gen Physiol, 1997. **109**(5): p. 619-31.

29. Boron, W.F. and E.L. Boulpaep, *Medical physiology : a cellular and molecular approach*. 2nd ed. 2009, Philadelphia, PA: Saunders/Elsevier. xii, 1337 p.

30. Sherwood, L. and Cengage Learning (Firm), *Human physiology : from cells to systems*. 7th ed. 2010, Australia ; United States: Brooks/Cole, Cengage Learning.

31. Moore, K.L., A.F. Dalley, and A.M.R. Agur, *Clinically oriented anatomy*. 6th ed. 2010, Philadelphia: Wolters Kluwer/Lippincott Williams & Wilkins. xxix, 1134 p.

32. Rebbeck, R.T., et al., *Skeletal muscle excitation-contraction coupling: who are the dancing partners?* Int J Biochem Cell Biol, 2014. **48**: p. 28-38.

33. Beam, K.G. and R.A. Bannister, *Looking for answers to EC coupling's persistent questions.* J Gen Physiol, 2010. **136**(1): p. 7-12.

34. Dibb, K.M., et al., *A functional role for transverse (t-) tubules in the atria.* J Mol Cell Cardiol, 2013. **58**: p. 84-91.

35. Dibb, K.M., et al., *Characterization of an extensive transverse tubular network in sheep atrial myocytes and its depletion in heart failure.* Circ Heart Fail, 2009. **2**(5): p. 482-9.

36. Brette, F. and C. Orchard, *T-tubule function in mammalian cardiac myocytes.* Circ Res, 2003. **92**(11): p. 1182-92.

37. Smyrnias, I., et al., *Comparison of the T-tubule system in adult rat ventricular and atrial myocytes, and its role in excitation-contraction coupling and inotropic stimulation.* Cell Calcium, 2010. **47**(3): p. 210-23.

38. Haddock, P.S., et al., *Subcellular [Ca2+]i gradients during excitation-contraction coupling in newborn rabbit ventricular myocytes.* Circ Res, 1999. **85**(5): p. 415-27.

39. Scriven, D.R., P. Dan, and E.D. Moore, *Distribution of proteins implicated in excitation-contraction coupling in rat ventricular myocytes.* Biophys J, 2000. **79**(5): p. 2682-91.

40. Carl, S.L., et al., *Immunolocalization of sarcolemmal dihydropyridine receptor and sarcoplasmic reticular triadin and ryanodine receptor in rabbit ventricle and atrium.* J Cell Biol, 1995. **129**(3): p. 673-82.

41. Franzini-Armstrong, C., *Simultaneous maturation of transverse tubules and sarcoplasmic reticulum during muscle differentiation in the mouse.* Dev Biol, 1991. **146**(2): p. 353-63.

42. DiFranco, M., et al., *DNA transfection of mammalian skeletal muscles using in vivo electroporation.* J Vis Exp, 2009(32).

43. Inui, M., et al., *Characterization of junctional and longitudinal sarcoplasmic reticulum from heart muscle.* J Biol Chem, 1988. **263**(22): p. 10843-50.

44. Franzini-Armstrong, C. and A.O. Jorgensen, *Structure and development of E-C coupling units in skeletal muscle.* Annu Rev Physiol, 1994. **56**: p. 509-34.

45. Scriven, D.R., P. Asghari, and E.D. Moore, *Microarchitecture of the dyad.* Cardiovasc Res, 2013. **98**(2): p. 169-76.

46. Ito, K., et al., *Deficiency of triad junction and contraction in mutant skeletal muscle lacking junctophilin type 1.* J Cell Biol, 2001. **154**(5): p. 1059-67.

47. Buck, E.D., et al., *Dyspedic mouse skeletal muscle expresses major elements of the triadic junction but lacks detectable ryanodine receptor protein and function.* J Biol Chem, 1997. **272**(11): p. 7360-7.

48. Felder, E., et al., *Morphology and molecular composition of sarcoplasmic reticulum surface junctions in the absence of DHPR and RyR in mouse skeletal muscle.* Biophys J, 2002. **82**(6): p. 3144-9.

49. Catterall, W.A., M.J. Seagar, and M. Takahashi, *Molecular properties of dihydropyridine-sensitive calcium channels in skeletal muscle.* J Biol Chem, 1988. **263**(8): p. 3535-8.

50. Catterall, W.A., *Structure and regulation of voltage-gated Ca2+ channels.* Annu Rev Cell Dev Biol, 2000. **16**: p. 521-55.

51. Brillantes, A.M., S. Bezprozvannaya, and A.R. Marks, *Developmental and tissue-specific regulation of rabbit skeletal and cardiac muscle calcium channels involved in excitation-contraction coupling.* Circ Res, 1994. **75**(3): p. 503-10.

52. Lee, C.S., et al., *Ca(2+) permeation and/or binding to CaV1.1 fine-tunes skeletal muscle Ca(2+) signaling to sustain muscle function.* Skelet Muscle, 2015. **5**: p. 4.

53. Schredelseker, J., et al., *Non-Ca2+-conducting Ca2+ channels in fish skeletal muscle excitation-contraction coupling.* Proc Natl Acad Sci U S A, 2010. **107**(12): p. 5658-63.

54. Gregg, R.G., et al., *Absence of the beta subunit (cchb1) of the skeletal muscle dihydropyridine receptor alters expression of the alpha 1 subunit and eliminates excitation-contraction coupling.* Proc Natl Acad Sci U S A, 1996. **93**(24): p. 13961-6.

55. Strube, C., et al., *Reduced Ca2+ current, charge movement, and absence of Ca2+ transients in skeletal muscle deficient in dihydropyridine receptor beta 1 subunit.* Biophys J, 1996. **71**(5): p. 2531-43.

56. Richards, M.W., A.J. Butcher, and A.C. Dolphin, *Ca2+ channel beta-subunits: structural insights AID our understanding.* Trends Pharmacol Sci, 2004. **25**(12): p. 626-32.

57. Acosta, L., et al., *Regional expression of L-type calcium channel subunits during cardiac development.* Dev Dyn, 2004. **230**(1): p. 131-6.

58. Flucher, B.E., et al., *The role of auxiliary dihydropyridine receptor subunits in muscle.* J Muscle Res Cell Motil, 2005. **26**(1): p. 1-6.

59. Pai, A.C., *Developmental Genetics of a Lethal Mutation, Muscular Dysgenesis (Mdg), in the Mouse. Ii. Developmental Analysis.* Dev Biol, 1965. **11**: p. 93-109.

60. Pai, A.C., *Developmental Genetics of a Lethal Mutation, Muscular Dysgenesis (Mdg), in the Mouse. I. Genetic Analysis and Gross Morphology.* Dev Biol, 1965. **11**: p. 82-92.

61. Gluecksohn-Waelsch, S., *Lethal Genes and Analysis of Differentiation.* Science, 1963. **142**(3597): p. 1269-76.

62. Klaus, M.M., et al., *Evidence for dysfunction in the regulation of cytosolic Ca2+ in excitation-contraction uncoupled dysgenic muscle.* Dev Biol, 1983. **99**(1): p. 152-65.

63. Knudson, C.M., et al., *Specific absence of the alpha 1 subunit of the dihydropyridine receptor in mice with muscular dysgenesis.* J Biol Chem, 1989. **264**(3): p. 1345-8.

64. Chaudhari, N., *A single nucleotide deletion in the skeletal muscle-specific calcium channel transcript of muscular dysgenesis (mdg) mice.* J Biol Chem, 1992. **267**(36): p. 25636-9.

65. Takekura, H., et al., *Restoration of junctional tetrads in dysgenic myotubes by dihydropyridine receptor cDNA.* Biophys J, 1994. **67**(2): p. 793-803.

66. Weissgerber, P., et al., *Reduced cardiac L-type Ca2+ current in Ca(V)beta2-/- embryos impairs cardiac development and contraction with secondary defects in vascular maturation.* Circ Res, 2006. **99**(7): p. 749-57.

67. Blitz, E., et al., *Bone ridge patterning during musculoskeletal assembly is mediated through SCX regulation of Bmp4 at the tendon-skeleton junction.* Dev Cell, 2009. **17**(6): p. 861-73.

68. Sharir, A., et al., *Muscle force regulates bone shaping for optimal load-bearing capacity during embryogenesis.* Development, 2011. **138**(15): p. 3247-59.

69. Bournaud, R. and A. Mallart, *An electrophysiological study of skeletal muscle fibres in the 'muscular dysgenesis' mutation of the mouse.* Pflugers Arch, 1987. **409**(4-5): p. 468-76.

70. Rieger, F., J.A. Powell, and M. Pincon-Raymond, *Extensive nerve overgrowth and paucity of the tailed asymmetric form (16 S) of acetylcholinesterase in the developing skeletal neuromuscular system of the dysgenic (mdg/mdg) mouse.* Dev Biol, 1984. **101**(1): p. 181-91.

71. Chen, F., et al., *Neuromuscular synaptic patterning requires the function of skeletal muscle dihydropyridine receptors.* Nat Neurosci, 2011. **14**(5): p. 570-7.

72. Powell, J.A., et al., *Distribution and quantification of ACh receptors and innervation in diaphragm muscle of normal and mdg mouse embryos.* Dev Biol, 1984. **101**(1): p. 168-80.

73. Lanner, J.T., et al., *Ryanodine receptors: structure, expression, molecular details, and function in calcium release.* Cold Spring Harb Perspect Biol, 2010. **2**(11): p. a003996.

74. Rousseau, E., J.S. Smith, and G. Meissner, *Ryanodine modifies conductance and gating behavior of single Ca2+ release channel.* Am J Physiol, 1987. **253**(3 Pt 1): p. C364-8.

75. Zorzato, F., et al., *Molecular cloning of cDNA encoding human and rabbit forms of the Ca2+ release channel (ryanodine receptor) of skeletal muscle sarcoplasmic reticulum.* J Biol Chem, 1990. **265**(4): p. 2244-56.

76. Lai, F.A., et al., *Purification and reconstitution of the calcium release channel from skeletal muscle.* Nature, 1988. **331**(6154): p. 315-9.

77. Anderson, K., et al., *Structural and functional characterization of the purified cardiac ryanodine receptor-Ca2+ release channel complex.* J Biol Chem, 1989. **264**(2): p. 1329-35.

78. Inui, M., A. Saito, and S. Fleischer, *Isolation of the ryanodine receptor from cardiac sarcoplasmic reticulum and identity with the feet structures.* J Biol Chem, 1987. **262**(32): p. 15637-42.

79. Franzini-Armstrong, C., *STUDIES OF THE TRIAD : I. Structure of the Junction in Frog Twitch Fibers.* J Cell Biol, 1970. **47**(2): p. 488-99.

80. Takeshima, H., et al., *Excitation-contraction uncoupling and muscular degeneration in mice lacking functional skeletal muscle ryanodine-receptor gene.* Nature, 1994. **369**(6481): p. 556-9.

81. Takeshima, H., et al., *Embryonic lethality and abnormal cardiac myocytes in mice lacking ryanodine receptor type 2.* EMBO J, 1998. **17**(12): p. 3309-16.

82. Lu, X., L. Xu, and G. Meissner, *Activation of the skeletal muscle calcium release channel by a cytoplasmic loop of the dihydropyridine receptor.* J Biol Chem, 1994. **269**(9): p. 6511-6.

83. Fabiato, A., *Calcium-induced release of calcium from the cardiac sarcoplasmic reticulum.* Am J Physiol, 1983. **245**(1): p. C1-14.

84. Meissner, G., *Adenine nucleotide stimulation of Ca2+-induced Ca2+ release in sarcoplasmic reticulum.* J Biol Chem, 1984. **259**(4): p. 2365-74.

85. Ikemoto, N., B. Antoniu, and L.G. Meszaros, *Rapid flow chemical quench studies of calcium release from isolated sarcoplasmic reticulum.* J Biol Chem, 1985. **260**(26): p. 14096-100.

86. Mosbah, A., et al., *A new fold in the scorpion toxin family, associated with an activity on a ryanodine-sensitive calcium channel.* Proteins, 2000. **40**(3): p. 436-42.

87. Zorzato, F., et al., *Chlorocresol: an activator of ryanodine receptor-mediated Ca2+ release.* Mol Pharmacol, 1993. **44**(6): p. 1192-201.

88. Marty, I., et al., *Biochemical evidence for a complex involving dihydropyridine receptor and ryanodine receptor in triad junctions of skeletal muscle.* Proc Natl Acad Sci U S A, 1994. **91**(6): p. 2270-4.

89. Paolini, C., et al., *Evidence for conformational coupling between two calcium channels.* Proc Natl Acad Sci U S A, 2004. **101**(34): p. 12748-52.

90. Flucher, B.E. and C. Franzini-Armstrong, *Formation of junctions involved in excitation-contraction coupling in skeletal and cardiac muscle.* Proc Natl Acad Sci U S A, 1996. **93**(15): p. 8101-6.

91. Franzini-Armstrong, C., M. Pincon-Raymond, and F. Rieger, *Muscle fibers from dysgenic mouse in vivo lack a surface component of peripheral couplings.* Dev Biol, 1991. **146**(2): p. 364-76.

92. Nakai, J., et al., *Enhanced dihydropyridine receptor channel activity in the presence of ryanodine receptor.* Nature, 1996. **380**(6569): p. 72-5.

93. Sheridan, D.C., et al., *Bidirectional signaling between calcium channels of skeletal muscle requires multiple direct and indirect interactions.* Proc Natl Acad Sci U S A, 2006. **103**(52): p. 19760-5.

94. Avila, G., et al., *Ca2+ release through ryanodine receptors regulates skeletal muscle L-type Ca2+ channel expression.* J Biol Chem, 2001. **276**(21): p. 17732-8.

95. Lee, E.H., et al., *Conformational coupling of DHPR and RyR1 in skeletal myotubes is influenced by long-range allosterism: evidence for a negative regulatory module.* Am J Physiol Cell Physiol, 2004. **286**(1): p. C179-89.

96. Grabner, M. and A. Dayal, *Crosstalk via the Sarcoplasmic Gap: The DHPR-RyR Interaction.* Curr Top Membr, 2010. **66**: p. 115-38.

97. Lorenzon, N.M. and K.G. Beam, *Accessibility of targeted DHPR sites to streptavidin and functional effects of binding on EC coupling.* J Gen Physiol, 2007. **130**(4): p. 379-88.

98. Tanabe, T., et al., *Regions of the skeletal muscle dihydropyridine receptor critical for excitation-contraction coupling.* Nature, 1990. **346**(6284): p. 567-9.

99. Bannister, R.A., et al., *Effects of inserting fluorescent proteins into the alpha1S II-III loop: insights into excitation-contraction coupling.* J Gen Physiol, 2009. **134**(1): p. 35-51.

100. Grabner, M., et al., *The II-III loop of the skeletal muscle dihydropyridine receptor is responsible for the Bi-directional coupling with the ryanodine receptor.* J Biol Chem, 1999. **274**(31): p. 21913-9.

101. Lu, X., L. Xu, and G. Meissner, *Phosphorylation of dihydropyridine receptor II-III loop peptide regulates skeletal muscle calcium release channel function. Evidence for an essential role of the beta-OH group of Ser687.* J Biol Chem, 1995. **270**(31): p. 18459-64.

102. El-Hayek, R., et al., *Identification of calcium release-triggering and blocking regions of the II-III loop of the skeletal muscle dihydropyridine receptor.* J Biol Chem, 1995. **270**(38): p. 22116-8.

103. El-Hayek, R. and N. Ikemoto, *Identification of the minimum essential region in the II-III loop of the dihydropyridine receptor alpha 1 subunit required for activation of skeletal muscle-type excitation-contraction coupling.* Biochemistry, 1998. **37**(19): p. 7015-20.

104. Dulhunty, A.F., et al., *Activation and inhibition of skeletal RyR channels by a part of the skeletal DHPR II-III loop: effects of DHPR Ser687 and FKBP12.* Biophys J, 1999. **77**(1): p. 189-203.

105. Casarotto, M.G., et al., *A structural requirement for activation of skeletal ryanodine receptors by peptides of the dihydropyridine receptor II-III loop.* J Biol Chem, 2000. **275**(16): p. 11631-7.

106. Altafaj, X., et al., *Maurocalcine interacts with the cardiac ryanodine receptor without inducing channel modification.* Biochem J, 2007. **406**(2): p. 309-15.

107. Esteve, E., et al., *Critical amino acid residues determine the binding affinity and the Ca2+ release efficacy of maurocalcine in skeletal muscle cells.* J Biol Chem, 2003. **278**(39): p. 37822-31.

108. Szappanos, H., et al., *Differential effects of maurocalcine on Ca2+ release events and depolarization-induced Ca2+ release in rat skeletal muscle.* J Physiol, 2005. **565**(Pt 3): p. 843-53.

109. Fajloun, Z., et al., *Chemical synthesis and characterization of maurocalcine, a scorpion toxin that activates Ca(2+) release channel/ryanodine receptors.* FEBS Lett, 2000. **469**(2-3): p. 179-85.

110. Lukacs, B., et al., *Charged surface area of maurocalcine determines its interaction with the skeletal ryanodine receptor.* Biophys J, 2008. **95**(7): p. 3497-509.

111. Kugler, G., et al., *Structural requirements of the dihydropyridine receptor alpha1S II-III loop for skeletal-type excitation-contraction coupling.* J Biol Chem, 2004. **279**(6): p. 4721-8.

112. Proenza, C., C.M. Wilkens, and K.G. Beam, *Excitation-contraction coupling is not affected by scrambled sequence in residues 681-690 of the dihydropyridine receptor II-III loop.* J Biol Chem, 2000. **275**(39): p. 29935-7.

113. Nakai, J., et al., *Functional nonequality of the cardiac and skeletal ryanodine receptors.* Proc Natl Acad Sci U S A, 1997. **94**(3): p. 1019-22.

114. Nakai, J., et al., *Two regions of the ryanodine receptor involved in coupling with L-type Ca2+ channels.* J Biol Chem, 1998. **273**(22): p. 13403-6.

115. Yamazawa, T., et al., *A region of the ryanodine receptor critical for excitation-contraction coupling in skeletal muscle.* J Biol Chem, 1997. **272**(13): p. 8161-4.

116. Perez, C.F., et al., *RyR1/RyR3 chimeras reveal that multiple domains of RyR1 are involved in skeletal-type E-C coupling.* Biophys J, 2003. **84**(4): p. 2655-63.

117. Perez, C.F., S. Mukherjee, and P.D. Allen, *Amino acids 1-1,680 of ryanodine receptor type 1 hold critical determinants of skeletal type for excitation-contraction coupling. Role of divergence domain D2.* J Biol Chem, 2003. **278**(41): p. 39644-52.

118. Leong, P. and D.H. MacLennan, *A 37-amino acid sequence in the skeletal muscle ryanodine receptor interacts with the cytoplasmic loop between domains II and III in the skeletal muscle dihydropyridine receptor.* J Biol Chem, 1998. **273**(14): p. 7791-4.

119. Leong, P. and D.H. MacLennan, *The cytoplasmic loops between domains II and III and domains III and IV in the skeletal muscle dihydropyridine receptor bind to a contiguous site in the skeletal muscle ryanodine receptor.* J Biol Chem, 1998. **273**(45): p. 29958-64.

120. Monnier, N., et al., *Malignant-hyperthermia susceptibility is associated with a mutation of the alpha 1-subunit of the human dihydropyridine-sensitive L-type voltage-dependent calcium-channel receptor in skeletal muscle.* Am J Hum Genet, 1997. **60**(6): p. 1316-25.

121. Weiss, R.G., et al., *Functional analysis of the R1086H malignant hyperthermia mutation in the DHPR reveals an unexpected influence of the III-IV loop on skeletal muscle EC coupling.* Am J Physiol Cell Physiol, 2004. **287**(4): p. C1094-102.

122. Bannister, R.A., M. Grabner, and K.G. Beam, *The alpha(1S) III-IV loop influences 1,4-dihydropyridine receptor gating but is not directly involved in excitation-contraction coupling interactions with the type 1 ryanodine receptor.* J Biol Chem, 2008. **283**(34): p. 23217-23.

123. MacLennan, D.H. and M.S. Phillips, *Malignant hyperthermia.* Science, 1992. **256**(5058): p. 789-94.

124. Mickelson, J.R. and C.F. Louis, *Malignant hyperthermia: excitation-contraction coupling, Ca2+ release channel, and cell Ca2+ regulation defects.* Physiol Rev, 1996. **76**(2): p. 537-92.

125. Tong, J., T.V. McCarthy, and D.H. MacLennan, *Measurement of resting cytosolic Ca2+ concentrations and Ca2+ store size in HEK-293 cells transfected with malignant hyperthermia or central core disease mutant Ca2+ release channels.* J Biol Chem, 1999. **274**(2): p. 693-702.

126. Zhao, F., et al., *Dantrolene inhibition of ryanodine receptor Ca2+ release channels. Molecular mechanism and isoform selectivity.* J Biol Chem, 2001. **276**(17): p. 13810-6.

127. Amburgey, K., et al., *Genotype-phenotype correlations in recessive RYR1-related myopathies.* Orphanet J Rare Dis, 2013. **8**: p. 117.

128. Robinson, R., et al., *Mutations in RYR1 in malignant hyperthermia and central core disease.* Hum Mutat, 2006. **27**(10): p. 977-89.

129. Zhou, H., et al., *Multi-minicore disease and atypical periodic paralysis associated with novel mutations in the skeletal muscle ryanodine receptor (RYR1) gene.* Neuromuscul Disord, 2010. **20**(3): p. 166-73.

130. Zhang, Y., et al., *A mutation in the human ryanodine receptor gene associated with central core disease.* Nat Genet, 1993. **5**(1): p. 46-50.

131. Ferreiro, A., et al., *A recessive form of central core disease, transiently presenting as multi-minicore disease, is associated with a homozygous mutation in the ryanodine receptor type 1 gene.* Ann Neurol, 2002. **51**(6): p. 750-9.

132. Capacchione, J.F., et al., *Exertional rhabdomyolysis and malignant hyperthermia in a patient with ryanodine receptor type 1 gene, L-type calcium channel alpha-1 subunit gene, and calsequestrin-1 gene polymorphisms.* Anesthesiology, 2010. **112**(1): p. 239-44.

133. Morrill, J.A., R.H. Brown, Jr., and S.C. Cannon, *Gating of the L-type Ca channel in human skeletal myotubes: an activation defect caused by the hypokalemic periodic paralysis mutation R528H.* J Neurosci, 1998. **18**(24): p. 10320-34.

134. Jurkat-Rott, K., et al., *A calcium channel mutation causing hypokalemic periodic paralysis.* Hum Mol Genet, 1994. **3**(8): p. 1415-9.

135. Wehrens, X.H., et al., *FKBP12.6 deficiency and defective calcium release channel (ryanodine receptor) function linked to exercise-induced sudden cardiac death.* Cell, 2003. **113**(7): p. 829-40.

136. Jiang, D., et al., *Enhanced basal activity of a cardiac Ca2+ release channel (ryanodine receptor) mutant associated with ventricular tachycardia and sudden death.* Circ Res, 2002. **91**(3): p. 218-25.

137. George, C.H., G.V. Higgs, and F.A. Lai, *Ryanodine receptor mutations associated with stress-induced ventricular tachycardia mediate increased calcium release in stimulated cardiomyocytes.* Circ Res, 2003. **93**(6): p. 531-40.

138. Lahat, H., et al., *A missense mutation in a highly conserved region of CASQ2 is associated with autosomal recessive catecholamine-induced polymorphic ventricular tachycardia in Bedouin families from Israel.* Am J Hum Genet, 2001. **69**(6): p. 1378-84.

139. Song, L., et al., *Calsequestrin 2 (CASQ2) mutations increase expression of calreticulin and ryanodine receptors, causing catecholaminergic polymorphic ventricular tachycardia.* J Clin Invest, 2007. **117**(7): p. 1814-23.

140. Postma, A.V., et al., *Absence of calsequestrin 2 causes severe forms of catecholaminergic polymorphic ventricular tachycardia.* Circ Res, 2002. **91**(8): p. e21-6.

141. Nyegaard, M., et al., *Mutations in calmodulin cause ventricular tachycardia and sudden cardiac death.* Am J Hum Genet, 2012. **91**(4): p. 703-12.

142. Roux-Buisson, N., et al., *Absence of triadin, a protein of the calcium release complex, is responsible for cardiac arrhythmia with sudden death in human.* Hum Mol Genet, 2012. **21**(12): p. 2759-67.

143. Rampazzo, A., et al., *A new locus for arrhythmogenic right ventricular cardiomyopathy (ARVD2) maps to chromosome 1q42-q43.* Hum Mol Genet, 1995. **4**(11): p. 2151-4.

144. Tiso, N., et al., *Identification of mutations in the cardiac ryanodine receptor gene in families affected with arrhythmogenic right ventricular cardiomyopathy type 2 (ARVD2).* Hum Mol Genet, 2001. **10**(3): p. 189-94.

145. Brugada, P. and J. Brugada, *Right bundle branch block, persistent ST segment elevation and sudden cardiac death: a distinct clinical and electrocardiographic syndrome. A multicenter report.* J Am Coll Cardiol, 1992. **20**(6): p. 1391-6.

146. Alings, M. and A. Wilde, *"Brugada" syndrome: clinical data and suggested pathophysiological mechanism.* Circulation, 1999. **99**(5): p. 666-73.

147. Priori, S.G., et al., *Natural history of Brugada syndrome: insights for risk stratification and management.* Circulation, 2002. **105**(11): p. 1342-7.

148. Nademanee, K., et al., *Arrhythmogenic marker for the sudden unexplained death syndrome in Thai men.* Circulation, 1997. **96**(8): p. 2595-600.

149. Cordeiro, J.M., et al., *Accelerated inactivation of the L-type calcium current due to a mutation in CACNB2b underlies Brugada syndrome.* J Mol Cell Cardiol, 2009. **46**(5): p. 695-703.

150. Antzelevitch, C., et al., *Loss-of-function mutations in the cardiac calcium channel underlie a new clinical entity characterized by ST-segment elevation, short QT intervals, and sudden cardiac death.* Circulation, 2007. **115**(4): p. 442-9.

151. Antzelevitch, C., et al., *Brugada syndrome: report of the second consensus conference: endorsed by the Heart Rhythm Society and the European Heart Rhythm Association.* Circulation, 2005. **111**(5): p. 659-70.

152. Splawski, I., et al., *Ca(V)1.2 calcium channel dysfunction causes a multisystem disorder including arrhythmia and autism.* Cell, 2004. **119**(1): p. 19-31.

153. Yazawa, M., et al., *Using induced pluripotent stem cells to investigate cardiac phenotypes in Timothy syndrome.* Nature, 2011. **471**(7337): p. 230-4.

154. Splawski, I., et al., *Severe arrhythmia disorder caused by cardiac L-type calcium channel mutations.* Proc Natl Acad Sci U S A, 2005. **102**(23): p. 8089-96; discussion 8086-8.

155. Marks, M.L., D.L. Trippel, and M.T. Keating, *Long QT syndrome associated with syndactyly identified in females.* Am J Cardiol, 1995. **76**(10): p. 744-5.

156. Reichenbach, H., E.M. Meister, and H. Theile, *[The heart-hand syndrome. A new variant of disorders of heart conduction and syndactylia including osseous changes in hands and feet]*. Kinderarztl Prax, 1992. **60**(2): p. 54-6.

157. Bers, D.M., *Cardiac excitation-contraction coupling.* Nature, 2002. **415**(6868): p. 198-205.

158. Bassani, J.W., R.A. Bassani, and D.M. Bers, *Relaxation in rabbit and rat cardiac cells: species-dependent differences in cellular mechanisms.* J Physiol, 1994. **476**(2): p. 279-93.

159. Shigekawa, M. and T. Iwamoto, *Cardiac Na(+)-Ca(2+) exchange: molecular and pharmacological aspects.* Circ Res, 2001. **88**(9): p. 864-76.

160. Crespo, L.M., C.J. Grantham, and M.B. Cannell, *Kinetics, stoichiometry and role of the Na-Ca exchange mechanism in isolated cardiac myocytes.* Nature, 1990. **345**(6276): p. 618-21.

161. Ren, X. and K.D. Philipson, *The topology of the cardiac Na(+)/Ca(2)(+) exchanger, NCX1.* J Mol Cell Cardiol, 2013. **57**: p. 68-71.

162. Liao, J., et al., *Structural insight into the ion-exchange mechanism of the sodium/calcium exchanger.* Science, 2012. **335**(6069): p. 686-90.

163. Reeves, J.P. and C.C. Hale, *The stoichiometry of the cardiac sodium-calcium exchange system.* J Biol Chem, 1984. **259**(12): p. 7733-9.

164. Philipson, K.D. and D.A. Nicoll, *Sodium-calcium exchange: a molecular perspective.* Annu Rev Physiol, 2000. **62**: p. 111-33.

165. Shattock, M.J., et al., *Na+/Ca2+ exchange and Na+/K+-ATPase in the heart.* J Physiol, 2015. **593**(6): p. 1361-82.

166. Pitts, B.J., *Stoichiometry of sodium-calcium exchange in cardiac sarcolemmal vesicles. Coupling to the sodium pump.* J Biol Chem, 1979. **254**(14): p. 6232-5.

167. Blaustein, M.P. and W.J. Lederer, *Sodium/calcium exchange: its physiological implications.* Physiol Rev, 1999. **79**(3): p. 763-854.

168. Nicoll, D.A., et al., *Cloning of a third mammalian Na+-Ca2+ exchanger, NCX3.* J Biol Chem, 1996. **271**(40): p. 24914-21.

169. Li, Z., et al., *Cloning of the NCX2 isoform of the plasma membrane Na(+)-Ca2+ exchanger.* J Biol Chem, 1994. **269**(26): p. 17434-9.

170. Nicoll, D.A., S. Longoni, and K.D. Philipson, *Molecular cloning and functional expression of the cardiac sarcolemmal Na(+)-Ca2+ exchanger.* Science, 1990. **250**(4980): p. 562-5.

171. Quednau, B.D., D.A. Nicoll, and K.D. Philipson, *Tissue specificity and alternative splicing of the Na+/Ca2+ exchanger isoforms NCX1, NCX2, and NCX3 in rat.* Am J Physiol, 1997. **272**(4 Pt 1): p. C1250-61.

172. Bers, D.M., *Calcium fluxes involved in control of cardiac myocyte contraction.* Circ Res, 2000. **87**(4): p. 275-81.

173. Larbig, R., et al., *Activation of reverse Na+-Ca2+ exchange by the Na+ current augments the cardiac Ca2+ transient: evidence from NCX knockout mice.* J Physiol, 2010. **588**(Pt 17): p. 3267-76.

174. Lines, G.T., et al., *Contribution of the Na+/Ca2+ exchanger to rapid Ca2+ release in cardiomyocytes.* Biophys J, 2006. **91**(3): p. 779-92.

175. Goldhaber, J.I. and K.D. Philipson, *Cardiac sodium-calcium exchange and efficient excitation-contraction coupling: implications for heart disease.* Adv Exp Med Biol, 2013. **961**: p. 355-64.

176. Schillinger, W., et al., *Relevance of Na+-Ca2+ exchange in heart failure.* Cardiovasc Res, 2003. **57**(4): p. 921-33.

177. Armoundas, A.A., et al., *Role of sodium-calcium exchanger in modulating the action potential of ventricular myocytes from normal and failing hearts.* Circ Res, 2003. **93**(1): p. 46-53.

178. De Stefani, D., et al., *A forty-kilodalton protein of the inner membrane is the mitochondrial calcium uniporter.* Nature, 2011. **476**(7360): p. 336-40.

179. Perocchi, F., et al., *MICU1 encodes a mitochondrial EF hand protein required for Ca(2+) uptake.* Nature, 2010. **467**(7313): p. 291-6.

180. Baughman, J.M., et al., *Integrative genomics identifies MCU as an essential component of the mitochondrial calcium uniporter.* Nature, 2011. **476**(7360): p. 341-5.

181. Raffaello, A., et al., *The mitochondrial calcium uniporter is a multimer that can include a dominant-negative pore-forming subunit.* EMBO J, 2013. **32**(17): p. 2362-76.

182. Williams, G.S., et al., *Mitochondrial calcium uptake.* Proc Natl Acad Sci U S A, 2013. **110**(26): p. 10479-86.

183. Pan, X., et al., *The physiological role of mitochondrial calcium revealed by mice lacking the mitochondrial calcium uniporter.* Nat Cell Biol, 2013. **15**(12): p. 1464-72.

184. Kielley, W.W. and O. Meyerhof, *Studies on adenosinetriphosphatase of muscle; a new magnesium-activated a denosinetriphosphatase.* J Biol Chem, 1948. **176**(2): p. 591-601.

185. Marsh, B.B., *The effects of adenosine triphosphate on the fibre volume of a muscle homogenate.* Biochim Biophys Acta, 1952. **9**(3): p. 247-60.

186. MacLennan, D.H., *Purification and properties of an adenosine triphosphatase from sarcoplasmic reticulum.* J Biol Chem, 1970. **245**(17): p. 4508-18.

187. Olesen, C., et al., *The structural basis of calcium transport by the calcium pump.* Nature, 2007. **450**(7172): p. 1036-42.

188. Toyoshima, C., et al., *Crystal structure of the calcium pump of sarcoplasmic reticulum at 2.6 A resolution.* Nature, 2000. **405**(6787): p. 647-55.

189. MacLennan, D.H. and N.M. Green, *Structural biology. Pumping ions.* Nature, 2000. **405**(6787): p. 633-4.

190. Kuhlbrandt, W., *Biology, structure and mechanism of P-type ATPases.* Nat Rev Mol Cell Biol, 2004. **5**(4): p. 282-95.

191. Periasamy, M. and A. Kalyanasundaram, *SERCA pump isoforms: their role in calcium transport and disease.* Muscle Nerve, 2007. **35**(4): p. 430-42.

192. Kho, C., et al., *SUMO1-dependent modulation of SERCA2a in heart failure.* Nature, 2011. **477**(7366): p. 601-5.

193. Tilemann, L., et al., *SUMO-1 gene transfer improves cardiac function in a large-animal model of heart failure.* Sci Transl Med, 2013. **5**(211): p. 211ra159.

194. Kho, C., et al., *Small-molecule activation of SERCA2a SUMOylation for the treatment of heart failure.* Nat Commun, 2015. **6**: p. 7229.

195. Hawkins, C., A. Xu, and N. Narayanan, *Sarcoplasmic reticulum calcium pump in cardiac and slow twitch skeletal muscle but not fast twitch skeletal muscle undergoes phosphorylation by endogenous and exogenous Ca2+/calmodulin-dependent protein*

kinase. Characterization of optimal conditions for calcium pump phosphorylation. J Biol Chem, 1994. **269**(49): p. 31198-206.

196. Odermatt, A., K. Kurzydlowski, and D.H. MacLennan, *The vmax of the Ca2+-ATPase of cardiac sarcoplasmic reticulum (SERCA2a) is not altered by Ca2+/calmodulin-dependent phosphorylation or by interaction with phospholamban.* J Biol Chem, 1996. **271**(24): p. 14206-13.

197. Anderson, D.M., et al., *A micropeptide encoded by a putative long noncoding RNA regulates muscle performance.* Cell, 2015. **160**(4): p. 595-606.

198. Lytton, J., M. Westlin, and M.R. Hanley, *Thapsigargin inhibits the sarcoplasmic or endoplasmic reticulum Ca-ATPase family of calcium pumps.* J Biol Chem, 1991. **266**(26): p. 17067-71.

199. Wiggers, C.J. and L.N. Katz, *THE CONTOUR OF THE VENTRICULAR VOLUME CURVES UNDER DIFFERENT CONDITIONS*. Vol. 58. 1922. 439-475.

200. Sarnoff, S.J., *Myocardial Contractility as Described by Ventricular Function Curves; Observations on Starling's Law of the Heart*. Vol. 35. 1955. 107-122.

201. Buss, J.E. and J.T. Stull, *Calcium binding to cardiac troponin and the effect of cyclic AMP-dependent protein kinase.* FEBS Lett, 1977. **73**(1): p. 101-4.

202. Katz, A.M., *Discovery of phospholamban. A personal history.* Ann N Y Acad Sci, 1998. **853**: p. 9-19.

203. Tada, M., M.A. Kirchberger, and A.M. Katz, *Phosphorylation of a 22,000-dalton component of the cardiac sarcoplasmic reticulum by adenosine 3':5'-monophosphate-dependent protein kinase.* J Biol Chem, 1975. **250**(7): p. 2640-7.

204. Kirchberger, M.A., et al., *Cyclic adenosine 3',5'-monophosphate-dependent protein kinase stimulation of calcium uptake by canine cardiac microsomes.* J Mol Cell Cardiol, 1972. **4**(6): p. 673-80.

205. Kirchberger, M.A., M. Tada, and A.M. Katz, *Adenosine 3':5'-monophosphate-dependent protein kinase-catalyzed phosphorylation reaction and its relationship to calcium transport in cardiac sarcoplasmic reticulum.* J Biol Chem, 1974. **249**(19): p. 6166-73.

206. Tada, M., et al., *The stimulation of calcium transport in cardiac sarcoplasmic reticulum by adenosine 3':5'-monophosphate-dependent protein kinase.* J Biol Chem, 1974. **249**(19): p. 6174-80.

207. Inui, M., M. Kadoma, and M. Tada, *Purification and characterization of phospholamban from canine cardiac sarcoplasmic reticulum.* J Biol Chem, 1985. **260**(6): p. 3708-15.

208. Jones, L.R., et al., *Purification and characterization of phospholamban from canine cardiac sarcoplasmic reticulum.* J Biol Chem, 1985. **260**(12): p. 7721-30.

209. Fujii, J., et al., *Characterization of structural unit of phospholamban by amino acid sequencing and electrophoretic analysis.* Biochem Biophys Res Commun, 1986. **138**(3): p. 1044-50.

210. Simmerman, H.K., et al., *Sequence analysis of phospholamban. Identification of phosphorylation sites and two major structural domains.* J Biol Chem, 1986. **261**(28): p. 13333-41.

211. Fujii, J., et al., *Expression and site-specific mutagenesis of phospholamban. Studies of residues involved in phosphorylation and pentamer formation.* J Biol Chem, 1989. **264**(22): p. 12950-5.

212. Le Peuch, C.J., J. Haiech, and J.G. Demaille, *Concerted regulation of cardiac sarcoplasmic reticulum calcium transport by cyclic adenosine monophosphate dependent and calcium--calmodulin-dependent phosphorylations.* Biochemistry, 1979. **18**(23): p. 5150-7.

213. Fujii, J., et al., *Complete complementary DNA-derived amino acid sequence of canine cardiac phospholamban.* J Clin Invest, 1987. **79**(1): p. 301-4.

214. Gustavsson, M., et al., *Allosteric regulation of SERCA by phosphorylation-mediated conformational shift of phospholamban.* Proc Natl Acad Sci U S A, 2013. **110**(43): p. 17338-43.

215. Kimura, Y., et al., *Phospholamban domain Ib mutations influence functional interactions with the Ca2+-ATPase isoform of cardiac sarcoplasmic reticulum.* J Biol Chem, 1998. **273**(23): p. 14238-41.

216. Asahi, M., et al., *Transmembrane helix M6 in sarco(endo)plasmic reticulum Ca(2+)-ATPase forms a functional interaction site with phospholamban. Evidence for physical interactions at other sites.* J Biol Chem, 1999. **274**(46): p. 32855-62.

217. Wawrzynow, A., et al., *Sarcolipin, the "proteolipid" of skeletal muscle sarcoplasmic reticulum, is a unique, amphipathic, 31-residue peptide.* Arch Biochem Biophys, 1992. **298**(2): p. 620-3.

218. Butler, J., et al., *The effects of sarcolipin over-expression in mouse skeletal muscle on metabolic activity.* Arch Biochem Biophys, 2015. **569**: p. 26-31.

219. Odermatt, A., et al., *Sarcolipin regulates the activity of SERCA1, the fast-twitch skeletal muscle sarcoplasmic reticulum Ca2+-ATPase.* J Biol Chem, 1998. **273**(20): p. 12360-9.

220. Asahi, M., et al., *Cardiac-specific overexpression of sarcolipin inhibits sarco(endo)plasmic reticulum Ca2+ ATPase (SERCA2a) activity and impairs cardiac function in mice.* Proc Natl Acad Sci U S A, 2004. **101**(25): p. 9199-204.

221. Bhupathy, P., et al., *Threonine-5 at the N-terminus can modulate sarcolipin function in cardiac myocytes.* J Mol Cell Cardiol, 2009. **47**(5): p. 723-9.

222. Mall, S., et al., *The presence of sarcolipin results in increased heat production by Ca(2+)-ATPase.* J Biol Chem, 2006. **281**(48): p. 36597-602.

223. Smith, W.S., et al., *Sarcolipin uncouples hydrolysis of ATP from accumulation of Ca2+ by the Ca2+-ATPase of skeletal-muscle sarcoplasmic reticulum.* Biochem J, 2002. **361**(Pt 2): p. 277-86.

224. Bal, N.C., et al., *Sarcolipin is a newly identified regulator of muscle-based thermogenesis in mammals.* Nat Med, 2012. **18**(10): p. 1575-9.

225. Magny, E.G., et al., *Conserved regulation of cardiac calcium uptake by peptides encoded in small open reading frames.* Science, 2013. **341**(6150): p. 1116-20.

226. Nelson, B.R., D.M. Anderson, and E.N. Olson, *Small open reading frames pack a big punch in cardiac calcium regulation.* Circ Res, 2014. **114**(1): p. 18-20.

227. Toyoshima, C., et al., *Crystal structures of the calcium pump and sarcolipin in the Mg2+-bound E1 state.* Nature, 2013. **495**(7440): p. 260-4.

228. Winther, A.M., et al., *The sarcolipin-bound calcium pump stabilizes calcium sites exposed to the cytoplasm.* Nature, 2013. **495**(7440): p. 265-9.

229. Asahi, M., et al., *Sarcolipin regulates sarco(endo)plasmic reticulum Ca2+-ATPase (SERCA) by binding to transmembrane helices alone or in association with phospholamban.* Proc Natl Acad Sci U S A, 2003. **100**(9): p. 5040-5.

230. Chen, Z., et al., *Spatial and Dynamic Interactions between Phospholamban and the Canine Cardiac Ca2+ Pump Revealed with Use of Heterobifunctional Cross-linking Agents.* Journal of Biological Chemistry, 2003. **278**(48): p. 48348-48356.

231. Bidwell, P., et al., *Phospholamban binds with differential affinity to calcium pump conformers.* J Biol Chem, 2011. **286**(40): p. 35044-50.

232. Chen, Z., et al., *Cross-linking of C-terminal residues of phospholamban to the Ca2+ pump of cardiac sarcoplasmic reticulum to probe spatial and functional interactions within the transmembrane domain.* J Biol Chem, 2006. **281**(20): p. 14163-72.

233. Toyoshima, C., et al., *Modeling of the inhibitory interaction of phospholamban with the Ca2+ ATPase.* Proc Natl Acad Sci U S A, 2003. **100**(2): p. 467-72.

234. Collins, J.H. and J. Leszyk, *The "gamma subunit" of Na,K-ATPase: a small, amphiphilic protein with a unique amino acid sequence.* Biochemistry, 1987. **26**(26): p. 8665-8.

235. Han, F., et al., *Phospholemman phosphorylation mediates the protein kinase C-dependent effects on Na+/K+ pump function in cardiac myocytes.* Circ Res, 2006. **99**(12): p. 1376-83.

236. Presti, C.F., L.R. Jones, and J.P. Lindemann, *Isoproterenol-induced phosphorylation of a 15-kilodalton sarcolemmal protein in intact myocardium.* J Biol Chem, 1985. **260**(6): p. 3860-7.

237. Mercer, R.W., et al., *Molecular cloning and immunological characterization of the gamma polypeptide, a small protein associated with the Na,K-ATPase.* J Cell Biol, 1993. **121**(3): p. 579-86.

238. Fuller, W. and M.J. Shattock, *Phospholemman and the cardiac sodium pump: protein kinase C, take a bow.* Circ Res, 2006. **99**(12): p. 1290-2.

239. Navarre, C., et al., *Purification and complete sequence of a small proteolipid associated with the plasma membrane H(+)-ATPase of Saccharomyces cerevisiae.* J Biol Chem, 1992. **267**(9): p. 6425-8.

240. Navarre, C., et al., *Two distinct genes encode small isoproteolipids affecting plasma membrane H(+)-ATPase activity of Saccharomyces cerevisiae.* J Biol Chem, 1994. **269**(33): p. 21262-8.

241. Takeshima, H., E. Venturi, and R. Sitsapesan, *New and notable ion-channels in the sarcoplasmic/endoplasmic reticulum: do they support the process of intracellular Ca2+ release?* J Physiol, 2014.

242. Yazawa, M., et al., *TRIC channels are essential for Ca2+ handling in intracellular stores.* Nature, 2007. **448**(7149): p. 78-82.

243. Guo, T., et al., *Sarcoplasmic reticulum K(+) (TRIC) channel does not carry essential countercurrent during Ca(2+) release.* Biophys J, 2013. **105**(5): p. 1151-60.

244. Kuum, M., et al., *Endoplasmic reticulum potassium-hydrogen exchanger and small conductance calcium-activated potassium channel activities are essential for ER calcium uptake in neurons and cardiomyocytes.* J Cell Sci, 2012. **125**(Pt 3): p. 625-33.

245. Louch, W.E., et al., *No rest for the weary: diastolic calcium homeostasis in the normal and failing myocardium.* Physiology (Bethesda), 2012. **27**(5): p. 308-23.

246. Swift, F., et al., *Extreme sarcoplasmic reticulum volume loss and compensatory T-tubule remodeling after Serca2 knockout.* Proc Natl Acad Sci U S A, 2012. **109**(10): p. 3997-4001.

247. Song, L.S., et al., *Orphaned ryanodine receptors in the failing heart.* Proc Natl Acad Sci U S A, 2006. **103**(11): p. 4305-10.

248. Louch, W.E., et al., *T-tubule disorganization and reduced synchrony of Ca2+ release in murine cardiomyocytes following myocardial infarction.* J Physiol, 2006. **574**(Pt 2): p. 519-33.

249. Heinzel, F.R., et al., *Remodeling of T-tubules and reduced synchrony of Ca2+ release in myocytes from chronically ischemic myocardium.* Circ Res, 2008. **102**(3): p. 338-46.

250. Brette, F., et al., *Spatiotemporal characteristics of SR Ca(2+) uptake and release in detubulated rat ventricular myocytes.* J Mol Cell Cardiol, 2005. **39**(5): p. 804-12.

251. Houser, S.R., V. Piacentino, 3rd, and J. Weisser, *Abnormalities of calcium cycling in the hypertrophied and failing heart.* J Mol Cell Cardiol, 2000. **32**(9): p. 1595-607.

252. Allen, D.G., et al., *Calcium and the damage pathways in muscular dystrophy.* Can J Physiol Pharmacol, 2010. **88**(2): p. 83-91.

253. Whitehead, N.P., E.W. Yeung, and D.G. Allen, *Muscle damage in mdx (dystrophic) mice: role of calcium and reactive oxygen species.* Clin Exp Pharmacol Physiol, 2006. **33**(7): p. 657-62.

254. Millay, D.P., et al., *Calcium influx is sufficient to induce muscular dystrophy through a TRPC-dependent mechanism.* Proc Natl Acad Sci U S A, 2009. **106**(45): p. 19023-8.

255. Burr, A.R., et al., *Na+ dysregulation coupled with Ca2+ entry through NCX1 promotes muscular dystrophy in mice.* Mol Cell Biol, 2014. **34**(11): p. 1991-2002.

256. Allen, D.G., G.D. Lamb, and H. Westerblad, *Skeletal muscle fatigue: cellular mechanisms.* Physiol Rev, 2008. **88**(1): p. 287-332.

257. Goonasekera, S.A., et al., *Mitigation of muscular dystrophy in mice by SERCA overexpression in skeletal muscle.* J Clin Invest, 2011. **121**(3): p. 1044-52.

258. del Monte, F., et al., *Abrogation of ventricular arrhythmias in a model of ischemia and reperfusion by targeting myocardial calcium cycling.* Proc Natl Acad Sci U S A, 2004. **101**(15): p. 5622-7.

259. del Monte, F., et al., *Improvement in survival and cardiac metabolism after gene transfer of sarcoplasmic reticulum Ca(2+)-ATPase in a rat model of heart failure.* Circulation, 2001. **104**(12): p. 1424-9.

260. Schmidt, U., et al., *Restoration of diastolic function in senescent rat hearts through adenoviral gene transfer of sarcoplasmic reticulum Ca(2+)-ATPase.* Circulation, 2000. **101**(7): p. 790-6.

261. Miyamoto, M.I., et al., *Adenoviral gene transfer of SERCA2a improves left-ventricular function in aortic-banded rats in transition to heart failure.* Proc Natl Acad Sci U S A, 2000. **97**(2): p. 793-8.

262. Hajjar, R.J., et al., *Modulation of ventricular function through gene transfer in vivo.* Proc Natl Acad Sci U S A, 1998. **95**(9): p. 5251-6.

263. Byrne, M.J., et al., *Recirculating cardiac delivery of AAV2/1SERCA2a improves myocardial function in an experimental model of heart failure in large animals.* Gene Ther, 2008. **15**(23): p. 1550-7.

264. Kawase, Y., et al., *Reversal of cardiac dysfunction after long-term expression of SERCA2a by gene transfer in a pre-clinical model of heart failure.* J Am Coll Cardiol, 2008. **51**(11): p. 1112-9.

265. Sakata, S., et al., *Restoration of mechanical and energetic function in failing aortic-banded rat hearts by gene transfer of calcium cycling proteins.* J Mol Cell Cardiol, 2007. **42**(4): p. 852-61.

266. Hajjar, R.J., *Potential of gene therapy as a treatment for heart failure.* J Clin Invest, 2013. **123**(1): p. 53-61.

267. Zsebo, K., et al., *Long-term effects of AAV1/SERCA2a gene transfer in patients with severe heart failure: analysis of recurrent cardiovascular events and mortality.* Circ Res, 2014. **114**(1): p. 101-8.

268. Jessup, M., et al., *Calcium Upregulation by Percutaneous Administration of Gene Therapy in Cardiac Disease (CUPID): a phase 2 trial of intracoronary gene therapy of sarcoplasmic reticulum Ca2+-ATPase in patients with advanced heart failure.* Circulation, 2011. **124**(3): p. 304-13.

269. Jaski, B.E., et al., *Calcium upregulation by percutaneous administration of gene therapy in cardiac disease (CUPID Trial), a first-in-human phase 1/2 clinical trial.* J Card Fail, 2009. **15**(3): p. 171-81.

270. *Celladon Reports Negative Results for CUPID2 Trial of MYDICAR(R) in Advanced Heart Failure*. 2015, Celladon Corporation: Company Website.

271. Ratner, M., *Heart failure gene therapy disappoints but experts keep the faith.* Nat Biotechnol, 2015. **33**(6): p. 573-4.

272. *Creative Commons License 3.0*. [cited 2015 June 5]; Available from: https://creativecommons.org/licenses/by/3.0/deed.en.

273. CNX, O. *OpenStax College, Skeletal Muscle*. 2013 [cited 2015 June 8]; Available from: http://cnx.org/contents/6df8aab3-1741-4016-b5a9-ac51b52fade0@3.

274. Catterall, W.A., *Voltage-gated calcium channels.* Cold Spring Harb Perspect Biol, 2011. **3**(8): p. a003947.

275. Zalk, R., et al., *Structure of a mammalian ryanodine receptor.* Nature, 2015. **517**(7532): p. 44-9.

276. Wilkens, C.M., et al., *Excitation-contraction coupling is unaffected by drastic alteration of the sequence surrounding residues L720-L764 of the alpha 1S II-III loop.* Proc Natl Acad Sci U S A, 2001. **98**(10): p. 5892-7.

CHAPTER 2. ROLE OF STAC3 IN EXCITATION-CONTRACTION COUPLING

2.1 PROLOGUE

The following section titled "Skeletal muscle-specific T-tubule protein STAC3 mediates voltage-induced calcium release and contractility" has been reformatted from its original source in the Proceedings of the National Academy of Sciences, USA [1]. Permission from the publisher is not required in this instance. Portions of the data included in this section were contributed by authors Fenfen Wu, Yun Liu, and Douglas M. Anderson.

2.2 SKELETAL MUSCLE-SPECIFIC T-TUBULE PROTEIN STAC3 MEDIATES VOLTAGE-INDUCED CALCIUM RELEASE AND CONTRACTILITY

2.2.1 Abstract

Excitation–contraction (EC) coupling comprises events in muscle that convert electrical signals to Ca^{2+} transients, which then trigger contraction of the sarcomere. Defects in these processes cause a spectrum of muscle diseases. We report that STAC3, a skeletal muscle-specific protein that localizes to T-tubules, is essential for coupling membrane depolarization to Ca^{2+} release from the sarcoplasmic reticulum (SR). Consequently, homozygous deletion of src homology 3 and cysteine rich domain 3 (*Stac3*) in mice results in complete paralysis and perinatal lethality with a range of musculoskeletal defects that reflect a blockade of ECC. Muscle contractility and Ca^{2+} release from the SR of cultured myotubes from *Stac3* mutant mice could be restored by application of 4-chloro-*m*-cresol, a ryanodine receptor agonist, indicating that the sarcomeres, SR Ca^{2+} store, and ryanodine receptors are functional in *Stac3* mutant skeletal

muscle. These findings reveal a previously uncharacterized, but required, component of the ECC machinery of skeletal muscle and introduce a candidate for consideration in myopathic disorders.

2.2.2 Introduction

Muscle contraction requires a series of events known as excitation–contraction coupling (ECC) that links electrical depolarization, initiated by motor neuron innervation, to muscle contraction by releasing Ca^{2+} from its storage site in the sarcoplasmic reticulum (SR), which consequently activates the sarcomere. In both cardiac and skeletal muscle, this process requires the function of two Ca^{2+} channels, the dihydropyridine receptor (DHPR) and the ryanodine receptor (RyR) [2, 3], but the isoforms of each and the functional relationship between these channels are distinct in each striated muscle tissue.

In cardiac muscle, membrane depolarization results in inward flow of extracellular Ca^{2+} through the DHPR [2]. Calcium that enters the cytoplasm through the DHPR then acts as a second messenger upon the RyR, causing the channel to open and release more Ca^{2+} from the SR. By contrast, skeletal muscle does not require extracellular Ca^{2+} to trigger Ca^{2+} release from the SR, and DHPR serves primarily as a voltage sensor [3]. The skeletal muscle DHPR does in fact conduct inward Ca^{2+} current, known as L-type current, which is enhanced by retrograde signaling with the RyR [4], but this current is not required for normal ECC. Instead, DHPR triggers opening of the RyR in the SR membrane by an unknown physical coupling mechanism, which results in a massive release of Ca^{2+} to activate the sarcomere [2, 4, 5].

The exact coupling mechanism that links the skeletal-type DHPR to the skeletal muscle-specific isoform of RyR (RyR1) has proven difficult to define, although studies using chimeric constructs of skeletal and cardiac DHPR isoforms have successfully mapped the regions that are

functionally required for the skeletal-type coupling mechanism [3, 6]. There is substantial evidence that the cytoplasmic loop between transmembrane regions II and III (II-III loop) of the DHPR pore-forming subunit (α1s) conveys the skeletal-specific properties of this channel. Whereas the C-terminal portion of the II-III loop has been shown to be sufficient to convey the skeletal muscle-specific properties of the II-III loop [7], other groups have demonstrated that a positively charged portion of the N-terminal region can activate RyR [8, 9], despite the fact that ECC was normal when this region was disrupted or deleted [7, 10]. Thus, it is unlikely that the N-terminal region of the II-III loop directly activates RyR1 in a normal physiological context. RyR1 has also been shown to be modulated by a variety of accessory proteins including FK506 binding protein 1A (FKBP1A) [11], S100 calcium-binding protein A1 (S100A1) [12], and calmodulin [13].

In a bioinformatic screen for uncharacterized muscle-specific conserved genes with probable function in intracellular signaling, we identified src homology 3 (SH3) and cysteine rich domain 3 (*Stac3*), which we show encodes a skeletal muscle-specific protein that localizes to T-tubules. Using a knockout (KO) mouse model and primary myoblast cultures, we demonstrate that STAC3 is required for coupling membrane depolarization to SR Ca^{2+} release and is required for electrically evoked skeletal muscle contraction. Surprisingly, skeletal muscle contractility could be fully restored in the absence of STAC3 by application of the RyR agonist 4-chloro-*m*-cresol (4-CMC). Based on this evidence, we propose that STAC3 may promote coupling between or possibly link the DHPR voltage sensor and the RyR Ca^{2+} release channel. This work expands understanding of ECC and may provide insight into Ca^{2+} regulation in other tissues such as the central nervous system, where the related genes *Stac* and *Stac2* are expressed.

2.2.3 Materials and Methods

2.2.3.1 Mice

All experiments involving animals were approved by the Institutional Animal Care and Use Committee at the University of Texas Southwestern Medical Center. The *Stac3* knockout strain was re-derived on a mixed background by *in vitro* fertilization using germplasm stock obtained from the National Institutes of Health Knock-Out Mouse Project (KOMP; www.komp.org; Project ID CSD41137).

2.2.3.2 Muscle Electroporation and Imaging

Flexor digitorum brevis (FDB) muscles were electroporated following a published protocol [14]. Following anesthesia by isoflurane, 15 μL of 2 mg/mL hyaluronidase was injected beneath the skin of the foot and footpad. One hour later the mice were anesthetized again and DNA expression vector containing a green fluorescent fusion gene was injected. The foot was then pierced with two sterile gold-plated acupuncture needles and 20 1-s pulses of 100 V were applied. Following a 3-d recovery, the mice were killed, their feet were skinned, and the unfixed FDB was examined directly in imaging buffer by two-photon laser scanning microscopy (Zeiss; LSM 780) with reverse second harmonic generation to visualize the A bands as an internal reference.

2.2.3.3 Electrophysiology

Measurement of neuromuscular synaptic and muscle activity was carried out on acutely isolated E18.5 phrenic nerve-diaphragm muscle preparations, as previously described [15]. Miniature end-plate potentials and action potentials were acquired by sharp intracellular microglass electrodes via an intracellular amplifier (AxoClamp-2B; Molecular Devices),

digitized with Digidata 1332 (Molecular Devices), and analyzed with pClamp 9.0 (Molecular Devices) and Mini Analysis Program (Synaptosoft). Data are presented as the mean ± SEM, and statistical differences were determined by Student's t test.

2.2.3.4 Contraction Assays

The measurement of muscle contraction was carried out as described previously [16, 17]. In brief, E18.5 diaphragm muscles were isolated *in situ* at room temperature in oxygenated Ringer's solution containing 118 mM NaCl, 4.75 mM KCl, 1.18 mM $MgSO_4$, 2.54 mM $CaCl_2$, 1.18 mM NaH_2PO_4, 10 mM glucose, and 24.8 mM $NaHCO_3$. A muscle strip cut from the right dorsal diaphragm was vertically mounted in an isometric tissue clamp of a force transducer (FORT25; WPI) suspended in a 25-mL organ bath (Myobath; WPI) filled with Ringer's solution continuously bubbled with a mixture of 95% O_2 and 5% CO_2 at 37 °C. To block neuromuscular transmission from phrenic-nerve terminals, 10 μM tubocurarine (Sigma-Aldrich) was added to the bath solution [16]. Muscle contraction was elicited by field stimulation with parallel wire electrodes. Isometric contractions were evoked by a train of 50 pulses of 1-ms duration, 80 mA (A385 Stimulator; WPI) at 50 Hz delivered every 20 s. Data were acquired using a transbridge (4M; WPI) and pCLAMP 9 software (Molecular Devices) at a sampling rate of 2 kHz. Data were analyzed using Clampfit (Molecular Devices) and Origin 6 (OriginLab). After measurement of muscle contraction by field electrical stimulation, the same diaphragm muscle strip was sequentially bathed in 4-chloro-*m*-cresol (4-CMC; 1 mM; 1:500 dilution from a 0.5 M stock solution in 100% ethanol)/Ringer's solution, a high-potassium (120 mM) solution, and 4-CMC (1 mM)/Ringer's solution for 5 min each exposure. Each exposure was separated by a 5-min Ringer's solution incubation to allow the muscle to recover. The high-potassium solution was made by reducing the NaCl concentration in the Ringer's solution. Test solutions were pre-

warmed to 37 °C and applied by perfusion of eight times the bath volume at a flow rate of ~2.5 mL/s. Muscle contraction was recorded at a sampling rate of 2 Hz for 40 min. On completion of contraction measurement, the wet weight of the muscle strip was determined.

2.2.3.5 Electron Microscopy

Tongues were harvested from E18.5 fetuses and fixed by immersion in 2.5% (vol/vol) glutaraldehyde in 0.1 M sodium cacodylate buffer (pH 7.4) containing 50 mM $CaCl_2$, rinsed in buffer, and then postfixed in buffered 2% (wt/vol) osmium tetroxide containing 0.8% (wt/vol) potassium ferricyanide for 3 h. Tissues were rinsed with dH_2O, *en bloc* stained in 4% (wt/vol) uranyl acetate in 50% (vol/vol) ethanol, dehydrated with a graded series of ethanol, and embedded in EMbed 812 resin (Electron Microscopy Sciences). Thin sections were cut on a Leica Ultracut UCT ultramicrotome and then stained with 2% (wt/vol) uranyl acetate and lead citrate. Images were acquired on an FEI Tecnai G^2 Spirit electron microscope equipped with an LaB_6 source Gatan CCD camera and operated at 120 kV.

2.2.3.6 Calcium Measurements

Primary myoblasts were plated at ~90% confluence on laminin-coated 35-mm dishes and then differentiated for 6 d. Myotubes were loaded with the fluorescent calcium indicator fluo-4-AM (Invitrogen) by 30-min incubation at 37 °C with medium containing 5 μM fluo-4-AM, 0.02% (wt/vol) Pluronic F-127 (Invitrogen), and 0.1% (wt/vol) probenecid. Myotubes were subsequently washed and incubated for another 30 min at 37 °C with probenecid-containing medium. Calcium transients were recorded using a DeltaVision pDV microscope (Applied Precision) with a 20× objective, FITC filters, and a heated chamber. A total of 4,200 frames were collected at 100-ms intervals for each sample. Beginning just before imaging, medium was

continuously perfused at a rate of 12.5 mL/min through a closed-bath perfusion chamber (Harvard Apparatus). The perfusion buffers were as follows: Ca^{2+}-free Ringer's solution for wash (118 mM NaCl, 4.75 mM KCl, 1.18 mM $MgSO_4$, 1.18 mM NaH_2PO_4, 10 mM glucose, 24.8 mM $NaHCO_3$); Ca^{2+}-free high-K^+ Ringer's solution (2.75 mM NaCl, 120 mM KCl); high-K^+ Ringer's solution (2.75 mM NaCl, 120 mM KCl, 2.54 mM $CaCl_2$); and Ca^{2+}-free Ringer's solution with 1 mM 4-CMC. Each treatment lasted a total of 600 frames or 1 min. z-axis plots were generated using ImageJ [18] by selecting the outlines of mature myotubes. z-axis plots for background regions were also generated and then subtracted from the myotube signal to yield the corrected value.

2.2.3.7 cDNA and Real-Time PCR

For mRNA quantification in knockout mice, total RNA was isolated using TRIzol (Invitrogen) from pooled embryonic day 18.5 (E18.5) hindlimb muscles, primarily quadriceps, gastrocnemius, soleus, and tibialis anterior. Purified RNA was DNase-treated and then reverse-transcribed with random hexamers using a SuperScript III First-Strand Synthesis Kit (Invitrogen). cDNA samples were analyzed using a StepOne Real-Time PCR instrument (Applied Biosystems) with TaqMan probes for *Ryr1* [the skeletal muscle-specific isoform of the ryanodine receptor (RyR)] (Mm01175211_m1), voltage-dependent L-type calcium channel, alpha 1S subunit (*Cacna1s*) (Mm00489257_m1), voltage-dependent L-type calcium channel, beta 1 subunit (*Cacnb1*) (Mm0136805_m1), and myogenin (Mm00446195_g1). SYBR Green was used for *Stac* (5′-TCCAGCCAACTTTGTTCAGA-3′, 5′-ATGAAGCCGTCCTGTTCTTC-3′), *Stac2* (5′-AGAATGTTTGGCGATGCTGT-3′, 5′-TGCTTCTGCTCACGCCTAC-3′), and *Stac3* (5′-CGGATTCTTCCCTCCAAACT-3′, 5′-CCACCAGCTTCATCTCCTTT-3′). Values for each sample were normalized to ribosomal RNA control probes (Invitrogen).

2.2.3.8 In Situ Hybridization

Tissues for in situ hybridization were harvested from anesthetized mice following fixation via transcardial perfusion with 4% (wt/vol) paraformaldehyde, Bouin's, or 10% (vol/vol) neutral-buffered formalin. Subsequent paraffin processing, embedding, and sectioning and histological stains were performed by standard procedures [19, 20]. Probe template corresponding to the full-length coding sequence of mouse *Stac3* was PCR-amplified with the primers 5′-ATGACAGAAAAGGAAGTGGTGGA-3′ and 5′-AATCTCCTCCAGGAAGTCG- 3′ and cloned into pCRII-TOPO (Invitrogen). ^{35}S-labeled probes were generated from linearized cDNA templates by in vitro transcription using a MAXIscript Kit (Ambion). Radioisotopic *in situ* hybridization was performed as previously described in Shelton et al. [21]. Briefly, sagittal sections of E15.5 embryos and transverse thoracic sections of E14.5 embryos were deparaffinized, permeabilized, and acetylated before hybridization at 55 °C with riboprobes diluted in a mixture containing 50% (vol/ vol) formamide, 0.3 M NaCl, 20 mM Tris·HCl (pH 8.0), 5 mM EDTA (pH 8.0), 10 mM $NaPO_4$ (pH 8.0), 10% (wt/vol) dextran sulfate, 1× Denhardt's, 0.5 mg/mL tRNA. Following hybridization, the sections were rinsed with increasing-stringency washes, subjected to RNase A (2 μg/mL, 30 min at 37 °C), and dehydrated before dipping in K.5 nuclear emulsion gel (Ilford). Autoradiographic exposure was 42 d. Bright-field and darkfield images were obtained for each specimen. Using ImageJ [18] for all steps, the bright-field image was converted to grayscale. For the dark-field image containing the signal, the saturation and brightness thresholds were set to capture the signal (approximately the upper third of each scale). The image was then converted to grayscale and the look-up table was converted to cyan. The resulting signal image was then subtracted from the grayscale bright-field image to yield the final image. All adjustments were made uniformly to the entire images.

2.2.3.9 Northern Blot

A Northern blot containing 20 μg total RNA per lane from 15 mouse tissues was purchased from Zyagen (MN-MT-1). [^{32}P]dCTP-labeled probe was transcribed *in vitro* using the full-length *Stac3* coding sequence. Following overnight hybridization at 68 °C and washing, the blot was exposed to autoradiographic film for 3 h.

2.2.3.10 Genotyping

Tail biopsies were digested overnight at 55 °C in tail digest buffer [50 mM KCl, 10 mM Tris·HCl, pH 8.3, 2.5 mM $MgCl_2$, 0.2 mg/mL gelatin, 0.45% (vol/vol) Nonidet P-40, 0.45% (vol/vol) Tween 20, 0.15 mg/mL proteinase K]. Samples were then vortexed to dissociate tissue and centrifuged (15,000 × g). Multiplex PCR reactions (25 μL) were prepared on ice as follows: 800 nM common primer: 5′-CTCCTCACCTGTGAGTATTTGG-3′; 400 nM wild-type primer: 5′-CTCAACCTTCCTAATGCTGTGG-3′; 200 nM knockout primer: 5′-AACTTGTTGATATCGTGGTATCGTT-3′; 1× FailSafe PCR buffer D (Epicentre); 1 μL tail digest buffer (no proteinase K); 1 μL tail lysate; 1 U Taq DNA polymerase (New England BioLabs). The thermal protocol was 94 °C for 5 min; 40 cycles of 94 °C for 15 s, 58.5 °C for 30 s, 72 °C for 15 s; 72 °C for 5 min. The wild-type allele produced a band of 507 bp and the knockout produced a band of 301 bp.

2.2.3.11 β-Galactosidase Staining

Embryos were harvested and fixed in 1× PBS, 0.8% (vol/vol) formaldehyde, 0.2% (vol/vol) glutaraldehyde for 30 min to 1 h at 4 °C followed by a washing in PBS for 30 min at 4 °C. Specimens were then placed in staining solution (5 mM potassium ferrocyanide, 5 mM potassium ferricyanide, 2 mM $MgCl_2$, 1 mg/mL X-gal, 1× PBS) for several hours to overnight at 37 °C, washed the next day, and further fixed in 1× PBS with 4% (vol/vol) formaldehyde.

2.2.3.12 Diaphragm Immunostaining

E18.5 diaphragm muscles were fixed with 2% (vol/vol) paraformaldehyde in 0.1 M phosphate buffer (pH 7.3) overnight at 4 °C. Muscle samples were incubated with 2 nM Texas red-conjugated α-bungarotoxin (Invitrogen) for 30 min, and then with the antibody against syntaxin 1 (1:1,000) (gift from Thomas Südhof, Stanford University School of Medicine, Stanford, CA) overnight at 4 °C. Then muscle samples were incubated with fluorescein isothiocyanate-conjugated goat anti-rabbit IgG overnight at 4 °C. Muscle samples were washed with PBS and mounted in Vectashield mounting medium. Fluorescent images were acquired using a Zeiss LSM 510 Meta confocal microscope.

2.2.3.13 Skeleton Staining

Alizarin red S/alcian blue skeletal preparations were carried out using standard procedures (7). Briefly, neonatal carcasses were skinned and eviscerated. Carcasses were dehydrated in 95% (vol/vol) ethanol for several hours and then incubated in alcian blue staining solution [150 mg/L alcian blue 8GX, 20% (vol/vol) glacial acetic acid, 75% (vol/vol) ethanol] for 2 d with constant rotation. The solution was changed to fresh 95% (vol/vol) ethanol for 12 h with rotation and then to 1% (wt/vol) KOH overnight. The skeletons were transferred to alizarin red S staining solution [25 mg/L alizarin red S, 1% (wt/vol) KOH] for several hours until the bone tissue reached the desired hue. Processed specimens were stored and imaged in one part 70% (vol/vol) ethanol, one part glycerin.

2.2.3.14 Primary Myoblast Cultures

Myoblasts were isolated from the forelimbs and hindlimbs of E18.5 fetuses. Briefly, skin was re- moved from limbs, which were then incubated at 37 °C for 4 h in tissue dissociation buffer [1× PBS, 0.05% (wt/vol) collagenase D (Roche), 2 mM $CaCl_2$, 1×

penicillin/streptomycin/glutamine (Invitrogen)] with shaking at 70 rpm. The dissociated tissue solution was diluted with myoblast culture medium [Ham's F-10 (Invitrogen), 20% (vol/vol) fetal bovine serum (Invitrogen), 1× penicillin/streptomycin (Invitrogen), 2.5 ng/mL human basic fibroblast growth factor (Promega)] and pelleted by centrifugation (150 × g). The pellet was re-suspended in myoblast growth medium, passed through a 70-μm nylon cell strainer, and pre-plated on a 10-cm uncoated cell-culture dish. The cells were incubated for 1.5 h at 37 °C in a humidified incubator with 5% CO_2 atmosphere. The cell suspension was then re-plated onto a 10-cm laminin-coated cell-culture dish. Cells were passaged by trypsinization and pre-plating until relatively homogeneous for myoblasts. Medium was replenished every day. For differentiation, myoblasts were plated on laminin-coated dishes at high density. When the cells were nearing confluence, the culture medium was changed to differentiation medium [DMEM (HyClone), 2% (vol/vol) heat-inactivated horse serum (Invitrogen), 1× penicillin/streptomycin/glutamine (Invitrogen)] for 5 d.

2.2.3.15 Western Blots

Tissue samples were snap-frozen in liquid nitrogen for storage and then dounce-homogenized in RIPA [150 mM NaCl; 1% (vol/vol) IGEPAL CA-630; 50 mM Tris-HCl, pH 8.0; 1% (wt/vol) sodium deoxycholate; 0.1% (wt/vol) sodium dodecyl sulfate; complete protease inhibitor cocktail tablet (Roche)] buffer. Cell cultures were scraped free and collected with RIPA buffer and then snap-frozen. *N*-ethylmaleimide was added at 5 mM final concentration and the samples were incubated on ice for 30 min before boiling with reducing SDS loading buffer. Samples were electrophoresed in denaturing SDS buffer on 6% polyacrylamide gels with no stacking gel for dihydropyridine receptor (DHPR) α1s and RyR1 and an Any kD gel (Bio-Rad) for α-tubulin. Gels were electroblotted onto PVDF membranes with a semidry blotter (Bio-Rad)

and then blocked in 5% (wt/vol) nonfat milk in TBST [25 mM Tris-HCl, pH 7.5; 125 mM NaCl; 0.1% (vol/vol) Tween-20]. Primary antibodies were as follows: DHPR α1s (Thermo Scientific; mouse monoclonal 1A; 1:500), RyR1 (Thermo Scientific; mouse monoclonal 34C; 1:5,000), and α-tubulin (Sigma; mouse monoclonal DM1A; 1:5,000). Primary antibodies were diluted in TBST with 1% (wt/vol) nonfat milk and incubated with blots overnight at 4 °C with rotation. Blots were washed five times with TBST before addition of the secondary antibody in TBST (Bio-Rad; 1:10,000). Blots were incubated with secondary antibody for 30 min at room temperature with vigorous shaking before five washes with TBST. Blots were dipped in West Pico chemiluminescent substrate (Thermo Scientific) and exposed to autoradiographic film.

2.2.4 Results

2.2.4.1 Skeletal Muscle-Specific Expression of Stac3

STAC3 is a 360-amino acid protein containing a polyglutamic acid region (Poly-E), a domain with similarity to the C1 domain of protein kinase C, and two SH3 protein-interaction domains (Figure 2-1A). We determined that *Stac3* expression is highly restricted to skeletal muscle throughout development and into adulthood (Figure 2-1 and Figure 2-7), consistent with *in situ* hybridization studies in zebrafish (ZFIN Database; http://zfin.org). In contrast, the mouse paralogs *Stac* and *Stac2* are excluded from skeletal muscle but are expressed in a variety of other tissues, including the central nervous system (Figure 2-1B). *Stac3* expression was absent in myoblasts but robustly up-regulated upon differentiation of C2C12 myoblasts to myotubes, suggesting a role in mature muscle (Figure 2-8). Interestingly, expression of *Stac3* and its related family members is absent in the heart.

2.2.4.2 Localization of STAC3 to T-tubules

As a first step toward understanding the function of STAC3, we determined the sub-cellular localization of the protein by electroporating an expression plasmid encoding a fusion protein of STAC3-GFP (GFP at the carboxyl end) into mouse flexor digitorum brevis muscles (FDB) *in vivo*. Following a 3-day recovery period, the FDB was imaged directly using two-photon laser scanning microscopy with second harmonic generation to visualize the myosin A bands as an internal reference, as described by DiFranco et al. [14]. STAC3-GFP localized in a repeating doublet pattern with the wider spaces correlating to the myosin heavy chains (Figure 2-1D), consistent with a report describing in vivo localization of the T-tubule protein DHPR α1s to the borders of A bands [22]. Using this technique, it is not possible to determine whether STAC3 localizes along the full length of the T-tubules or more specifically to the triads. Given the critical role of T-tubules in ECC, localization of STAC3 to these structures is consistent with a role in this process.

2.2.4.3 Loss of Stac3 Results in Complete Paralysis and Perinatal Lethality

To further study the expression and function of STAC3 in vivo, we re-derived *Stac3* KO mice from germplasm containing a β-galactosidase (LacZ) reporter gene inserted within the first intron of the *Stac3* locus, disrupting expression of the *Stac3* coding sequence (Figure 2-9). Expression of the *Stac3*-LacZ allele in heterozygous mice was detected as early as embryonic day 9.5 (E9.5) in somites and was robustly expressed in all fetal and postnatal skeletal muscles (Figure 2-10 and Figure 2-11). In concordance with our expression analysis in wild-type (WT) mice, we did not observe LacZ staining in any tissue other than skeletal muscle as examined by whole-mount staining (Figure 2-11).

Mice heterozygous for the LacZ knock-in allele were grossly normal in appearance and behavior. In contrast, *Stac3* homozygous KO mice were born with an overall "lunar" shape, characterized by a generally flaccid appearance, wrist drop, and abnormal spinal curvature (Figure 2-2A). The gross morphology of the KO neonates was similar to that described for mice with severe defects in muscle differentiation [23], neuromuscular junction (NMJ) formation or function [24-26], or ECC [27-30]. KO neonates were born in expected Mendelian ratios from heterozygous crosses of *Stac3*-LacZ knock-in mice, indicating that *Stac3* is not required for embryonic viability (Table 2-1); however, they were completely paralyzed and died rapidly following birth. Histological examination of KO neonatal lungs revealed that the alveoli were markedly smaller than those in comparable sections of WT lungs (Figure 2-2B), and KO lungs were not buoyant in saline. Although the mice were paralyzed, the hearts of *Stac3* KOs were observed beating for several minutes following birth. These results suggest that KO mice expire shortly after birth due to hypoxia resulting from the inability to inspire.

2.2.4.4 Musculoskeletal Defects of Stac3 KO Mice

To investigate the function of *Stac3*, we examined the musculoskeletal system in KO mice. In comparison with WT mice, the appendicular muscles and diaphragm of *Stac3* KO mice appeared smaller and more translucent. Staining of bone and cartilage revealed that the KO skeletons were abnormally kyphotic, with multiple abnormalities involving the ribs, sternum, and costal cartilages (Figure 2-2C). KO skeletons also had a dramatic reduction in bone ridge formation at major muscle insertion sites, including the deltoid tuberosity of the humerus and the trochanters of the femurs (Figure 2-12). Because bone growth at these sites requires muscle development and function, this evidence supports the conclusion that KO mice are paralyzed throughout development [31].

Based on the striking similarity between *Stac3* KO mice and other paralytic muscle phenotypes, we hypothesized that *Stac3* may be critical for muscle differentiation, NMJ formation, or ECC. Fundamental defects in muscle differentiation could be ruled out because skeletal muscle was formed in KO mice, albeit with reduced mass and aberrant morphology (Figure 2-2D). Myofibers from KO mice were clearly multinucleated in H&E sections, but the nuclei were typically seen clustered together instead of being distributed uniformly along the fiber as in normal muscle. Myonuclei of KO fibers also failed to migrate to the periphery of the fibers by E18.5, compared with WT muscle. Whereas striations were rarely observed in some regions of the KO muscle, visualized by H&E staining, overall the fibers appeared mottled and vacuolated. Transmission electron microscopy of tongue muscle demonstrated myofibril formation, although there were obvious signs of structural heterogeneity and disorganization in the KO (Figure 2-2E and Figure 2-13). In culture, primary myoblasts isolated from E18.5 forelimbs and hindlimbs of KO fetuses differentiated and fused normally, yielding multinucleated myotubes. However, differentiated KO myotubes never spontaneously twitched, as observed in cultures of normal myotubes. We conclude that although there are clear defects in muscle maturation, mass, and morphology, myoblast differentiation or fusion can occur in the absence of STAC3.

2.2.4.5 Neuromuscular Junctions Are Functional in Stac3 KO Mice

To determine whether the absence of STAC3 disrupts NMJ formation or function, we labeled acetylcholine receptors of E18.5 diaphragms with Texas red α-bungarotoxin and the phrenic nerve with an antibody against syntaxin (Figure 2-3). In the *Stac3* KO muscles, we found that NMJs were properly formed, with the nerve terminals directly apposing acetylcholine receptor clusters of the muscle (Figure 2-3B). However, there was increased branching of the

phrenic nerve and a slightly broader spatial distribution of the NMJs (Figure 2-3A), both of which are features that were previously described in mice lacking key components of ECC [32-34]. Interestingly, E18.5 KO diaphragms displayed an in- crease in miniature end-plate potentials (Figure 2-4), a feature reported previously with loss of ECC components [34]. We observed normal evoked end-plate potentials following electrical stimulation of the phrenic nerve (Figure 2-4 C and D). Muscle action potentials were also comparable in WT and KO mice, but the action potentials failed to induce contraction in the KO muscles (Figure 2-4E). These experiments demonstrate that STAC3 is not required for synaptic transmission or development of the NMJ, nor is it required for action potential generation or propagation. Because no contraction was observed in response to muscle action potentials evoked by nerve stimulation, the defect in the KO muscle must lie downstream of excitation.

2.2.4.6 Lack of Depolarization-Evoked Contraction in the Absence of STAC3

To further examine the mechanistic basis for the lack of electrically induced contraction in *Stac3* KO muscle, we conducted muscle contraction assays on dissected diaphragms from E18.5 embryos. Indeed, electrical field stimulation of WT or heterozygous (Het) diaphragms triggered robust contractions at all tested frequencies, but contractions of the KO diaphragms were barely detectable (Figure 2-5A). We tested whether addition of the RyR agonist 4-CMC could induce contraction, and found that 4-CMC–induced contractions in normal and KO diaphragms generated approximately the same magnitude of force when normalized for differences in muscle weight. Diaphragms from the KO mice were also insensitive to membrane depolarization with potassium chloride (Figure 2-5B). These results indicate that SR Ca^{2+} stores in the KO muscles are adequate for contraction and that the contractile apparatus functions normally, despite the disorganization observed by histology and electron microscopy. Therefore,

these abnormalities likely arise secondarily to complete lack of muscle function in the absence of STAC3.

2.2.4.7 Stac3 KO Myotubes Lack Depolarization-Induced Calcium Transients

From the muscle contraction experiments, we concluded that loss of *Stac3* likely blocks voltage-induced Ca^{2+} release from the SR. To test this hypothesis directly, we isolated myoblasts from E18.5 embryos and differentiated them in vitro. Next, we loaded normal and KO myotubes with the fluorescent Ca^{2+} indicator fluo-4-AM and imaged these cells during depolarization with KCl and stimulation with 4-CMC. In the absence of stimulation, we found spontaneous twitch-associated Ca^{2+} transients in WT and Het myotubes, but no spontaneous Ca^{2+} transients were seen in KO myotubes (Figure 2-5C). Occasionally, we observed slowly propagating waves of Ca^{2+} in KO myotubes, but never rapid, synchronous transients involving the entire myotube. Application of 120 mM KCl to WT or Het myotubes caused massive synchronous Ca^{2+} transients, whereas KO myotubes were unresponsive; however, Het and KO myotubes responded similarly to application of 4-CMC. These experiments demonstrate that the complete paralysis seen in *Stac3* KO mice results from a defect in voltage-induced Ca^{2+} release from the SR.

2.2.4.8 Expression of Known ECC Components in Stac3 KO Muscle

Collectively, our data reveal a previously unrecognized but essential role for STAC3 in voltage-induced Ca^{2+} release and consequently skeletal muscle contraction. This phenomenon may result from reduced expression or mislocalization of DHPR or RyR1, but we found that mRNA levels of these components are similar in WT and KO muscles (Figure 2-14A) and that KO muscles responded normally to 4-CMC, indicating normal RyR function (Figure 2-5C and Figure 2-15). Protein levels of DHPR α1s and RyR1 were decreased, but not absent, in tongue

muscle of KO compared with WT mice at E18.5 (Figure 2-14B). In primary myotube cultures, we found that expression of these components was slightly increased in the KO above those of Het myotubes, suggesting that there may be compensation in these cells or that the expression of these components in embryonic muscle may be dependent upon muscle use.

2.2.5 Discussion

The results of this study identify STAC3 as a previously unrecognized regulator of skeletal muscle contraction and demonstrate that STAC3 is required for voltage-induced Ca^{2+} release from the SR. Although the exact mechanism by which STAC3 functions in this process is still unknown, our results suggest that it is functionally involved in the coupling of voltage changes in the plasma membrane to Ca^{2+} release from the SR.

While this work was being completed, two other reports described the requirement of *Stac3* for skeletal muscle function, but the mechanistic basis of its role was unclear. Bower et al. reported that *Stac3* is required for myotube formation and differentiation of skeletal myoblasts in zebrafish, based on morpholino knockdown studies in zebrafish embryos and RNAi in cultured C2C12 mouse myoblasts [35]. In contrast, our results clearly demonstrate that *Stac3* is not required for myofiber formation in mice, and that myoblasts from *Stac3* KO mice differentiate in culture. Reinholt et al. described the lethal skeletal muscle phenotype of mice with the same insertional mutation analyzed in our studies [36]. They concluded that *Stac3* was required for correct sub-cellular localization of myonuclei and also that *Stac3* KO mice may have increased myoblast fusion. Although myofibers from *Stac3* KO mice are dysmorphic, our results suggest that this defect, as well as abnormalities in sub-cellular structure, result secondarily from the complete absence of muscle contractility, rather than from a primary role of STAC3 in these processes. Indeed, our finding that *Stac3* KO muscle is unresponsive to depolarization, but that

contraction can be rescued by exposure to the RyR agonist 4-CMC, demonstrates that the primary defect in these mice is the complete loss of voltage-dependent Ca^{2+} release from the SR. Thus, we can only conclude that other abnormalities result primarily from lack of Ca^{2+} transients or contraction.

We found that loss of *Stac3* in muscle results in non- autonomous effects on the skeleton and motor neurons. Although this pattern of defects is known to result from loss of ECC, the underlying mechanisms are still somewhat vague. Skeletal defects have been hypothesized to result from lack of mechanical stimulation of bone and maintenance of posture *in utero* [31]. Increased phrenic nerve branching and miniature end-plate potentials have been shown in other ECC null mutants, including muscular dysgenesis (DHPR α1s null), DHPR β1 null, and RyR1 null mice. The exact cause of this phenomenon is unclear, but it demonstrates the interdependence of muscle and motor neuron development and the importance of ECC in these processes.

Because STAC3 is a skeletal muscle-specific protein with no paralog in cardiac muscle, it is likely that it specifically facilitates skeletal-type ECC. To do this, STAC3 may act upon either DHPR or RyR to facilitate their activation or localization (Figure 2-6). Accordingly, STAC3 may be involved in the formation, trafficking, or stability of the DHPR complex or the formation of tetrads, the skeletal muscle-specific Ca^{2+} release units. Another possibility is that STAC3 may directly couple DHPR to RyR1 by a conformation-dependent mechanism, because these channels have long been known to physically interact, but conclusive evidence of direct interaction has been elusive. Further work will be necessary to fully elucidate the function of STAC3 in regard to its possible molecular interactions with other ECC components. Although

STAC3 is required for voltage-induced Ca^{2+} release in skeletal muscle, there may still be unknown proteins that are required for this process with which STAC3 might interact.

Because mutations in other ECC components are known to cause muscle diseases, it is expected that mutations in *Stac3* likely cause disease as well. Identification of individuals with hypomorphic or gain-of-function mutations in *Stac3* could be instrumental in understanding the function of this gene. For instance, are there mutations in *Stac3* that result in altered RyR1 gating, possibly resulting in susceptibility to malignant hyperthermia, nemaline myopathy, central core disease, or multiminicore disease? It would also be interesting to know whether *Stac* or *Stac2* can rescue the KO myotubes and whether chimeras between *Stac3* and these genes might be useful study tools. Finally, it would be interesting to explore whether *Stac3* paralogs may be involved in Ca^{2+} signaling in their respective tissues.

2.2.6 Figures

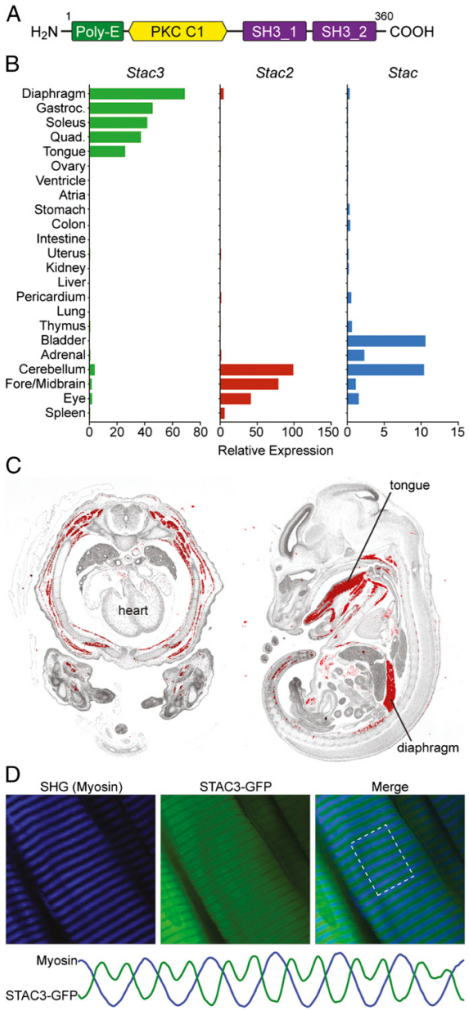

Figure 2-1. Domain structure and expression of *Stac3*.

(*A*) The domain architecture of STAC3 consists of a region containing 11 consecutive glutamic acid residues (Poly- E), a protein kinase C (PKC) C1 domain, and two SH3 protein-interaction domains. Scales of each domain are not directly proportional. (*B*) Expression profiles of *Stac*, *Stac2*, and *Stac3* determined by real-time PCR in adult mouse tissues. (*C*) In situ hybridization of an E14.5 mouse transverse thorax (*Left*) and an E15.5 sagittal section (*Right*) shows skeletal muscle-specific expression of Stac3. Hybridization signal is pseudocolored red. (*D*) T-tubule localization of STAC3. Flexor digitorum brevis muscles were electroporated *in vivo* with a *Stac3* C-terminal GFP fusion construct, and the live muscle was imaged after a 3-d recovery period. The fusion protein localized in a repeating doublet pattern alternating with the myosin A bands, as visualized by second harmonic generation (SHG). This pattern is consistent with localization to T-tubules. The plots for each channel, shown at the bottom, were generated using the ImageJ Plot Profiler tool within the highlighted region. The scales of these plots were arbitrarily adjusted to compare the patterns.

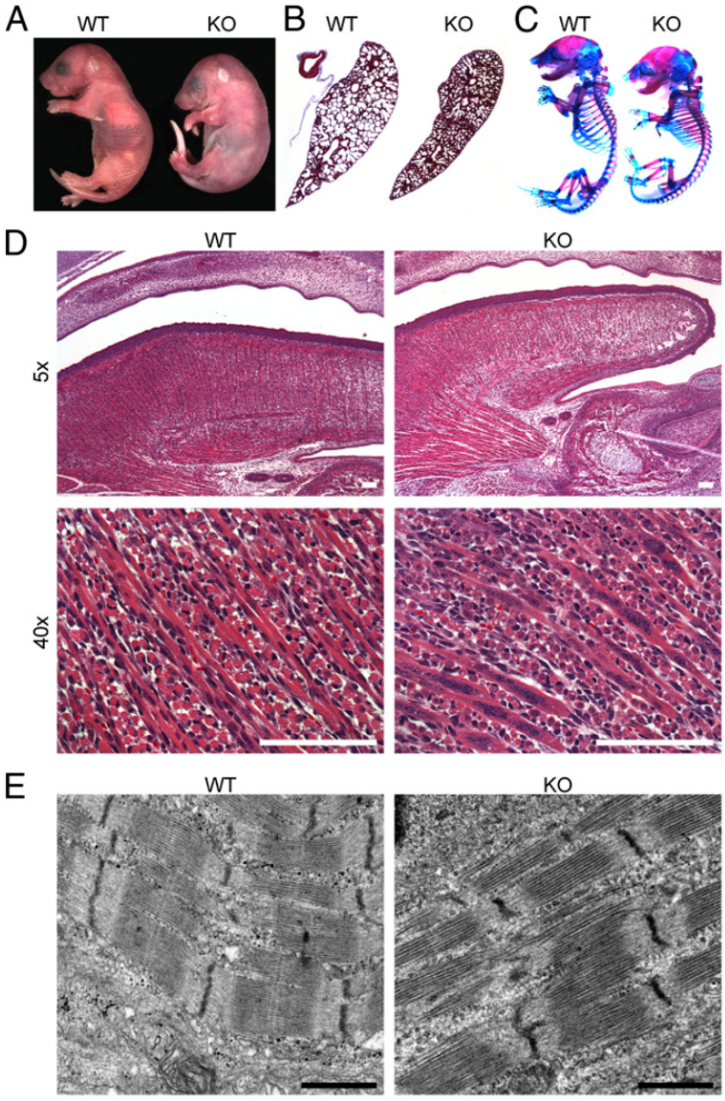

Figure 2-2. Abnormalities of *Stac3* KO mice.

(*A*) Complete paralysis, wrist drop, and abnormally rounded lunar appearance of a newborn *Stac3* KO mouse. (*B*) Alveoli of KO lungs are not inflated, as shown by Masson's trichrome staining. (*C*) Whole-mount E18.5 skeletons prepared with alcian blue, a cartilage stain, and alizarin red S, a bone stain, show numerous abnormalities in KOs, including abnormal spinal curvature, growth defects in costal cartilages, and decreased bone formation at muscle insertion sites. (*D*) H&E sagittal paraffin sections of E16.5 heads show decreased muscle mass of the tongue and abnormal clustering of nuclei in KOs. KO fibers also have fewer observable striations, and most have a vacuolated appearance. (*E*) Electron microscopy of E15.5 tongues shows that sarcomeres are present in KO fibers as seen here but overall, sarcomeres appear more disorganized (Figure 2-13). (Scale bars, 1 μm.)

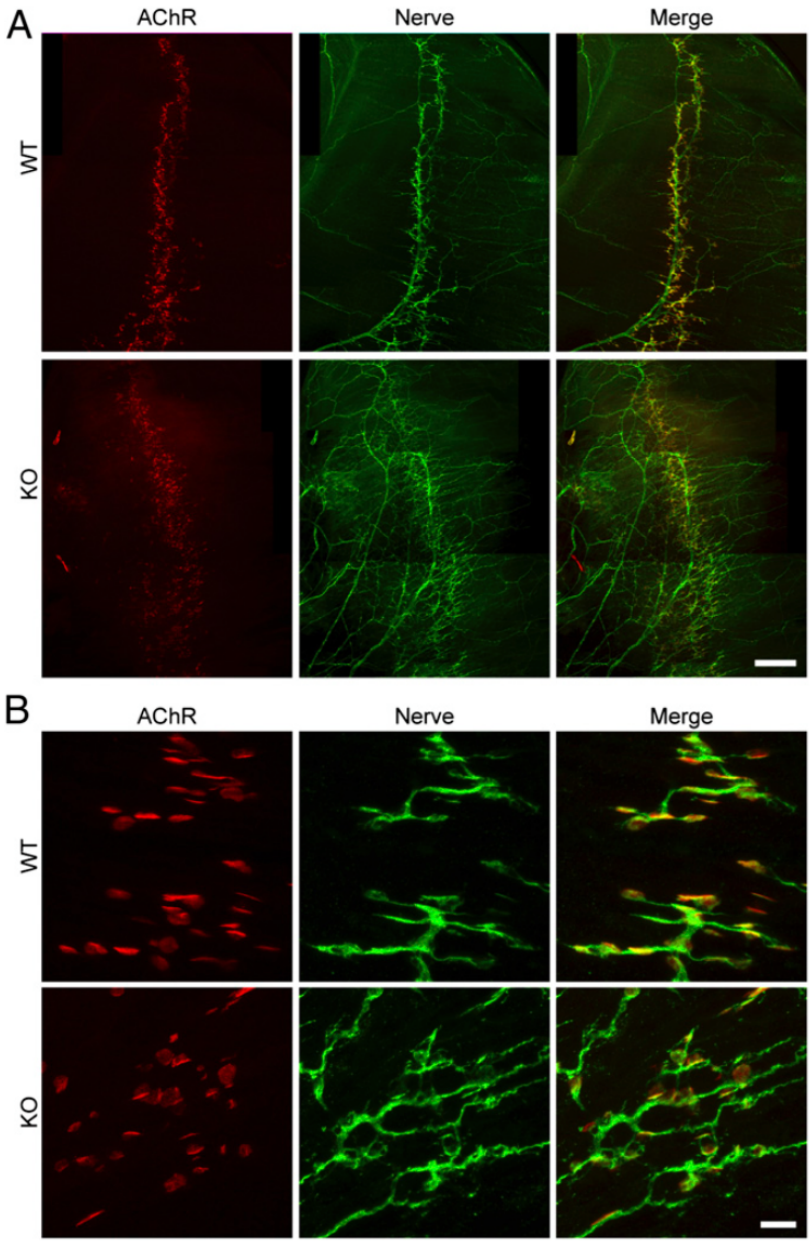

Figure 2-3. Normal NMJ formation but increased nerve branching in KO mice.

Whole mounts of E18.5 diaphragm muscles were double-stained with Texas red α-bungarotoxin to label postsynaptic AChRs and an antibody against syntaxin to label presynaptic nerves. In both WT and KO muscles, presynaptic nerve terminals formed in juxtaposition with postsynaptic AChR clusters (*B*). However, there were increased nerve branching and defasciculation in the KO diaphragm compared with the WT (*A*). AChR clusters also occupied a broader area in the central region of the KO diaphragm. [Scale bars, 400 μm (*A*), 20 μm (*B*).]

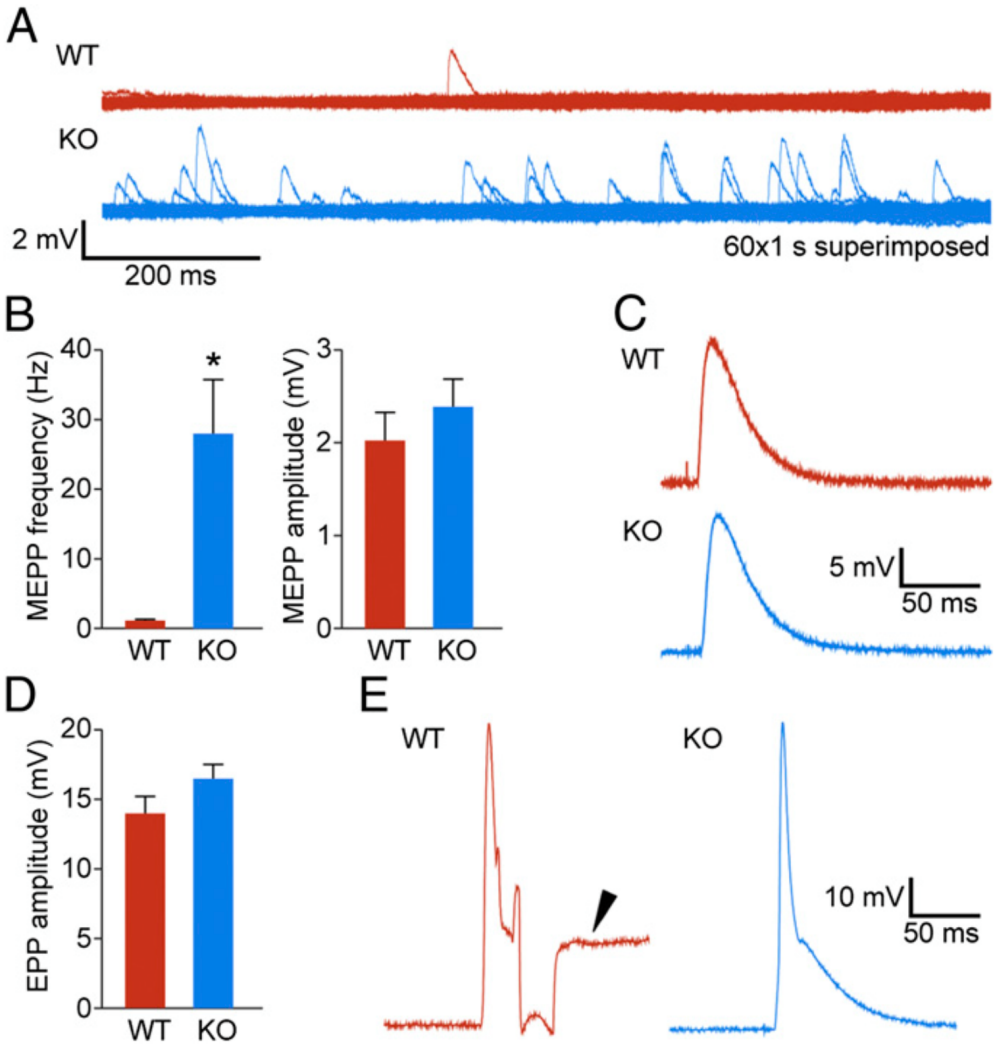

Figure 2-4. Increased neuromuscular synaptic activity.

(*A*) Examples of miniature end-plate potential (mEPP) traces obtained from 1-min continuous recording (superimposed traces are shown; 60×, 1-s). mEPP frequencies were significantly increased in E18.5 KO mice compared with WT. (*B*) Quantification of mEPP frequencies and amplitudes. Frequency: KO (27.99 ± 7.73 events per min, $n = 22$ cells), WT (1.15 ± 0.13 events per min, $n = 13$ cells), $^*P < 0.05$; mEPP amplitude (no statistical difference): KO (2.4 ± 0.3 mV, $n = 22$ cells), WT (2.04 ± 0.3 mV, $n = 13$ cells). (*C*) Sample traces of end-plate potentials. (*D*) Quantification of EPP amplitudes (no statistical difference): WT (14 ± 1.44 mV, $n = 9$ cells) and KO (16.46 ± 1.01 mV, $n = 16$ cells). Statistical data are represented as mean ± SEM. (*E*) Traces of muscle action potentials are comparable in WT and KO. The arrowhead indicates a contraction artifact, which was not observed in KO muscles due to their paralysis.

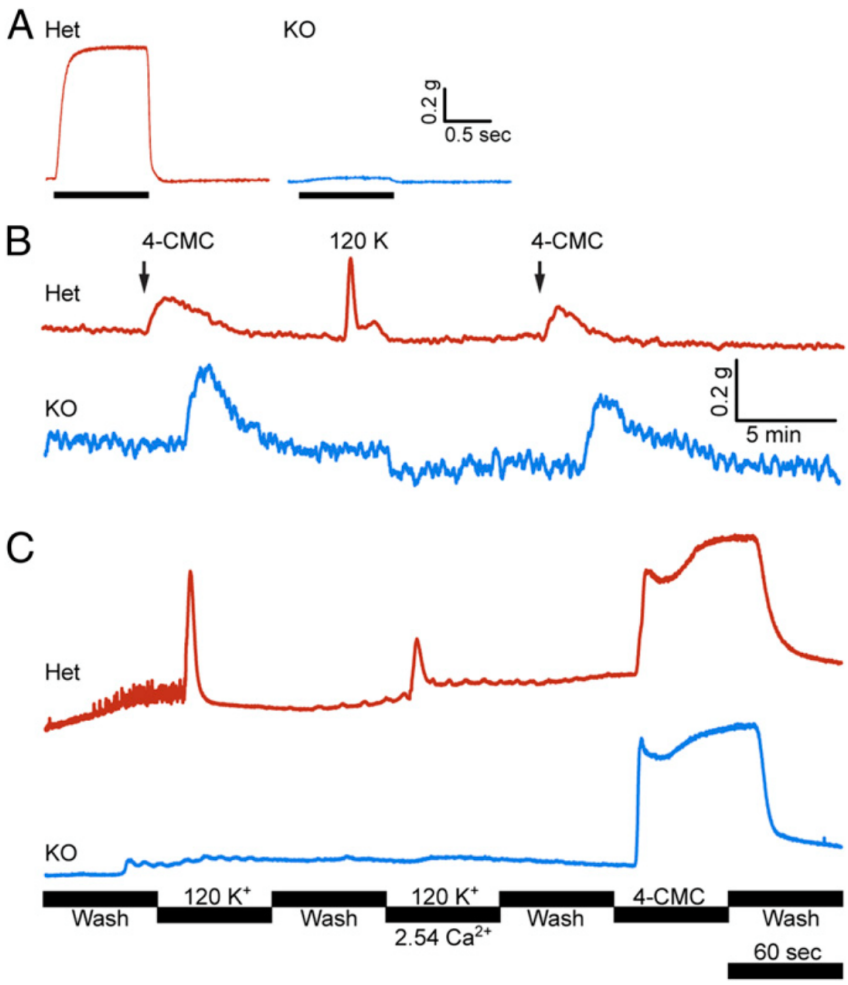

Figure 2-5. Muscle contraction and calcium transients.

(*A*) Contraction of E18.5 diaphragm was elicited by electrical field stimulation (50 Hz, 1-ms pulses) and measured with a force transducer. Stimulation yielded robust tetanic contraction in normal diaphragms, but barely detectable contraction in KOs. (*B*) Force measurements of diaphragm with application of 120 mM KCl and 1 mM 4-CMC. Het and KO responded comparably to 4-CMC when normalized for differences in weight, but the KO tissue was unresponsive to membrane depolarization by KCl. The amplitudes of the traces in A and B were normalized to the specimen weight. (*C*) Cultured myotubes loaded with the fluorescent calcium indicator fluo-4-AM. The cells were perfused continuously and the calcium transients were recorded with an inverted microscope. Het cells responded synchronously to KCl application and to 4-CMC. KO myotubes were unresponsive to KCl, but responded comparably with Het with application of 4-CMC. Each fluo-4-AM trace is the mean of ~10 myotubes within the field.

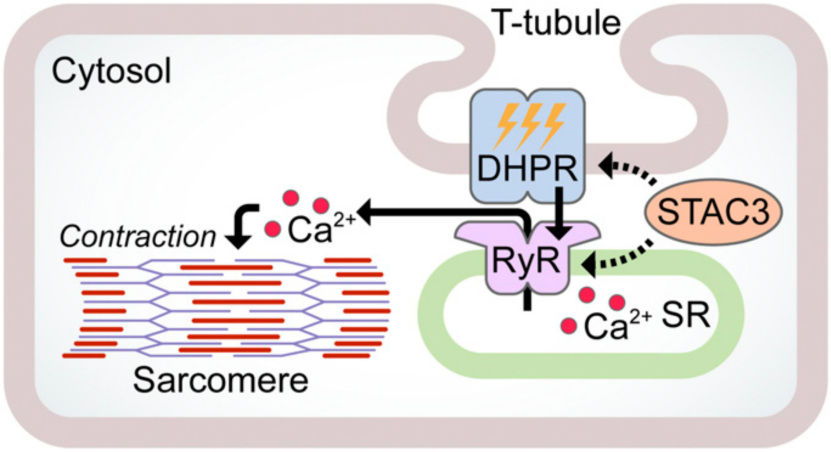

Figure 2-6. Hypothetical model of STAC3 function.

Upon activation of DHPR by an action potential, a conformational change is transmitted to RyR in the SR membrane, resulting in SR calcium release and sarcomere contraction. STAC3 may facilitate this process by interaction with DHPR, RyR, or both.

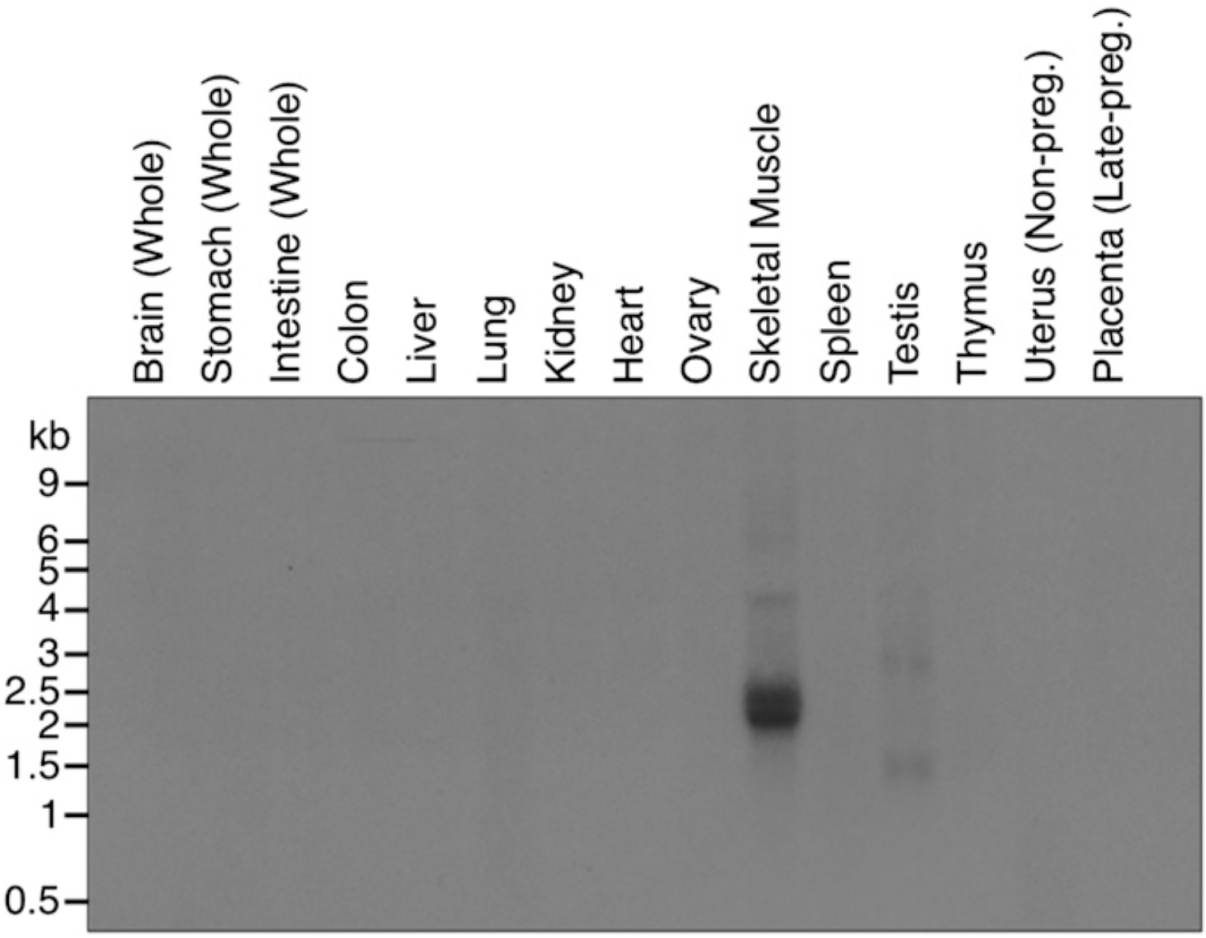

Figure 2-7. Multi-tissue northern blot.

A multi-tissue Northern blot shows expression of *Stac3* mRNA exclusively in adult skeletal muscle tissue. The double bands in skeletal muscle suggest two mRNA isoforms.

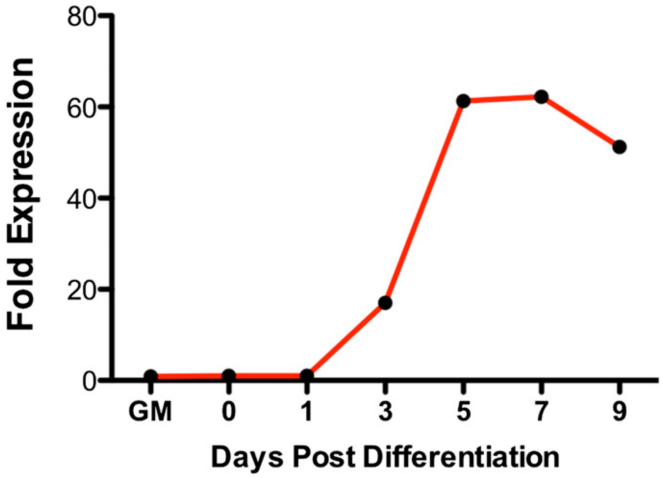

Figure 2-8. *Stac3* expression during C2C12 myoblast differentiation.

Over the course of differentiation, *Stac3* mRNA increases dramatically. Expression was measured by real-time PCR during differentiation of C2C12 myoblasts. The time course spans from proliferating myoblasts in growth medium (GM) to 9 d of differentiation medium. Values are fold over day 0.

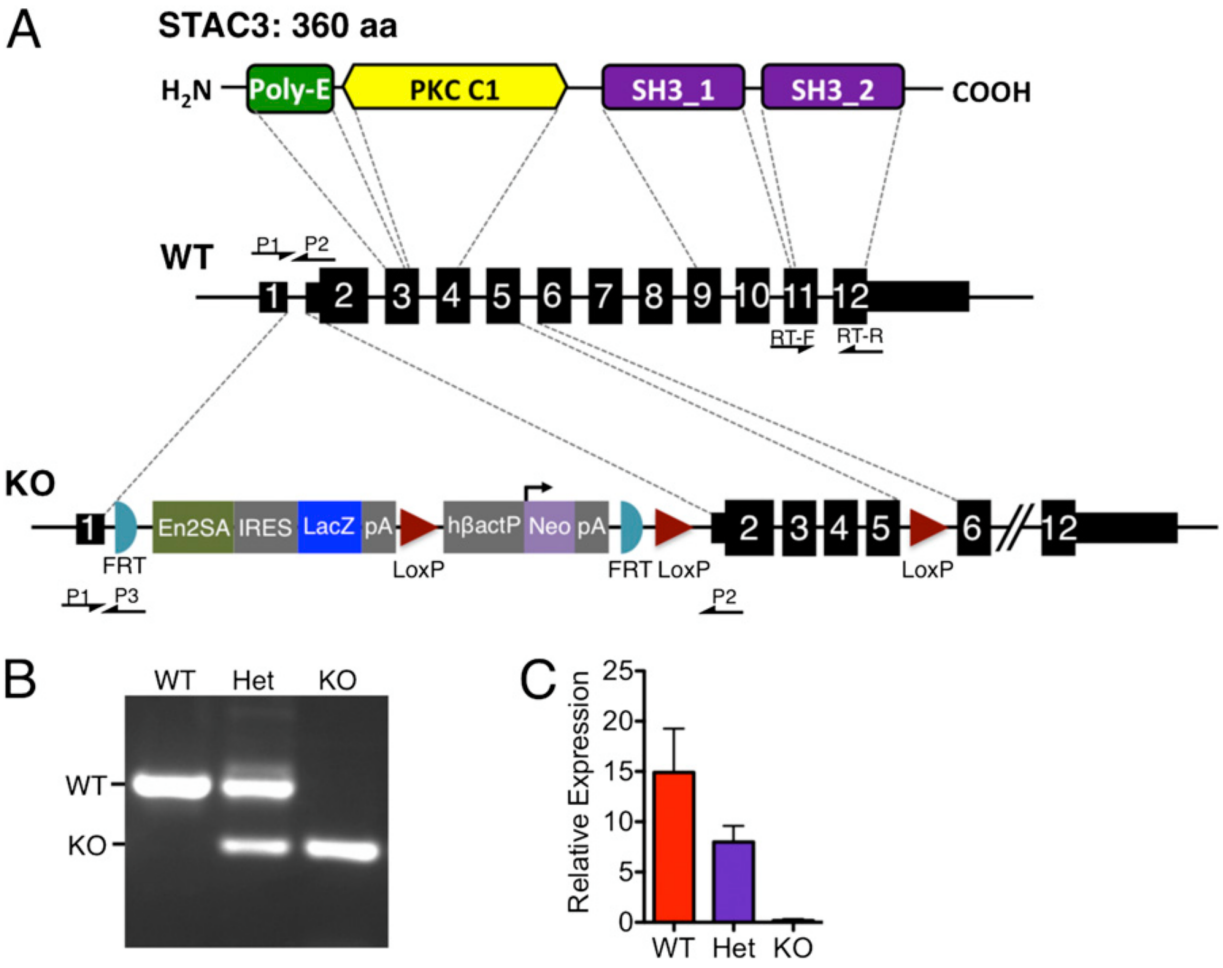

Figure 2-9. Knockout mouse allele.

(*A*) The National Institutes of Health Knock-Out Mouse Project "knockout first" allele for the *Stac3* locus, containing two FLP recombinase target sequences (FRT), an engrailed 2 splice acceptor (En2SA), an internal ribosome entry site (IRES), β-galactosidase (LacZ), two polyadenylation sequences (pA), three cre recombinase target sequences (LoxP), human β-actin promoter (hβactP), and a neomycin resistance gene (Neo) inserted into the first intron of the *Stac3* locus. Scale is not proportionally accurate. Poly-E, 11 consecutive glutamic acid residues; PKC C1, protein kinase C C1 domain-like; SH3, src homology 3. (*B*) Genotype-specific multiplex PCR using primers P1, P2, and P3 shows homozygosity of the knockout allele. Het, heterozygous. (*C*) Real-time PCR for *Stac3* demonstrating elimination of the transcript in E18.5 hindlimb muscles using primers RT-F and RT-R (mean ± SD; $n = 4$ for WT and KO, $n = 8$ for Het).

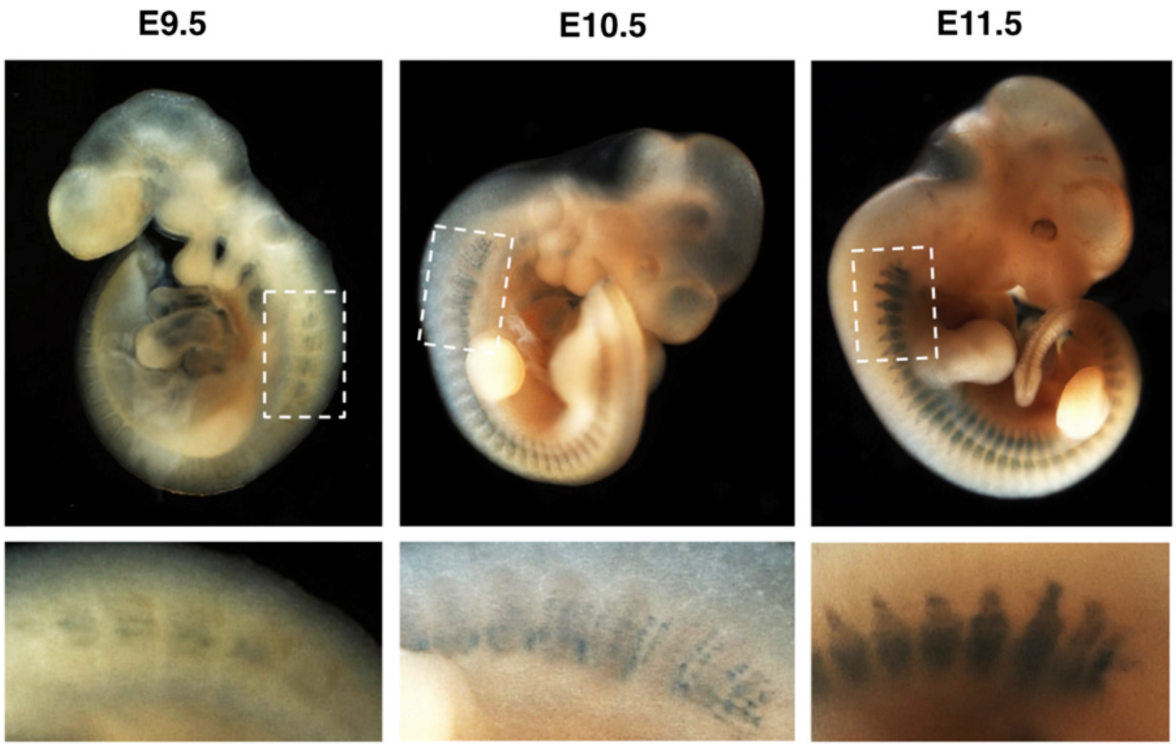

Figure 2-10. Expression of the *Stac3*-LacZ knockin in embryogenesis.

Expression of the *Stac3*-LacZ knock-in allele is observed in somites at early stages in muscle development. Shown here are E9.5, E10.5, and E11.5. (*Lower*) Zoomed-in images from the boxed portions (*Upper*). Heterozygotes are shown.

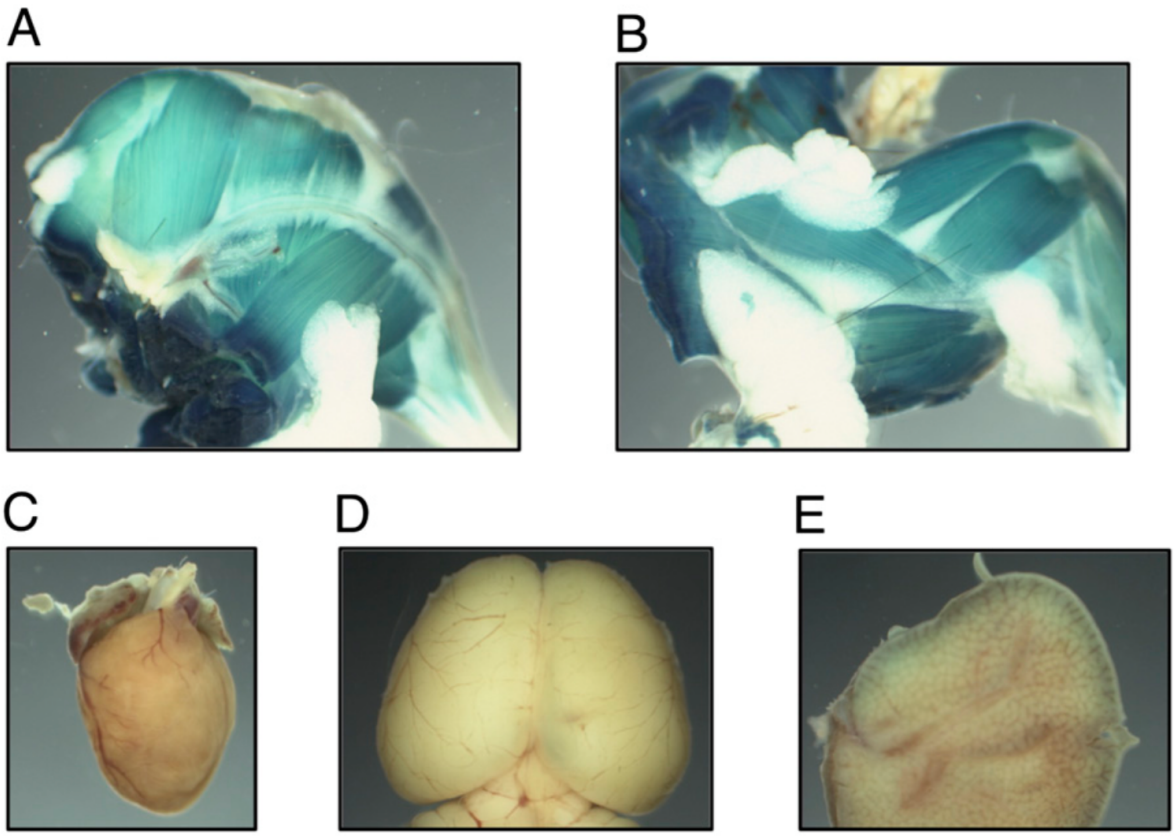

Figure 2-11. Expression of the *Stac3*-LacZ knock-in in postnatal mice.

The *Stac3*-LacZ knock-in allele is robustly expressed in postnatal skeletal muscle, but not in any other tissues. (*A*) Medial hindlimb. (*B*) Lateral hindlimb. (*C*) Heart. (*D*) Brain. (*E*) Liver. A heterozygous adult is shown.

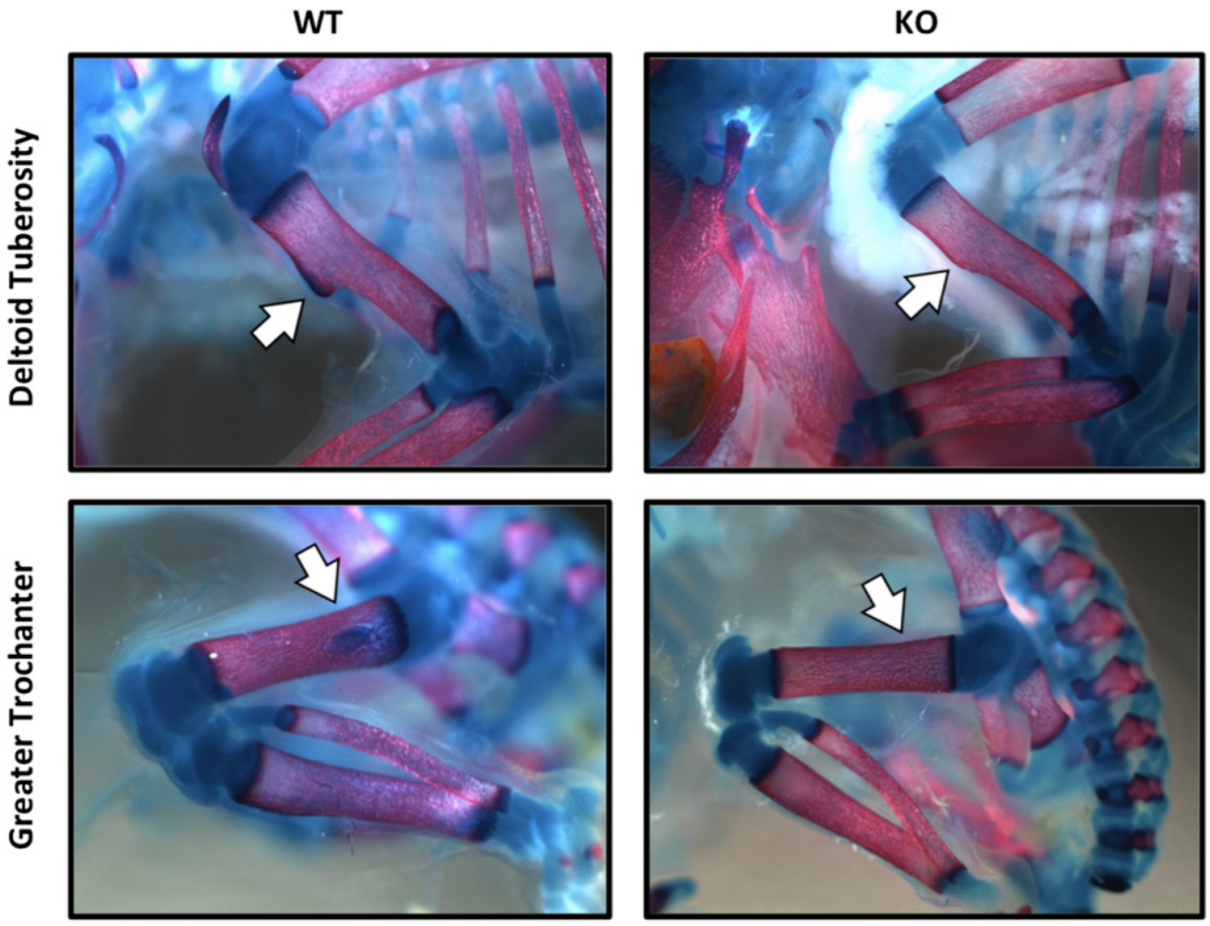

Figure 2-12. Decreased bone development at muscle insertion sites.

The deltoid tuberosity (arrows in *Upper*) and greater trochanter (arrows in *Lower*) of the femur are severely underdeveloped in KO mice, suggesting lack of fetal muscle contraction. Remaining cervical and scapular fat tissue is also visible in the knockouts.

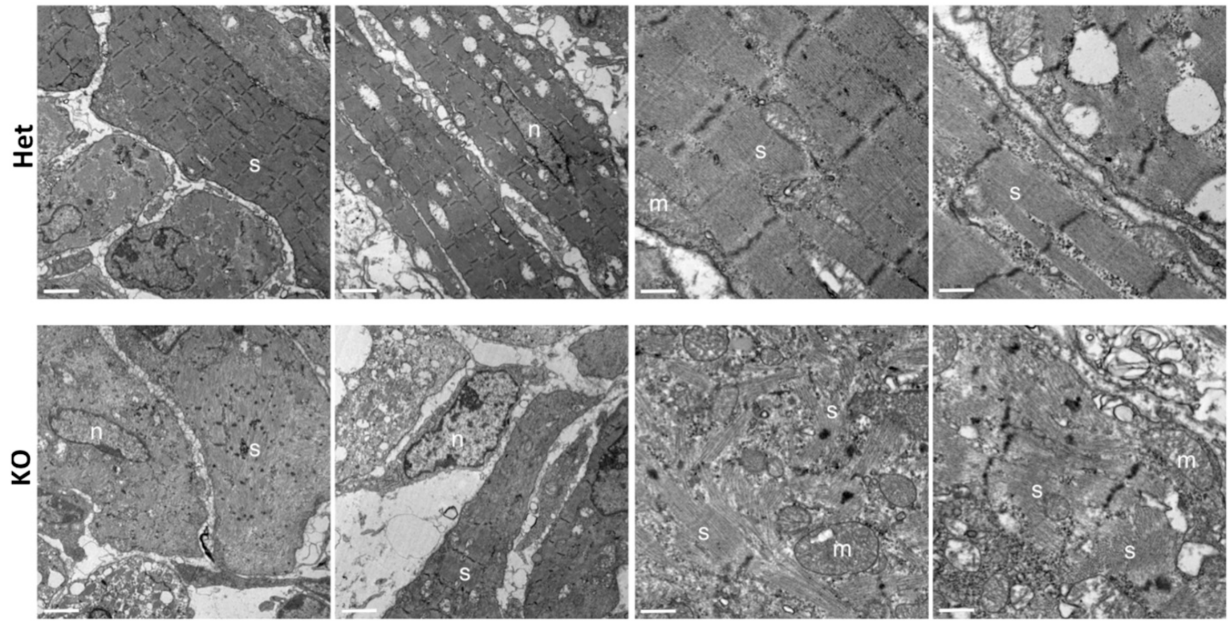

Figure 2-13. Transmission electron microscopy of E18.5 tongues.

Transmission electron microscopy images of tongues from *Stac3* Het and KO E18.5 mice shows the presence of sarcomeres in KO muscle, but with marked disorganization compared with a heterozygous littermate. [Scale bars, 2 μm (Left two images), 0.5 μm (Right two images).] m, mitochondrion; n, nucleus; s, sarcomere.

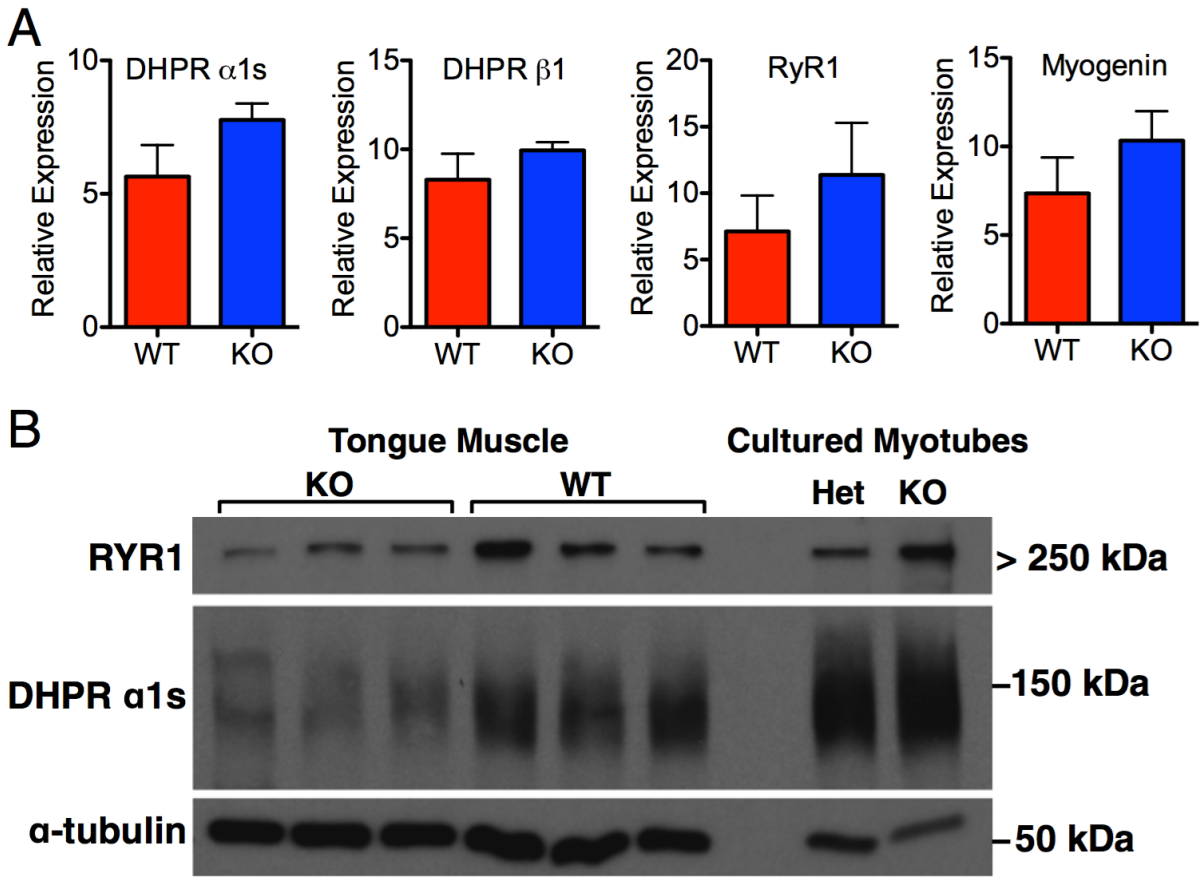

Figure 2-14. Expression of known excitation–contraction (EC) coupling components.

(*A*) mRNA expression of the ECC components DHPR α1s and β1 subunits and RyR1 is normal in E18.5 hindlimb muscles, as well as the skeletal muscle master transcription factor myogenin (mean ± SD; $n = 4$ for each genotype). (*B*) Protein expression of DHPR α1s and RyR1 by Western blot shows a reduction in E18.5 tongues but not in cultured myotubes (*Far Right*).

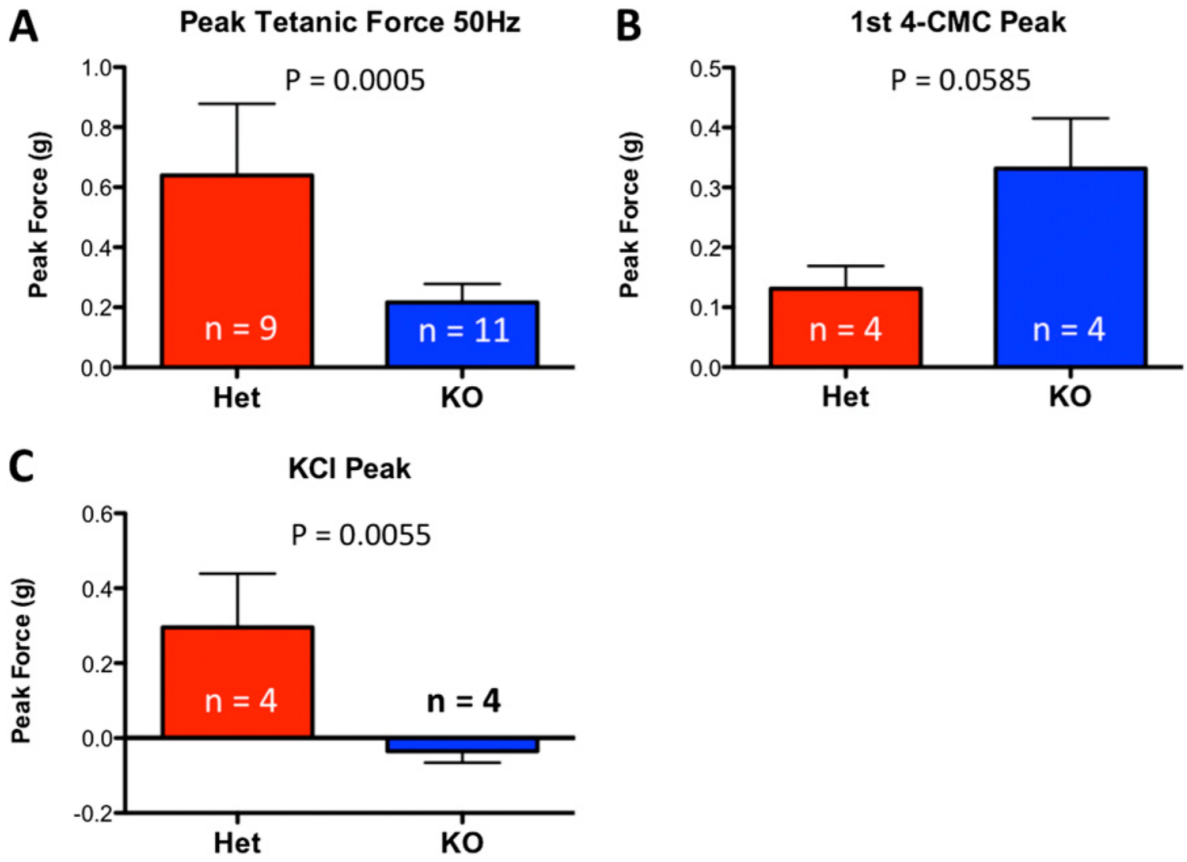

Figure 2-15. Quantification of contraction assays.

(*A*) Peak force in response to tetanic stimulus in E18.5 diaphragms is significantly reduced in STAC3 KO mice. (*B*) Peak force in response to the first 4-CMC application (a representative trace is shown in Figure 2-5B) is comparable in Het and KO diaphragms, but (*C*) is significantly reduced in KOs in response to KCl application. All values are weight-normalized means ± SD; *P* values were calculated using Student's unpaired *t* test.

2.2.7 Tables

Table 2-1. *Stac3*$^{-/-}$ mice are born in expected ratios.

E18.5	**+/+, *n* (%)**	**+/-, *n* (%)**	**-/-, *n* (%)**
Observed	14 (30)	17 (37)	15 (33)
Expected	11.5 (25)	23 (50)	11.5 (25)

Mice resulting from *Stac3*$^{+/-}$ crosses were born in the expected Mendelian ratios. χ^2 two-tailed *P* value = 0.2045.

2.3 EPILOGUE

Since publication of the findings outlined in section 2.2, some additional information has emerged concerning the function of *Stac3*. These recent studies and how they fit with our findings will be discussed below.

The same day that our paper was accepted for publication in *Proceedings of the National Academy of Sciences USA*, an excellent paper was published in *Nature Communications* by another group investigating the role of *stac3* in zebrafish [37]. Concordant with our observation that ECC is completely disrupted in *Stac3* knockout mice, they observed embryonic paralysis in their *stac3*^{mi34} homozygous mutant mice. Unlike our finding, however, they report normal sarcomere structure and triad formation as well as residual calcium flux in fast-twitch muscle groups. Given the clear requirement for *Stac3* in mouse, the most likely explanation is that in zebrafish wild-type *stac3* transcript is maternally inherited as they show, and this mRNA is sufficient for early muscle development.

Horstick et al. also reported that Stac3-GFP co-immunoprecipitates with DHPR α1s and RYR1β by mass spectrometry and that a Stac3 antibody can detect protein from DHPR α1 or RyR immunoprecipitation. While this seems reasonable, at least from a teleological perspective, this conclusion is relatively weak based on the evidence presented. In the case of the GFP pulldown and mass spectrometry, the control experiments are insufficient to demonstrate the specificity of these findings. The experiment compared immunoprecipitation of Stac3-GFP by a GFP antibody or IgG, but only the GFP precipitation was used for mass spectrometry. Furthermore, only selected protein hits are reported, which precludes critical interpretation by the reader. Last, the number of hits on the proteins shown is relatively low given their extremely large size. The western blot experiments are also concerning because of the protein size shown in

the blots. Although the size shown in their figures is the same as the predicted size, we have found in our hands that the apparent molecular weight of STAC3 is greater than 50 kDa (data not shown). This raises concerns about the specificity of the custom Stac3 antibody used in these experiments, although it is possible that this discrepancy could arise from species-specific differences.

Horstick et al. additionally report that a mutation in the first SH3 domain of *STAC3* is responsible for the rare human disease, Native American Myopathy. These patients suffer from severe muscle hypotonia and susceptibility to malignant hyperthermia. This finding is consistent with the clear necessity for *Stac3* in ECC in mice, but it is clear that some residual function of the protein is preserved given that the disease is much less severe than we observed in null mice.

More recently a report from Kurt Beam's lab has shown that STAC3 promotes plasma membrane expression of DHPR α1s in non-myocytes [38]. They show, too, that expression of DHPR α1s or DHPR α1c re-localizes STAC3 to the plasma membrane, whereas it is cytoplasmic in isolation. They also report that co-expression of STAC3 or STAC2 with DHPR α1s prolongs the inactivation of the channel. This may help to explain the function of other *Stac3* family members in neuronal tissues where other DHPR isoforms are expressed. Notably, this function appears to be unnecessary in the heart since no *Stac* family member is expressed there.

Currently the precise molecular mechanism that STAC3 fulfills in ECC is unknown, but there are several viable hypotheses. One is that STAC3 facilitates plasma membrane localization of the DHPR α1s subunit. Lack of membrane inserted DHPR α1s would certainly explain the complete lack of ECC that we observed. Another is that STAC3 stabilizes the DHPR or its ability to form tetrads, possibly through multiple contacts. This explanation is less satisfactory,

since calcium flux through the DHPR α1s pore would still be expected to cause calcium-induced calcium release as occurs in the heart despite a lack of organized tetrads. However, destabilization of DHPR α1s could foreseeably decrease the expression of the protein in the plasma membrane and possibly contribute or lead to the first explanation. Lastly, no evidence has ruled out the possibility that STAC3 may be the physical coupling unit between DHPR α1s and the RYR. It is possible then that STAC3 is necessary for retrograde stabilization of the DHPR α1s through contacts with RYR, since RYR expression has been reported to affect expression and function of DHPR α1s [4]. This explanation would be the most parsimonious, since it would also encompass the explanations above.

STAC3 has well-conserved electrostatic regions, including a negatively charged polyglutamic acid domain upstream of the C1 domain, which itself contains a positively charged face. Positively charged proteins such as the *peptide A-10* region of DHPR [8, 39-41], polylysine [42], the scorpion toxin maurocalcine [43-48] have been shown to potently activate the RYR. It seems conceivable that STAC3 may reversibly activate the RYR through the positively charged C1 domain, perhaps using the negatively charged helix of the RYR that is reported to bind and activate by calcium [49]. This interaction may be quenched by conformational changes that block the C1 domain with the polyglutamic acid region in an autoinhibitory fashion. This activating function is merely speculation at present, but it should be testable in future studies.

2.4 REFERENCES

1. Nelson, B.R., et al., *Skeletal muscle-specific T-tubule protein STAC3 mediates voltage-induced Ca2+ release and contractility.* Proc Natl Acad Sci U S A, 2013. **110**(29): p. 11881-6.

2. Block, B.A., et al., *Structural evidence for direct interaction between the molecular components of the transverse tubule/sarcoplasmic reticulum junction in skeletal muscle.* J Cell Biol, 1988. **107**(6 Pt 2): p. 2587-600.

3. Tanabe, T., et al., *Regions of the skeletal muscle dihydropyridine receptor critical for excitation-contraction coupling.* Nature, 1990. **346**(6284): p. 567-9.

4. Nakai, J., et al., *Enhanced dihydropyridine receptor channel activity in the presence of ryanodine receptor.* Nature, 1996. **380**(6569): p. 72-5.

5. Paolini, C., et al., *Evidence for conformational coupling between two calcium channels.* Proc Natl Acad Sci U S A, 2004. **101**(34): p. 12748-52.

6. Kugler, G., et al., *Structural requirements of the dihydropyridine receptor alpha1S II-III loop for skeletal-type excitation-contraction coupling.* J Biol Chem, 2004. **279**(6): p. 4721-8.

7. Wilkens, C.M., et al., *Excitation-contraction coupling is unaffected by drastic alteration of the sequence surrounding residues L720-L764 of the alpha 1S II-III loop.* Proc Natl Acad Sci U S A, 2001. **98**(10): p. 5892-7.

8. El-Hayek, R. and N. Ikemoto, *Identification of the minimum essential region in the II-III loop of the dihydropyridine receptor alpha 1 subunit required for activation of skeletal muscle-type excitation-contraction coupling.* Biochemistry, 1998. **37**(19): p. 7015-20.

9. Leong, P. and D.H. MacLennan, *A 37-amino acid sequence in the skeletal muscle ryanodine receptor interacts with the cytoplasmic loop between domains II and III in the skeletal muscle dihydropyridine receptor.* J Biol Chem, 1998. **273**(14): p. 7791-4.

10. Bannister, R.A., et al., *Effects of inserting fluorescent proteins into the alpha1S II-III loop: insights into excitation-contraction coupling.* J Gen Physiol, 2009. **134**(1): p. 35-51.

11. Avila, G., et al., *FKBP12 binding to RyR1 modulates excitation-contraction coupling in mouse skeletal myotubes.* J Biol Chem, 2003. **278**(25): p. 22600-8.

12. Prosser, B.L., et al., *S100A1 binds to the calmodulin-binding site of ryanodine receptor and modulates skeletal muscle excitation-contraction coupling.* J Biol Chem, 2008. **283**(8): p. 5046-57.

13. Rodney, G.G., et al., *Regulation of RYR1 activity by Ca(2+) and calmodulin.* Biochemistry, 2000. **39**(26): p. 7807-12.

14. DiFranco, M., et al., *DNA transfection of mammalian skeletal muscles using in vivo electroporation.* J Vis Exp, 2009(32).

15. Liu, Y., et al., *Essential roles of the acetylcholine receptor gamma-subunit in neuromuscular synaptic patterning.* Development, 2008. **135**(11): p. 1957-67.

16. Martin-Caraballo, M., et al., *Contractile and fatigue properties of the rat diaphragm musculature during the perinatal period.* J Appl Physiol (1985), 2000. **88**(2): p. 573-80.

17. Wu, F., et al., *A sodium channel knockin mutant (NaV1.4-R669H) mouse model of hypokalemic periodic paralysis.* J Clin Invest, 2011. **121**(10): p. 4082-94.

18. Schneider, C.A., W.S. Rasband, and K.W. Eliceiri, *NIH Image to ImageJ: 25 years of image analysis.* Nat Methods, 2012. **9**(7): p. 671-5.

19. Sheehan, D.C. and B.B. Hrapchak, *Theory and practice of histotechnology*. 2d ed. 1980, St. Louis: Mosby. xiii, 481 p., 1 leaf of plates.

20. Woods, A.E. and R.C. Ellis, *Laboratory histopathology: a complete reference*. 1996, New York: Churchill Livingstone.

21. Shelton, J.M., et al., *Microsomal triglyceride transfer protein expression during mouse development.* J Lipid Res, 2000. **41**(4): p. 532-7.

22. DiFranco, M., et al., *Functional expression of transgenic 1sDHPR channels in adult mammalian skeletal muscle fibres.* J Physiol, 2011. **589**(Pt 6): p. 1421-42.

23. Hasty, P., et al., *Muscle deficiency and neonatal death in mice with a targeted mutation in the myogenin gene.* Nature, 1993. **364**(6437): p. 501-6.

24. DeChiara, T.M., et al., *The receptor tyrosine kinase MuSK is required for neuromuscular junction formation in vivo.* Cell, 1996. **85**(4): p. 501-12.

25. Brandon, E.P., et al., *Aberrant patterning of neuromuscular synapses in choline acetyltransferase-deficient mice.* J Neurosci, 2003. **23**(2): p. 539-49.

26. An, M.C., et al., *Acetylcholine negatively regulates development of the neuromuscular junction through distinct cellular mechanisms.* Proc Natl Acad Sci U S A, 2010. **107**(23): p. 10702-7.

27. Pai, A.C., *Developmental Genetics of a Lethal Mutation, Muscular Dysgenesis (Mdg), in the Mouse. I. Genetic Analysis and Gross Morphology.* Dev Biol, 1965. **11**: p. 82-92.

28. Takeshima, H., et al., *Excitation-contraction uncoupling and muscular degeneration in mice lacking functional skeletal muscle ryanodine-receptor gene.* Nature, 1994. **369**(6481): p. 556-9.

29. Gregg, R.G., et al., *Absence of the beta subunit (cchb1) of the skeletal muscle dihydropyridine receptor alters expression of the alpha 1 subunit and eliminates excitation-contraction coupling.* Proc Natl Acad Sci U S A, 1996. **93**(24): p. 13961-6.

30. Zvaritch, E., et al., *An Ryr1I4895T mutation abolishes Ca2+ release channel function and delays development in homozygous offspring of a mutant mouse line.* Proc Natl Acad Sci U S A, 2007. **104**(47): p. 18537-42.

31. Blitz, E., et al., *Bone ridge patterning during musculoskeletal assembly is mediated through SCX regulation of Bmp4 at the tendon-skeleton junction.* Dev Cell, 2009. **17**(6): p. 861-73.

32. Powell, J.A., et al., *Distribution and quantification of ACh receptors and innervation in diaphragm muscle of normal and mdg mouse embryos.* Dev Biol, 1984. **101**(1): p. 168-80.

33. Rieger, F., J.A. Powell, and M. Pincon-Raymond, *Extensive nerve overgrowth and paucity of the tailed asymmetric form (16 S) of acetylcholinesterase in the developing skeletal neuromuscular system of the dysgenic (mdg/mdg) mouse.* Dev Biol, 1984. **101**(1): p. 181-91.

34. Chen, F., et al., *Neuromuscular synaptic patterning requires the function of skeletal muscle dihydropyridine receptors.* Nat Neurosci, 2011. **14**(5): p. 570-7.

35. Bower, N.I., et al., *Stac3 is required for myotube formation and myogenic differentiation in vertebrate skeletal muscle.* J Biol Chem, 2012. **287**(52): p. 43936-49.

36. Reinholt, B.M., et al., *Stac3 is a novel regulator of skeletal muscle development in mice.* PLoS One, 2013. **8**(4): p. e62760.

37. Horstick, E.J., et al., *Stac3 is a component of the excitation-contraction coupling machinery and mutated in Native American myopathy.* Nat Commun, 2013. **4**: p. 1952.

38. Polster, A., et al., *Stac adaptor proteins regulate trafficking and function of muscle and neuronal L-type Ca2+ channels.* Proc Natl Acad Sci U S A, 2015. **112**(2): p. 602-6.

39. Dulhunty, A.F., et al., *Activation and inhibition of skeletal RyR channels by a part of the skeletal DHPR II-III loop: effects of DHPR Ser687 and FKBP12.* Biophys J, 1999. **77**(1): p. 189-203.

40. Casarotto, M.G., et al., *A structural requirement for activation of skeletal ryanodine receptors by peptides of the dihydropyridine receptor II-III loop.* J Biol Chem, 2000. **275**(16): p. 11631-7.

41. El-Hayek, R., et al., *Identification of calcium release-triggering and blocking regions of the II-III loop of the skeletal muscle dihydropyridine receptor.* J Biol Chem, 1995. **270**(38): p. 22116-8.

42. Lu, X., L. Xu, and G. Meissner, *Activation of the skeletal muscle calcium release channel by a cytoplasmic loop of the dihydropyridine receptor.* J Biol Chem, 1994. **269**(9): p. 6511-6.

43. Fajloun, Z., et al., *Chemical synthesis and characterization of maurocalcine, a scorpion toxin that activates Ca(2+) release channel/ryanodine receptors.* FEBS Lett, 2000. **469**(2-3): p. 179-85.

44. Mosbah, A., et al., *A new fold in the scorpion toxin family, associated with an activity on a ryanodine-sensitive calcium channel.* Proteins, 2000. **40**(3): p. 436-42.

45. Esteve, E., et al., *Critical amino acid residues determine the binding affinity and the Ca2+ release efficacy of maurocalcine in skeletal muscle cells.* J Biol Chem, 2003. **278**(39): p. 37822-31.

46. Szappanos, H., et al., *Differential effects of maurocalcine on Ca2+ release events and depolarization-induced Ca2+ release in rat skeletal muscle.* J Physiol, 2005. **565**(Pt 3): p. 843-53.

47. Altafaj, X., et al., *Maurocalcine interacts with the cardiac ryanodine receptor without inducing channel modification.* Biochem J, 2007. **406**(2): p. 309-15.

48. Lukacs, B., et al., *Charged surface area of maurocalcine determines its interaction with the skeletal ryanodine receptor.* Biophys J, 2008. **95**(7): p. 3497-509.

49. Zalk, R., et al., *Structure of a mammalian ryanodine receptor.* Nature, 2015. **517**(7532): p. 44-9.

CHAPTER 3. DISCOVERY AND CHARACTERIZATION OF DWORF

3.1 ABSTRACT

Annotation of small proteins is a difficult task because of the large number of non-functional open reading frames found in RNA transcripts. We hypothesized that many genes currently annotated as long non-coding RNAs (lncRNAs) may encode previously unrecognized small proteins or peptides. We used codon substitution frequency to predict a number of hypothetical proteins. As a proof of principle, we confirmed the protein coding status of one of these genes, which we have named Dwarf Open Reading Frame (DWORF). The DWORF protein is a 34-amino-acid tail-anchored transmembrane protein with a predicted molecular weight of 3.8 kDa. We used CRISPR/Cas9 genome editing to insert a two base pair insertion into the DWORF coding sequence. This mutation results in a frame shift followed by nonsense sequence and a premature stop codon. We used these knockout mice and a DWORF-recognizing polyclonal antibody to confirm that the DWORF protein is produced endogenously in the mouse heart and soleus muscle. We produced GFP/DWORF fusion proteins and determined that DWORF localizes to the sarcoplasmic reticulum (SR) and interacts with the SERCA pump. Overexpression of DWORF in cardiac myocytes increases the amplitude and decay rate of calcium transients following electrical stimulation. These findings indicate that genes currently annotated as lncRNAs may encode small proteins, and we also report that the small protein DWORF is a regulator of muscle calcium handling.

3.2 INTRODUCTION

Eukaryotic transcriptomes contain thousands of short open reading frames (ORFs), but most are not thought to encode functional proteins. Because of the large number of potentially

spurious hypothetical small proteins, most gene predictions have discarded ORFs of fewer than 100 codons en bloc with little consideration for their coding potential. Polyadenylated transcripts for which no sufficiently long hypothetical ORF can be predicted are classified as long non-coding RNA (lncRNAs). Certainly, this classification is correct for most annotated lncRNAs, however, we hypothesized that many genes currently annotated lncRNAs actually encode small proteins that have evaded gene prediction algorithms.

We used a metric of evolutionary conservation of codons, called codon substitution frequency, to identify lncRNA ORFs that likely encode proteins. Using the PhyloCSF computer program, we identified many ORFs within the mouse lncRNA transcriptome that encode conserved hypothetical small proteins or peptides. As a proof of concept to validate these findings, we chose to explore one of these genes more thoroughly, which we have named Dwarf Open Reading Frame or DWORF. We have determined using knockout mice and a custom antibody that the *Dworf* gene encodes a bona fide protein product. This product is a tail-anchored transmembrane peptide of only 34 amino acids, making it one of the smallest known full-length proteins in vertebrates. Overexpression of DWORF in cardiac myocytes increases the rate of calcium clearance and peak calcium release.

Regulation of calcium release and clearance is vitally important to the function of striated muscle fibers and is altered in many muscle diseases. Upon electrical stimulation of the myocyte plasma membrane, a burst of calcium is released from the sarcoplasmic reticulum, which binds to the contractile apparatus and causes the muscle fiber to contract [1]. In order for the cell to relax, calcium must be stripped from the sarcomere and cytoplasm. A portion of this calcium is transported to the extracellular fluid, but the majority is recycled back to the SR, the primary site of calcium storage in myocytes. This task is accomplished unaided by the sarco/endoplasmic

reticulum ATPase (SERCA) which resides in the SR membrane. The isoform expressed in the heart and slow-twitch skeletal muscle is SERCA2a, which is inhibited by the small transmembrane peptides phospholamban, sarcolipin, and myoregulin. The secondary structure and sub-cellular localization of these proteins is remarkably similar to DWORF, yet DWORF shares no discernable primary sequence motifs.

3.3 MATERIALS AND METHODS

3.3.1 Identification of Conserved Small Open Reading Frames

Total RNA was extracted from adult mouse heart tissue using Trizol (Invitrogen). An RNA sequencing library was prepared using the TruSeq RNA Library Prep Kit (Illumina) according to the manufacturer's protocol. Reads were mapped to the USCS mm9 reference genome [2] using TopHat [3]. Final transcripts were assembled using Cufflinks and consolidated with the mm9 reference annotations [4]. Novel transcripts (i.e. those not existing in the reference annotation) were extracted and combined with transcripts annotated as long non-coding RNA in the UCSC database for a total of 3701 transcripts. Sequence alignments from fourteen mammalian species (mouse, rabbit, rat, human, chimpanzee, rhesus monkey, shrew, dog, cat, horse, cow, armadillo, elephant, and tenrec) were extracted using the "Stitch Gene blocks" tool in Galaxy [5-8]. PhyloCSF was used to calculate conservation scores for potential ORFs in three frames on both strands [9]. Only the highest scoring ORF for each transcript was reported.

3.3.2 Quantitative mRNA Measurement

Total RNA was extracted from adult mouse tissues using Trizol and reverse transcribed using the SuperScript III First-Strand Synthesis System (Invitrogen) with random hexamer primers. Quantitative Polymerase Chain Reaction (qPCR) was performed using 5' nuclease assays on the StepOne Real-Time PCR System (Life Technologies). The following

oligonucleotides were ordered from Integrated DNA Technologies to measure endogenous *Dworf* abundance: Forward – 5'-TTCTTCTCCTGGTTGGATGG-3'; Reverse – 5'-TCTTCTAAATGGTGTCAGATTGAAGT-3'; Probe – 5'-TTTACATTGTCTTCTTCTAGAAAAGGAAGAAG-3'. The following oligonucleotides were used to measure *Dworf* abundance from the αMHC promoter-driven transgene: Forward – 5'-ATAAGAGTTTGAGTCGACCGC-3'; Reverse – 5'- ACTGGGGAGGGGTCACAG-3'; Probe – 5'- TTGTCTTCTTCTAATAGAAGCTTGATGGGTG-3'. Probes were labeled with 5' 6-FAM, an internal ZEN quencher, and a 3' Iowa Black quencher and used in a 2:1 ratio with primers. Human RNA samples were obtained from a commercial source and prepared as described above. Human cDNAs were quantified using SYBR Green with the following primers: Forward 5'-CCACCCACCAACAGGAATA-3'; Reverse 5'-TTATGATGCAGCCCACAATC-3'. Each sample was normalized to a Eukaryotic 18S rRNA Endogenous Control (Life Technologies) reaction using Equation 3-1.

$$10^6 \times \left(\frac{2^{-\mathrm{Ct}_{Dworf}}}{2^{-\mathrm{Ct}_{18S}}} \right)$$

Equation 3-1. Calculation of Relative Abundance by qPCR.

3.3.3 Northern Blotting

A *Dworf* cDNA fragment was PCR purified with the following primers: Forward – 5'-XXXXXXX-3'; Reverse – 5'-XXXXXXX-3'. The fragment was gel purified and cloned into the TOPO pCR2.1 plasmid (Life Technologies). Following amplification in *E. coli*, the probe template was excised with EcoRI and gel purified. Radiolabeled probe was prepared using the RadPrime DNA Labeling System (Life Technologies) with α-^{32}P-dCTP. Radiolabeled probe was was hybridized overnight at 68 °C to a commercial northern blot (Zyagen, MN-MT-1)

containing 20 μg of total RNA per sample. The hybridized blot was washed four times and then exposed to autoradiography film for twenty-four hours. The blot was then stripped using a published protocol and probed for the 18S rRNA loading control using the same procedure described for *Dworf*.

3.3.4 Antibody Derivation

A custom polyclonal antibody was derived against the N-terminal region of the predicted DWORF protein by New England Peptide. Briefly, rabbits were immunized with a synthetic peptide with the following sequence MAEKESTSPHLIC. Sera were collected and affinity purified against the peptide immunogen.

3.3.5 Western Blotting

Lysates were prepared by pulverizing snap frozen tissues in liquid nitrogen and then homogenizing in RIPA buffer (150 mM NaCl; 1% v/v Igepal CA-630; 50 mM Tris-Cl, pH 8.3; 0.5% w/v sodium deoxycholate; 0.1% w/v sodium dodecyl sulfate) with added protease inhibitors (cOmplete ULTRA mini tablet, Roche) on ice using a 'tight' glass dounce homogenizer. Protein concentrations were determined using a BCA Protein Assay Kit (Pierce). For DWORF and PLN, samples were separated on a 16.5% tricine buffered polyacrylamide gel (BioRad). Samples for other experiments were separated on Any kD tris-glycine buffered polyacrylamide gels (BioRad). DWORF and PLN were electroblotted onto Immobilon P^{SQ} membranes (Millipore) using a semi-dry apparatus for 30 min at 20 V. Other experiments were electroblotted onto Immobilon P membranes using a semi-dry apparatus for 50 min at 20 V. Membranes were blocked overnight at 4 °C in blotto (5% w/v non-fat dry milk in TBST). Primary antibody hybridization was carried out overnight at 4 °C with the following antibodies: DWORF, 1:5,000; PLN (2D12, Pierce), 1:5,000; $pSer^{16}$-PLN (Badrilla), 1:5,000; $pThr^{17}$-PLN

(Badrilla), 1:5,000; GAPDH (MAB374, Millipore); 1:10,000. Blots were washed five times, 5 min each, in TBST and then incubated with HRP-conjugated secondary antibodies (BioRad) at 1:20,000. Blots were then developed with chemiluminescent substrate and exposed to either autoradiograph film or a digital ChemiDoc system (G:BOX, GeneSys).

3.3.6 Subcellular Fractionation

Adult mouse cardiac ventricle was snap frozen in liquid nitrogen and pulverized to a fine powder. The powdered sample was suspended in 1 mL of ice cold TE buffer (10 mM Tris-Cl, pH 8.0, 1 mM EDTA) with protease inhibitors (cOmplete ULTRA mini tablet, Roche) and incubated on ice for 30 min. The suspension was then homogenized with fifty strokes of a 'tight' glass douncer. The homogenates were spun at progressively higher speeds at 4 °C to fractionate the suspended particles: 1,000 x *g*, 5 min, discard pellet; 12,000 x *g*, 10 min, P12 pellet; 100,000 x *g*, 20 min, P100 pellet and supernatant. The pellets were suspended in equivalent starting volumes of 1:1 TE/PAGE loading buffer followed by western blotting.

3.3.7 Generation of Mouse Lines

All experiments involving animals were approved by the Institutional Animal Care and Use Committee at the University of Texas Southwestern Medical Center. Knockout mice were generated using the CRISPR/Cas9 system by pronuclear and cytoplasmic injection of mouse embryos with guide RNA (gRNA) and Cas9 mRNA as described previously [10]. Briefly, a gRNA was cloned that targeted the predicted coding sequence of DWORF. Cleavage efficiency was tested in cell culture, and then the gRNA and Cas9 mRNA were transcribed *in vitro* and spin-column purified. Mouse embryos were injected with an equal ratio of gRNA and Cas9 mRNA into the pronucleus and cytoplasm and then transferred to a surrogate dam for gestation. Because F_0 founders are expected to be mosaic, allelic disruption was confirmed in the F_0

generation pups using the T7E1 endonuclease assay on tail biopsies, and positive founders were bred to wild-type to clonally isolate potential alleles. Mutants in the F_1 generation were identified by T7E1 assay and then the alleles were cloned and sequenced. One mouse line with a two-bp insertion was chosen for further study.

Transgenic mice were derived by pronuclear injection of mouse embryos. Briefly, the DWORF coding sequence was cloned into an αMHC promoter-driven plasmid with a polyadenylation sequence from the human growth hormone (hGH) gene. The plasmid was injected into the pronucleus of mouse embryos and then implanted in a surrogate dam for gestation. F_0 generation pups were selected by presence of transgene by PCR from a tail biopsy and bred to wild-type. F_1 generation pups were bred and expression of the transgene was verified in the F_2 progeny by qPCR.

3.3.8 Genotyping of Mouse Lines

Knockout mice were genotyped using a custom TaqMan genotyping assay (Life Technologies). Briefly, tail biopsies were digested in lysis buffer (50 mM KCl; 10 mM Tris-Cl, pH 8.3; 2.5 mM $MgCl_2$; 0.1 mg/mL porcine gelatin; 0.45% v/v Igepal CA-630; 0.45% v/v Tween 20) with proteinase K (6 U/mL) overnight at 55 °C. Particulates were removed by high-speed centrifugation, and the supernatant was diluted 1:10 in water. The tail samples were then analyzed by qPCR with a mixture of the following oligonucleotides: Forward Primer 5'-TCATTGCTTCTAAGCAGAGTCAACA-3'; Reverse Primer 5'-ATGCAGCCTACAATCCATCCAA-3'; WT Probe 5'-CCAGGAGAAGAATG-3'; KO Probe 5'-CAGGAGACAAGAATG-3'.

Transgenic mice were genotyped based on presence or absence of the hGH sequence. Tail biopsies were processed as described for the *Dworf* KO mice, and used for PCR with a mixture of the following primers (myogenin primers are used as a positive control): hGH Forward Primer 5'-GTCTGACTAGGTGTCCTTCT-3'; hGH Reverse Primer 5'-CGTCCTCCTGCTGGTATAG-3'; Myogenin Forward Primer 5'-TTACGTCCATCGTGGACAGC-3'; Myogenin Reverse Primer 5'-TGGGCTGGGTGTTAGCCTTA-3'. PCR products were analyzed by agarose gel electrophoresis.

3.4 RESULTS

3.4.1 Identification of DWORF

Mouse transcripts annotated as lncRNAs in UCSC genome version mm9 [2] were extracted and pooled with *de novo* assembled un-annotated transcripts from mouse heart RNA-seq (Figure 3-1). Multispecies genome alignments were extracted for each transcript. The alignments were then analyzed using the PhyloCSF algorithm to return the best scoring conserved ORF using six possible frame orientations (i.e. frames +1, +2, +3, -1, -2, -3) [9]. High scoring ORFs were analyzed manually to verify presence of a bona fide conserved ORF, strictly requiring conservation of the start and stop codons and no indels that are not multiples of three to preserve coding frame. A number of novel ORFs were discovered using this method; therefore, the list was further filtered by muscle (heart or skeletal) expression based on multi-tissue RNA-seq data. Two stringently classified hypothetical ORFs remained following the expression filter. One was myoregulin, which had already been identified as a conserved ORF by our lab, and the other was encoded in a novel heart-specific RNA, which we called *Dworf*, for Dwarf Open

Reading Frame. At 34 codons, the *Dworf* ORF is the third smallest full-length protein in the mm9 annotation (Table 3-1).

In mice the *Dworf* RNA transcript is completely un-annotated in UCSC genome versions mm9 and mm10 (Figure 3-2A). Based on coverage maps from heart RNA-seq data, we designed cloning primers for the mouse transcript and successfully cloned a cDNA of 294 bp (Figure 3-3). The cDNA maps to a 2.8 kb locus of chromosome 3 and is transcribed as a three exon mRNA. The *Dworf* ORF begins in exon 1, which encodes the first four amino acids of the protein, and the remainder of the ORF is encoded in exon 2. The stop codon is only four base pairs from the end of exon 2, which likely prevents the transcript from being degraded by non-sense mediated decay [11]. In mice, RNA-seq suggested that alternative splicing between exons 1 and 2 produces an in-frame transcript with a 3 bp insertion. This finding was also confirmed in cloned cDNA. Based on RNA-seq reads mapping to the exon junction, the shorter isoform appears to be about five times more abundant. In humans the *DWORF* locus is annotated as a three exon lncRNA (LOC100507537), spanning about 3.4 kb of chromosome 3 (Figure 3-3B). RNA-seq data from human skeletal muscle suggests a single isoform. Unless otherwise stated, further discussion will focus on the mouse homolog.

The *Dworf* ORF encodes a 34 or 35 amino acid protein, depending on the isoform (Figure 3-4). The ORF also contains a single-nucleotide polymorphism (SNP), rs30878467, that replaces a thymine in the reference genome with cytosine. This variant results in codon 13 (of the 34 aa isoform) encoding either isoleucine (reference genome) or methionine. Combined, these variants produce four hypothetical DWORF proteins. The *Dworf* ORF is conserved to lamprey, the most distant extant vertebrate species for which a genome sequence is currently available (Figure 3-5). The C-terminal region is highly enriched in hydrophobic amino acids and is predicted to encode

a tail-anchored transmembrane peptide using the TMHMM algorithm [12-14]. The hydrophobicity of the C-terminal region is highly conserved across all species, although at most positions there is a degree of interchangeability between aliphatic amino acids. Within the transmembrane region, multiple amino acids are identically conserved. Notably, many of the identically conserved amino acids are often associated with unique structural or chemical properties, including proline, tryptophan, glycine, cysteine and tyrosine. The N-terminal region seems to be less stringently conserved, but most sequences (except for *Anolis carolensis*) contain multiple charged residues (primarily lysine and aspartic acid) in this region. Some species also contain serine or threonine residues which could be potential substrates for phosphorylation, but conservation of a specific motif is not clear.

3.4.2 *Dworf* mRNA is restricted to cardiac and slow-twitch muscle.

To confirm expression of the *Dworf* RNA transcript, the sequence shown in Figure 3-3 was used to probe a northern blot containing total RNA from multiple adult mouse tissues (Figure 3-6). This experiment revealed that *Dworf* is a very small RNA of about 500 bp. The size of the RNA is consistent with RNA-seq and cloning experiments if addition of a polyadenylated tail is considered. Signal was not detected in any other tissue on the blot, including skeletal muscle from fast-twitch muscle groups.

cDNA was prepared from a range of adult mouse tissues and analyzed using qPCR. The tissue with the highest expression of *Dworf* was the soleus, a postural muscle group of the distal hindlimb that contains the greatest enrichment of slow-twitch muscle fibers in the mice. The cardiac ventricle was the second most abundant in *Dworf*, followed by the diaphragm, the primary breathing muscle which contains some slow-twitch enrichment but is primarily a fast-twitch group in mice [15, 16]. A small amount of expression was observed also in the

gastrocnemius/plantaris and brain. Notably, *Dworf* was not detected in the quadriceps, a fast-twitch muscle group, consistent with our northern blot findings. *Dworf* was also surprisingly not detected in the cardiac atrial muscle. Expression analysis of a time course of cardiac development revealed that *Dworf* is not expressed in the prenatal heart (Figure 3-8). Expression gradually increases postnatally and by postnatal day 40, expression is comparable to adult heart. This pattern is also supported by publically available RNA-seq data that we remapped. This data also corroborates that *Dworf* is not expressed in atrial myocytes.

We examined *DWORF* expression in human tissues by qPCR and found very high expression in skeletal muscle, but surprisingly very low expression in the heart (Figure 3-9). Some expression was observed in esophagus, which in humans is composed of a mixture of skeletal and smooth muscle fibers, and in the prostate, which sometimes contains skeletal muscle fibers. We also examined published RNA-seq data that we re-mapped and found a similar expression pattern as in adult human with expression highest in skeletal muscle (Figure 3-10).

3.4.3 DWORF Protein Expression

In order to confirm that the *Dworf* transcript encodes a protein and for use in other experiments, we raised a custom polyclonal rabbit antibody against the N-terminal region of the predicted DWORF protein (Figure 3-11A). We used this antibody to probe a western blot containing protein from liver and multiple muscle groups (Figure 3-11B). We observed a single band at the expected molecular weight for DWORF at 3.8 kDa in soleus and heart, but no other tissues. As observed in the qPCR experiments, expression was highest in the soleus. The fact that only a single band was observed may suggest that the protein does not undergo posttranslational modification or possibly that modification blocks antibody binding.

To verify by an independent method that the *Dworf* transcript encodes a protein, we cloned the predicted 5' untranslated region (UTR) including the first thirteen codons of the *Dworf* RNA into a HaloTag expression vector that contains a protein tag but lacks a Kozak sequence and start codon (Figure 3-12A). We expressed the empty and *Dworf*-containing constructs in non-muscle cells followed by western blotting with an antibody against the HaloTag protein and our custom DWORF antibody (Figure 3-12B). We found that the *Dworf* 5' UTR is capable of initiating translation *in vivo*. Blotting with the DWORF antibody demonstrated that the full-length fusion protein was expressed as expected. We conclude from this experiment and the multi-tissue western blot that the *Dworf* RNA has intrinsic coding potential and produces a small peptide *in vivo*.

Because the *Dworf* gene may encode four protein variants, we examined whether our DWORF antibody could recognize these variant forms, since the differing regions are within the immunogenizing peptide sequence. Each of the four variant sequences were cloned to produce in frame fusion proteins with green fluorescent protein (GFP) and transfected into non-muscle cells. Lysates were used for western blots and probed with the DWORF antibody (Figure 3-13). The results show that the DWORF antibody reacts with apparent equal affinity to all variant proteins.

Because the epitope is in the N-terminal portion of the protein that is expected to be soluble, we next examined whether the antibody would bind the protein in a native membrane environment. We transfected a GFP-DWORF fusion construct into COS7 non-muscle cells followed by brief fixation and immunofluorescent labeling (Figure 3-14). We found that the DWORF antibody labeled only cells with GFP fluorescence; however, the antibody did not label cells transfected with a GFP fusion with the small transmembrane peptide sarcolipin. This

experiment demonstrates that the DWORF antibody is capable of recognizing the protein in a native membrane environment and that immunolabeling is specific to DWORF.

We next examined whether the DWORF antibody could recognize the protein in tissue cross-sections. We isolated the gastrocnemius with the adjacent plantaris muscle, which contains a small population of Type-I slow-twitch muscle fibers interspersed with fast-twitch muscle fibers. We snap froze the isolated muscles and sectioned them on a cryostat followed by permeabilization and immunolabeling with the DWORF antibody and the NOQ7.5.4D antibody against Type I muscle myosin (Figure 3-15). We observed punctate immunolabeling with the DWORF antibody within fibers labeled with the NOQ7.5.4D antibody. The specificity of this labeling demonstrates that the DWORF antibody only binds to Type-I fibers in skeletal muscle.

3.4.4 Subcellular Localization

Since DWORF is predicted to be a transmembrane peptide, we sought to understand the sub-cellular localization of the protein. We co-transfected GFP-DWORF and mCherry-SERCA1a expression vectors into COS7 cells and imaged the cells using live confocal fluorescence microscopy to avoid potential processing artifacts (Figure 3-16). mCherry-SERCA1a localizes to the endoplasmic reticulum with notable signal in peri-nuclear and reticular distributions. GFP-DWORF was observed to overlap substantially with the mCherry-SERCA1a signal. In addition to the clear signal localizing to the endoplasmic reticulum, we also noted the presence of a diffuse localization appearing to be cytosolic. It is unclear whether this signal is biologically representative or possibly an artifact of overexpression, since tail-anchored membrane proteins are integrated into membranes posttranslationally [17-19].

We investigated whether GFP-DWORF also localizes to the sarcoplasmic reticulum in skeletal muscle fibers by electroporation of the GFP-DWORF expression vector into the flexor digitorum brevis muscle of the foot (Figure 3-17A). We also transfected GFP-Sarcolipin and GFP-Phospholamban into muscles of separate mice for comparison. The muscles were whole mounted in physiologic buffer and imaged live using two-photon excitation microscopy to simultaneous visualize GFP and myosin (using second harmonic generation). We observed that GFP-DWORF localizes in an alternating pattern with myosin, similar to GFP-Sarcolipin and GFP-Phospholamban. At lower magnification, the overall similarity between GFP-Dworf and GFP-Sarcolipin is striking, with similar localization in the peri-nuclear region and notable longitudinal striations typical of longitudinal SR (Figure 3-17B).

We used a HaloTag-fused DWORF construct to stably express the protein at low-levels by viral transduction in COS7 cells. The cells were then lysed in hypotonic buffer and homogenized. The homogenates were centrifuged and pellets collected at increasing speeds to separate sub-cellular particles into multiple fractions. Western blots were then performed using a HaloTag antibody and an antibody against the ER marker protein disulfide-isomerase (PDI). HaloTag-DWORF was found primarily in the P12 fraction corresponding to the ER, while HaloTag alone was only in the supernatant or soluble fraction.

We next performed differential centrifugation on homogenates from cardiac ventricle followed by western blots for markers of sub-cellular compartments (Figure 3-19). We found that endogenous DWORF protein is bound primarily in the P12 fraction and to a lesser extent P100. No signal was observed in the supernatant. Unlike the differential centrifugation of COS7 cells, the sarcoplasmic reticulum appears to pellet in both the P12 and P100 fractions, based on the localization of phospholamban. The P12 fraction also contained the Na^+/K^+-ATPase.

Curiously, SERCA2a appears most abundant in the P100 fraction. These results appear to be inconsistent with those of experiments using GFP-tagged DWORF, but the basis for this discrepancy is currently unclear.

3.4.5 DWORF Protein-protein Interaction

Because GFP-DWORF co-localizes to the SR with SERCA, we sought to determine whether the two proteins physically interact (Figure 3-20). COS7 cells were co-transfected with GFP-DWORF and myc-SERCA2a or GFP alone and myc-SERCA2a. Immunoprecipitation of the GFP-DWORF/myc-SERCA2a lysate with a GFP antibody co-precipitates myc-SERCA2a by western blot, but GFP alone does not. This experiment suggests that DWORF and SERCA2a interact in the SR membrane.

3.4.6 Generation of DWORF Knockout

We used the CRISPR/Cas9 system to disrupt the coding frame of the DWORF protein. A guide RNA (gRNA) was designed to target the coding sequence of exon 2 before the transmembrane region (Figure 3-21). We injected purified gRNA and purified Cas9 mRNA into the pronucleus and cytoplasm of mouse single-cell embryos and transplanted the embryos in a surrogate dam. F_0 pups were screened for indels, and a founder with a two base pair insertion was chosen for further breeding. The predicted mutant protein is out of frame before the highly conserved transmembrane region and introduces a stop codon after seven nonsense codons.

Mice were bred to homozgozity and tissues were harvested to confirm disruption of the DWORF protein. cDNA was prepared from heart ventricle tissue and analyzed by qPCR (Figure 3-22A). Surprisingly, the *Dworf* transcript was up-regulated by about four fold in the knockout tissue, while several notable genes were not changed including the calcium-handling genes

SERCA2 and phospholamban and the cardiac stress markers MYH7 and ANP (NPPA). Although the predicted mutant protein contains a premature stop codon, in this case NMD is not expected since the new stop codon is fewer than fifty base pairs away from the last exon-exon junction. While lack of NMD may explain why the *Dworf* transcript is not down-regulated, the significant up-regulation is more difficult to explain. Perhaps the 2-bp mutation stabilizes the mRNA, or perhaps more likely, *Dworf* is involved in a transcriptional feedback loop and the transcript is up-regulated to compensate for loss of the protein product.

Western blots on the knockout ventricular and soleus muscle were probed with the DWORF antibody and show that the DWORF protein has been completely eliminated in both the cardiac and skeletal muscle tissues. Notably a smaller band indicating the predicted mutant protein was not observed, despite the fact that the protein contains the antibody epitope. This finding could result from several possibilities, including that the protein is not translated, that it is rapidly degraded, or that it does not blot well under the experimental conditions. The results of the knockout western blot conclusively confirm that the *Dworf* locus encodes a very small peptide.

3.4.7 Measurement of Calcium Transients in Transgenic Cardiomyocytes

To examine the effect of over-activity of *Dworf*, we generated transgenic mice overexpressing untagged *Dworf* under the control of the adult cardiomyocyte-specific alpha-myosin heavy chain (αMHC) promoter. A transgenic founder was selected that overexpresses the protein at very high levels. Western blots of the transgenic heart tissue demonstrate that the αMHC-DWORF mice robustly overexpress DWORF, but proteins involved in calcium handling are largely unaffected (Figure 3-23).

We next examined whether calcium flux was altered in isolated transgenic myocytes using the fluorescent calcium indicator dye, fluo-4. We observed that peak calcium release was significantly increased in the transgenic myocytes, likely indicating increased SR calcium stores. We also found that the calcium clearance rate was significantly higher in the transgenic myocytes, suggesting that SERCA was more active in those cells. In the absence of increased protein abundance of SERCA, these findings would suggest that SERCA activity is being modulated by a factor in the transgenic myocytes; however, protein abundance of phospholamban was unchanged and serine-16 phosphorylation may be decreased which would be expected to decrease SERCA activity under normal conditions.

3.4.8 DWORF Expression in Heart Failure

We examined the expression of *Dworf* mRNA and protein in αMHC-Calcineurin A transgenic hearts, a mouse model of hypertrophic heart disease that progresses to dilated cardiomyopathy by six months of age. We found that *Dworf* mRNA was down-regulated in dilated transgenic hearts of six month old mice. The level of DWORF protein was even more dramatically down-regulated in these hearts. Notably, we also observed some variation in the expression of DWORF protein in wild-type hearts. The cause of this is not understood at present, but this result would suggest that DWORF may be dynamically regulated by an uncontrolled variable.

3.5 DISCUSSION

Nearly fifteen years have now passed since the first draft of the human genome was published [20, 21]. Few, if any, publications in the history of science have had such an immediate and revolutionary impact. Today we enjoy unfettered and instantaneous access to complete or near complete sequences and annotations for human and most model organisms,

most notable being that of the house mouse, *Mus musculus*. These advances have made identification and retrieval of gene sequences an almost trivial matter. In some ways, however, the high overall quality of information and the somewhat dogmatic representation of genome browsers mask the remaining knowledge gaps. In practice, genome browsers often display faulty predictions and poorly supported annotations with the same certainty as high quality, well curated information. Therefore, many researchers, especially those who have only practiced science in the post-genome era, are sometimes given false assurance about the quality of annotations. With this prevalent ethos in mind, we thought it prudent to examine more thoroughly the reliability of annotations related to the emerging class of genes known as long non-coding RNAs (lncRNAs).

We used evolutionary conservation of codons as a guide to assess the coding potential of putative lncRNAs and novel transcripts using the PhyloCSF algorithm [9]. We hypothesized that potential small ORFs (typically fewer than 100 codons in length) had been systematically overlooked when determining coding potential of annotated lncRNAs. We found a number of small open reading frames that most likely encode proteins. We chose to further validate a hypothetical protein that we call DWORF using mouse models and found that the *Dworf* transcript does encode the conservation-predicted protein. In humans, the DWORF gene is classified as a lncRNA, however, quite remarkably it is completely un-annotated in the mouse genome. This fact should serve as a warning that the genome annotations are not complete, especially considering that the heart is one of the most intensively studied organ systems. It is worth mentioning that the well-known small peptides sarcolipin and phospholamban might not have been discovered by current bioinformatic techniques, as it is only for phosphorylation in the case of phospholamban or protein abundance in the case of sarcolipin that the proteins (not the

nucleotide sequences) were discovered in the 1970s. It is also interesting to note that within the *Dworf* mRNA, the DWORF ORF is not the longest ORF in the transcript, highlighting in this case the importance of using evolutionary conservation to guide the protein annotation.

Recently our lab published data showing that another putative lncRNA encodes a small peptide inhibitor of the skeletal muscle SR calcium pump that we named myoregulin (*Mrln*) (Figure 1-12) [22]. *Mrln* is similar in structure and function to the small peptides phospholamban and sarcolipin. Like DWORF, myoregulin is a tail-anchored membrane protein of the SR, although the two proteins have very little similarity in their primary sequences. It would seem that *Mrln* and *Dworf* have opposing effects on the activity of the SR calcium pump (Figure 3-26). This observation has caused us to ponder whether small peptides have generally evolved to serve as modulatory subunits of larger complexes, since it seems unlikely that very small proteins would function on their own.

It is tempting to think that very small proteins may evolve suddenly since they are unlikely to have extensive structural restraints and may require only a small number of contact residues to exert their function. Given the large number of potential ORFs in eukaryotic genomes, it seems likely that some of these are translated occasionally, even if very inefficiently. It is possible then that these ORFs could provide a substantial pool of novel proteins on which natural selection could act. With these considerations in mind, it would be reasonable to think that many interesting modulatory proteins may not be conserved across phyletic boundaries. While we used evolutionary conservation as a strict requirement in our study, other methods, such as ribosomal foot-printing, may yield important, yet un-conserved, small proteins. Perhaps these proteins would provide insight into the relatively subtle changes that occur during divergence of species.

In this regard, we find the species-specific differences in *Dworf* expression to be rather interesting. We have shown that *Dworf* is highly expressed in slow-twitch skeletal muscle of mice, predominately being found in the soleus muscle, but not in fast-twitch muscle (Figure 3-11). Similarly *Dworf* is highly expressed in human skeletal muscle (Figure 3-9), although it is unclear if *Dworf* is expressed in human fast-twitch muscle or simply that humans have a greater proportion of slow-twitch fibers in general. Interestingly, however, while *Dworf* is highly expressed in mouse heart, it does not appear to be expressed in human heart. Given also that *Dworf* is expressed in mouse ventricle but not atria suggests that *Dworf* may have evolved as a subtle regulator of calcium handling, which would explain the rather small changes observed in our study.

Alternatively, it may be that the modest changes we observed in calcium dynamics are secondary to some other process which *Dworf* regulates. Because DWORF localizes to the SR, we would presume that the function would involve this compartment. It could be that *Dworf* is responsible for balancing of SR ion species other than calcium, perhaps potassium, chloride, or magnesium. Such a role would have an indirect effect on calcium handling that we cannot rule out. However, it would seem odd that regulation of these factors would be specific to the heart and slow-muscle since presumably these ions and their transporters also have a major role in other muscle types. The expression of *Dworf* would seem to overlap most closely with the tissue-specific isoform expression of SERCA, particularly SERCA2a. In fact SERCA2a has been reported to be the slowest of the muscle SERCA isoforms with respect to calcium pumping, so it may be rational that an additional subunit is required for full activity [23].

Finally we think that because DWORF increases the activity of the SERCA pump, it may be an attractive candidate for gene therapy in the heart. Because of its demonstratively positive

effects on heart disease in model organisms, modulation of SERCA function *in situ* has been clinical goal for some time now, and overexpression of SERCA by viral delivery has been evaluated in human clinical trials. Unfortunately, the stage 2 clinical trial for mydicar (an AAV1-delivered SERCA2a transgene) recently failed to meet its clinical endpoints, time to re-hospitalization and time to lethal events. The cause of this failure is unclear since the therapy has proven successful in a number of rodent and large animal models, but it likely involves problems with transgene delivery. It could also be that the failing hearts were too sick to synthesize a therapeutic dose or quality of the SERCA protein. In this regard, perhaps a smaller, less complex protein such as DWORF may prove more successful. Since the human heart does not produce DWORF, perhaps a therapeutic dose would be easy to attain since it presumably only needs to match the stoichiometry of SERCA. We did not observe detrimental effects in our transgenic mice which express DWORF well beyond physiologic levels. Presumably this was the case because SERCA became saturated with DWORF and additional protein is inert.

Furthermore, we found that mRNA and protein levels of *Dworf* were disrupted in mice with cardiac overexpression of a calcineurin A transgene, a model of hypertrophic and dilated cardiomyopathy (Figure 3-25). It is unclear whether the changes in *Dworf* expression in these mice is due to direct regulation of *Dworf* by the calcineurin/NFAT regulatory or whether *Dworf* is responding indirectly through heart failure. We observed that *Dworf* mRNA expression increases about four fold in the knockout mice, suggesting that *Dworf* is a dynamically regulated gene and may be a homeostatic factor. In future studies, unrelated models of heart failure should be explored to understand better the transcriptional and translational regulation of *Dworf* in this context.

In conclusion, we have described a novel transmembrane peptide encoded by a gene that is currently annotated as a lncRNA in humans and un-annotated in mice. Our findings highlight the inadequacy of current genome annotations with regard to small protein-coding potential of transcripts. The DWORF peptide increases the apparent activity of the cardiac SERCA pump. While further work is required to understand the mechanistic basis for SERCA modulation, it may also be useful to evaluate the effect of exogenous DWORF expression in the context of heart failure.

3.6 FIGURES

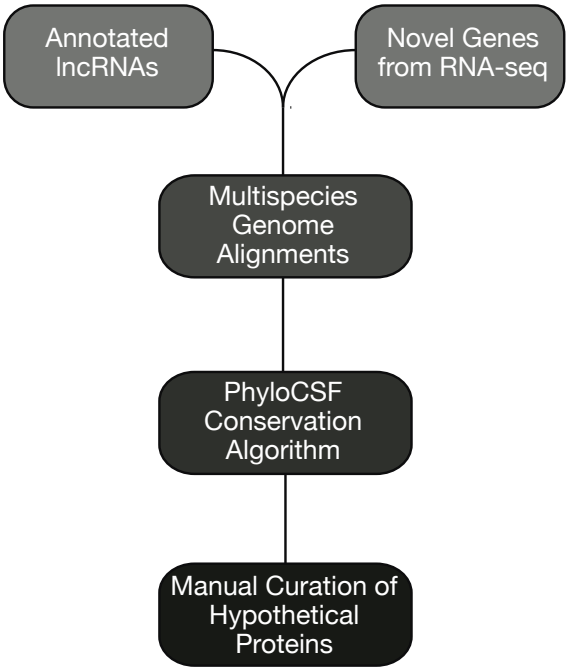

Figure 3-1. Workflow for discovery of small open reading frames.

Transcript annotations for lncRNAs were collected from the UCSC genome database and combined with novel transcript annotations from heart RNA-seq data. Multi-species genome alignments were extracted for fourteen mammalian species and then analyzed using the PhyloCSF computer program. High scoring ORFs were then examined manually to validate conservation.

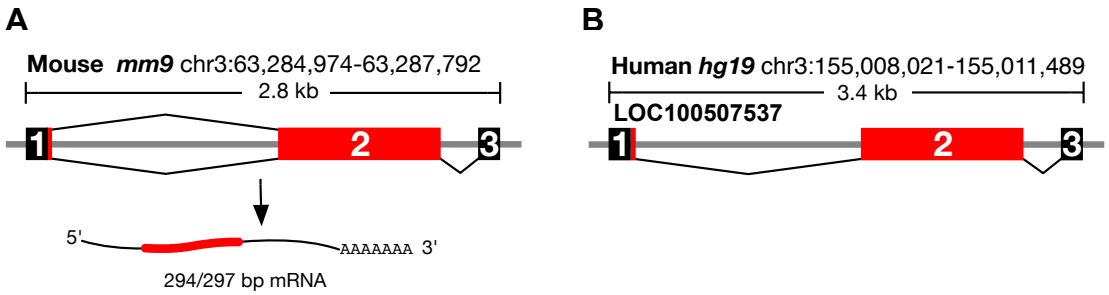

Figure 3-2. Overview of the *Dworf* locus.

In mice (*A*), *Dworf* is transcribed from an unannotated 2.8 kb locus on chromosome 3 to produce two transcript isoforms of approximately 300 bp that only differ by inclusion of three additional base pairs, producing a polyadenylated RNA. The predicted open reading frame (highlighted in red) begins in exon one and ends near the 3' end of exon two. In humans (*B*) the transcript is annotated as a lncRNA named LOC100507537 and appears to only produce a single isoform.

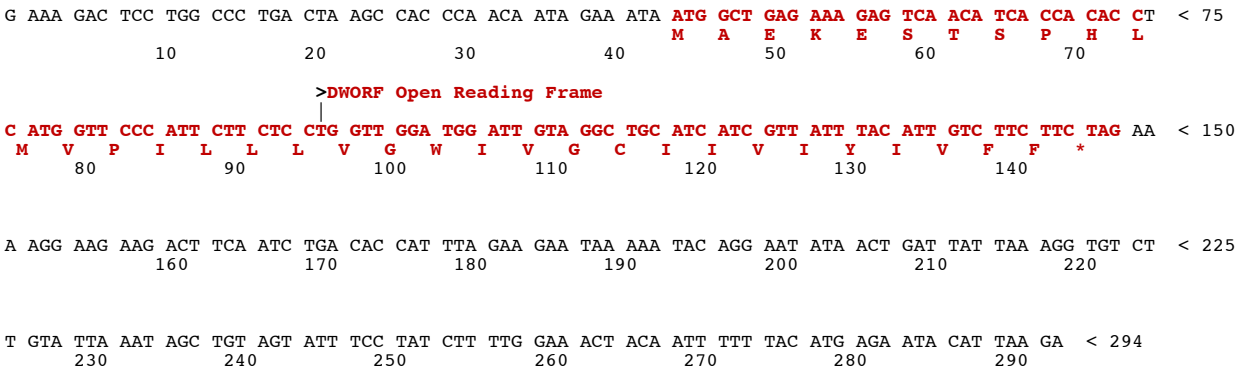

Figure 3-3. *Dworf* cDNA sequence from mouse.

Nucleotide sequence of a cloned fragment of *Dworf* from mouse heart cDNA. The ORF is highlighted in red with the amino acid sequence below.

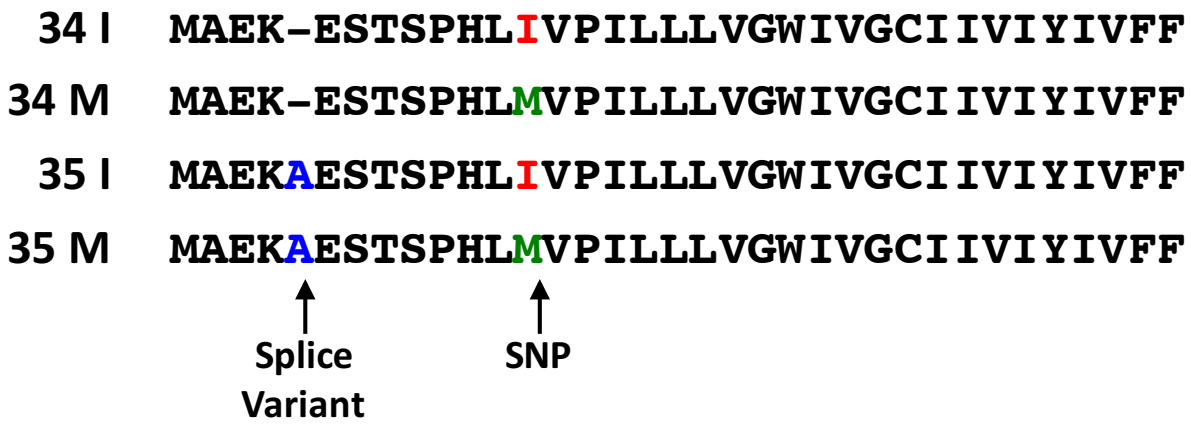

Figure 3-4. Four variants of the DWORF open reading frame.

In mice, the *Dworf* gene may produce four possible variant proteins. The 34- and 35-amino-acid variants differ by inclusion of three additional base pairs in the splicing of exons one and two. The "I" and "M" variations arise from a SNP that codes for isoleucine or methionine, respectively.

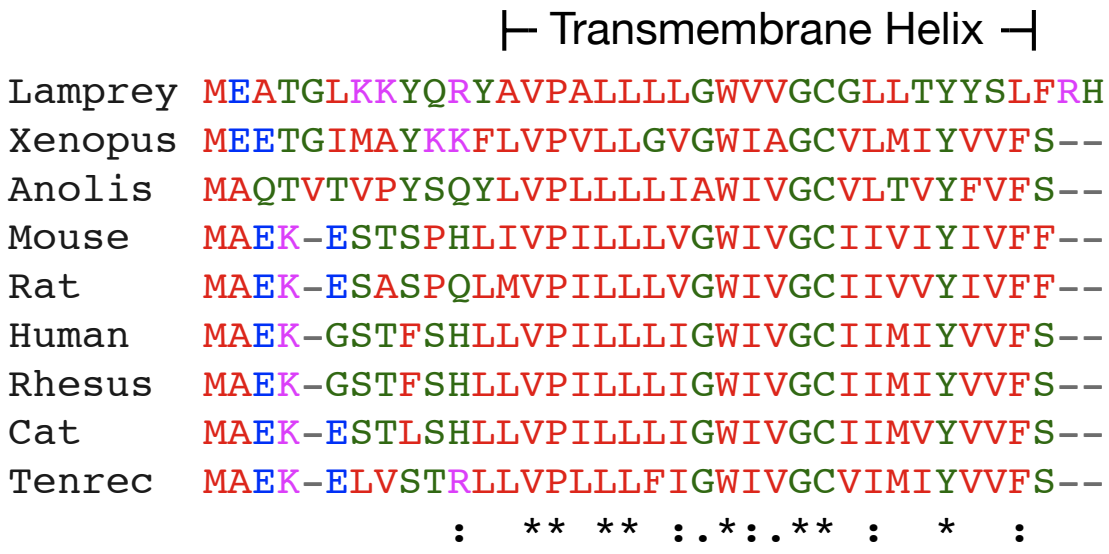

Figure 3-5. Multi-species protein alignment of predicted *Dworf* open reading frames.

The DWORF protein sequence is conserved in vertebrates and encodes a C-terminal transmembrane helix. Sequences were aligned using ClustalΩ. Transmembrane regions predicted by TMHMM.

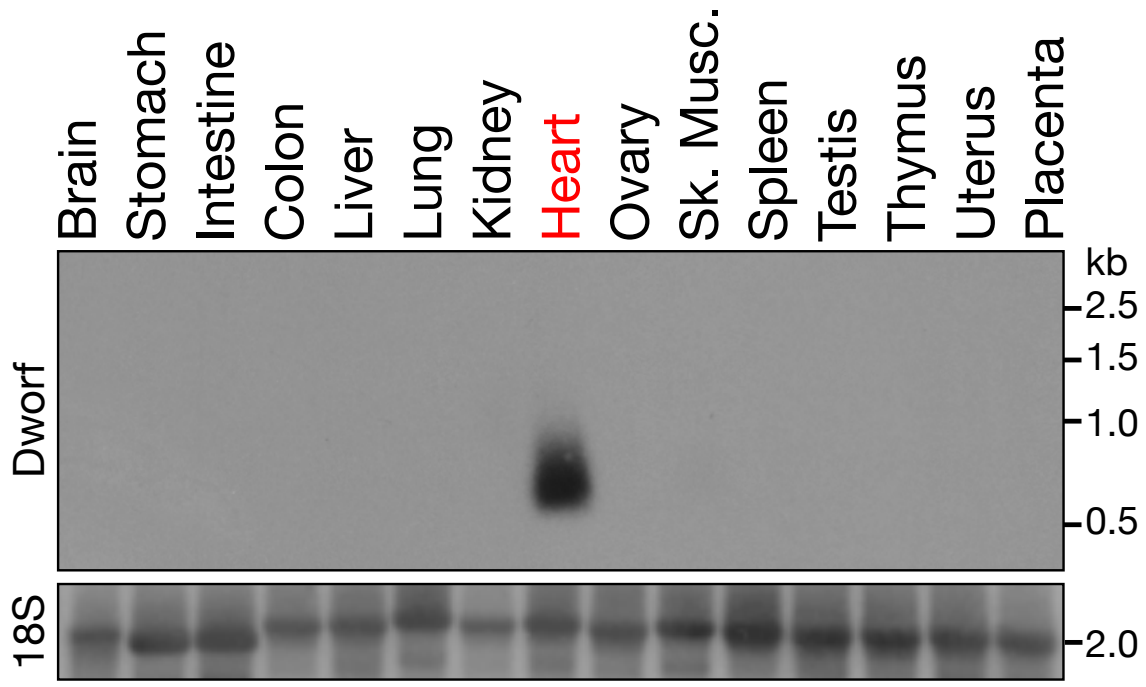

Figure 3-6. Multi-tissue northern blot from adult mouse.

A multi-tissue northern blot of adult mouse tissues was probed by radiolabeling the *Dworf* sequence shown in Figure 3-3. The *Dworf* signal is found only in the heart and measures approximately 500 bp in length. The blot was stripped and re-probed for the 18S rRNA as a loading control. Sk. Musc. = Skeletal Muscle. NB: The skeletal muscle sample only contains RNA from fast-twitch muscles of the gluteus and hindlimb muscles.

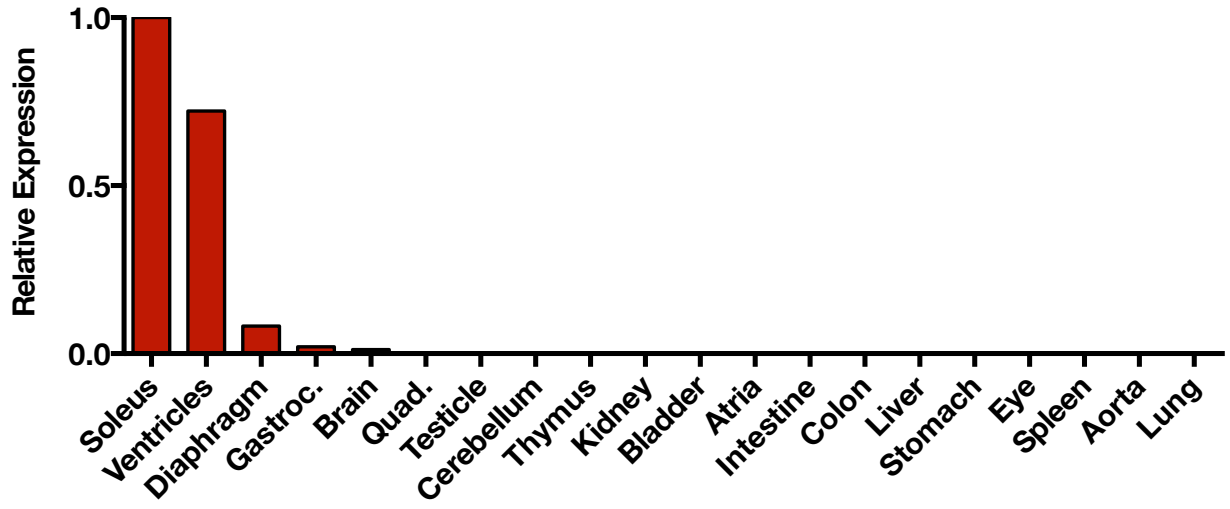

Figure 3-7. Multi-tissue qPCR from adult mouse.

Expression of *Dworf* is highest in adult soleus muscle and cardiac ventricle, but is not expressed in the cardiac atria or fast-twitch muscle groups such as the quadriceps. Gastroc. = Gastrocnemius (including plantaris muscle); Quad. = Quadriceps. cDNA courtesy of Kelly Anderson.

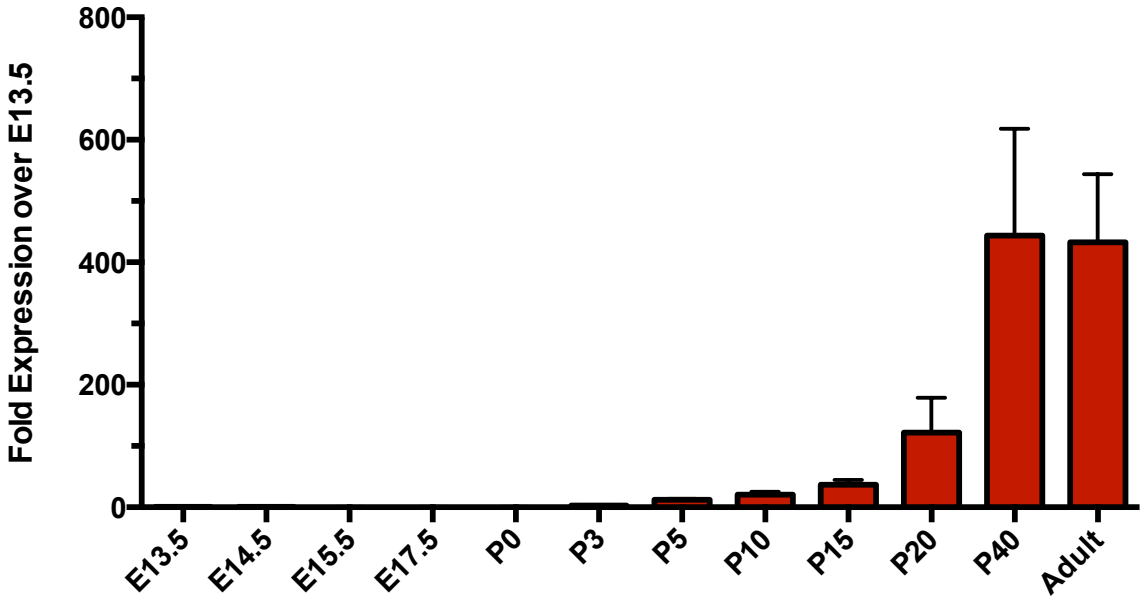

Figure 3-8. *Dworf* expression by qPCR during cardiac development.

Expression of *Dworf* is not expressed in the fetal heart and increases substantially after birth. By postnatal day forty, expression level is comparable to that of adult heart.

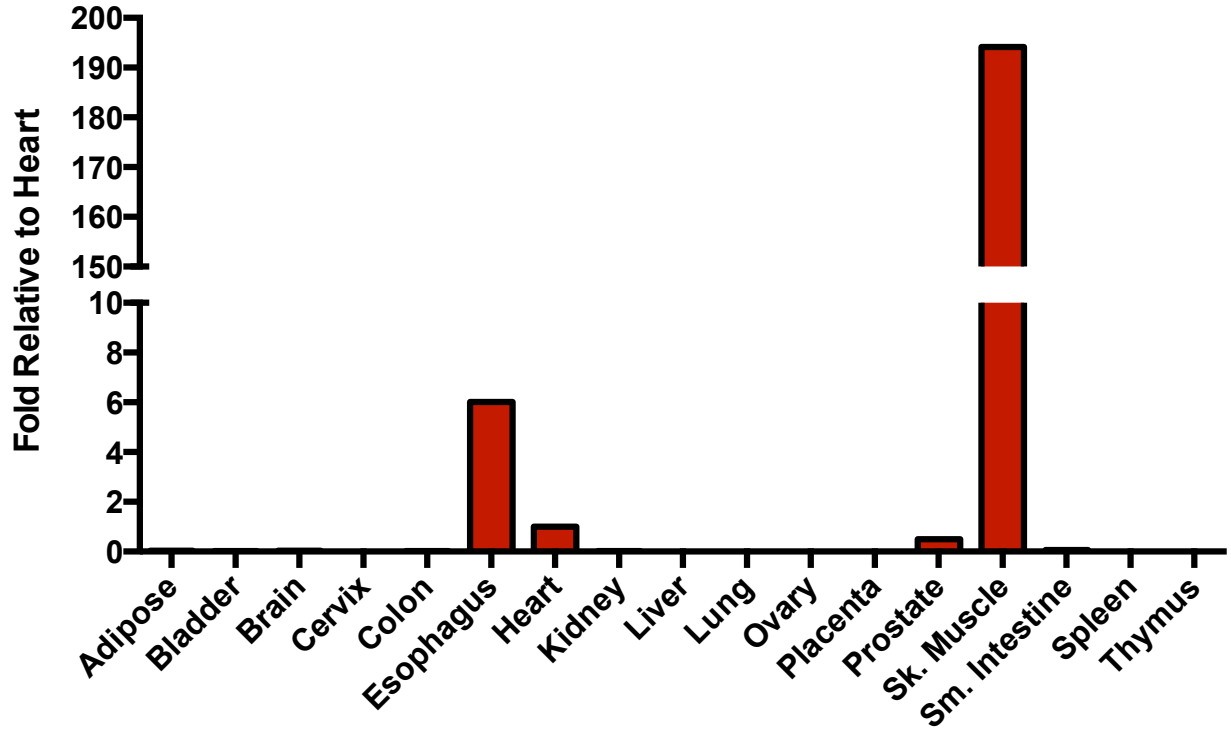

Figure 3-9. *Dworf* expression in adult human tissues by qPCR.

Expression of *Dworf* is highly enriched in adult skeletal muscle in humans. *Dworf* is also expressed in esophagus, which is composed of smooth and skeletal muscle in humans, and heart, although at a much lower level than adult mouse heart. Sk. Muscle = Skeletal Muscle; Sm. Intestine = Small Intestine.

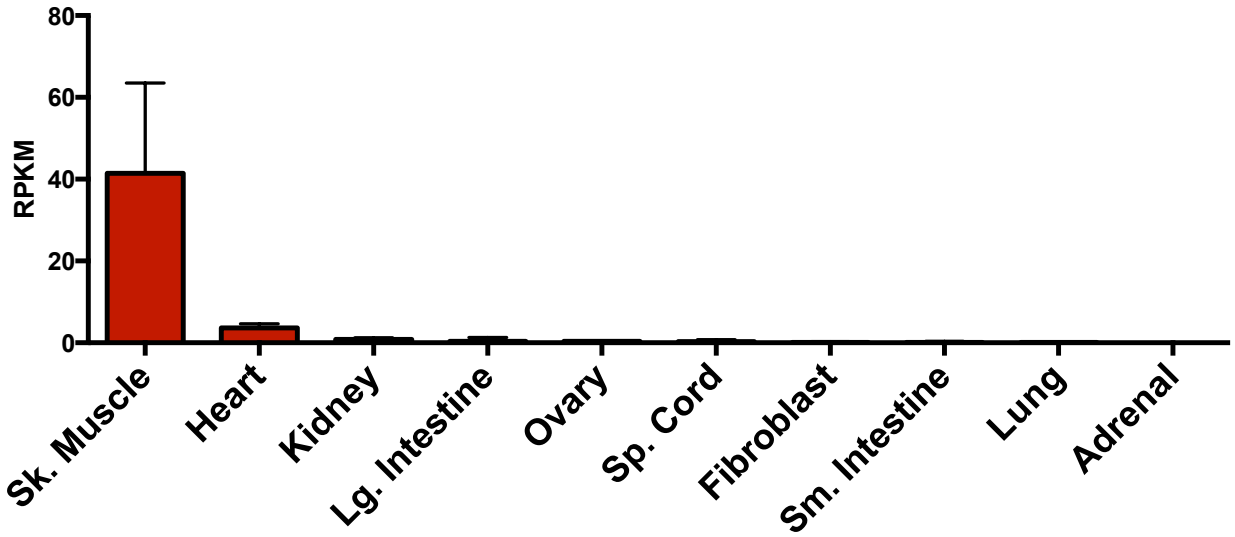

Figure 3-10. Expression of *Dworf* first exon by RNA-seq in fetal human tissues.

Dworf is expressed in fetal skeletal muscle and, to a lesser extent, heart. Human fetal RNA-seq data was downloaded from NCBI and mapped to the reference genome. An RPKM value was calculated for the first exon of the *Dworf* transcript. Data source accession number SRP001371. Sk. Muscle = Skeletal Muscle; Lg. Intestine = Large Intestine; Sp. Cord = Spinal Cord; Sm. Intestine = Small Intestine.

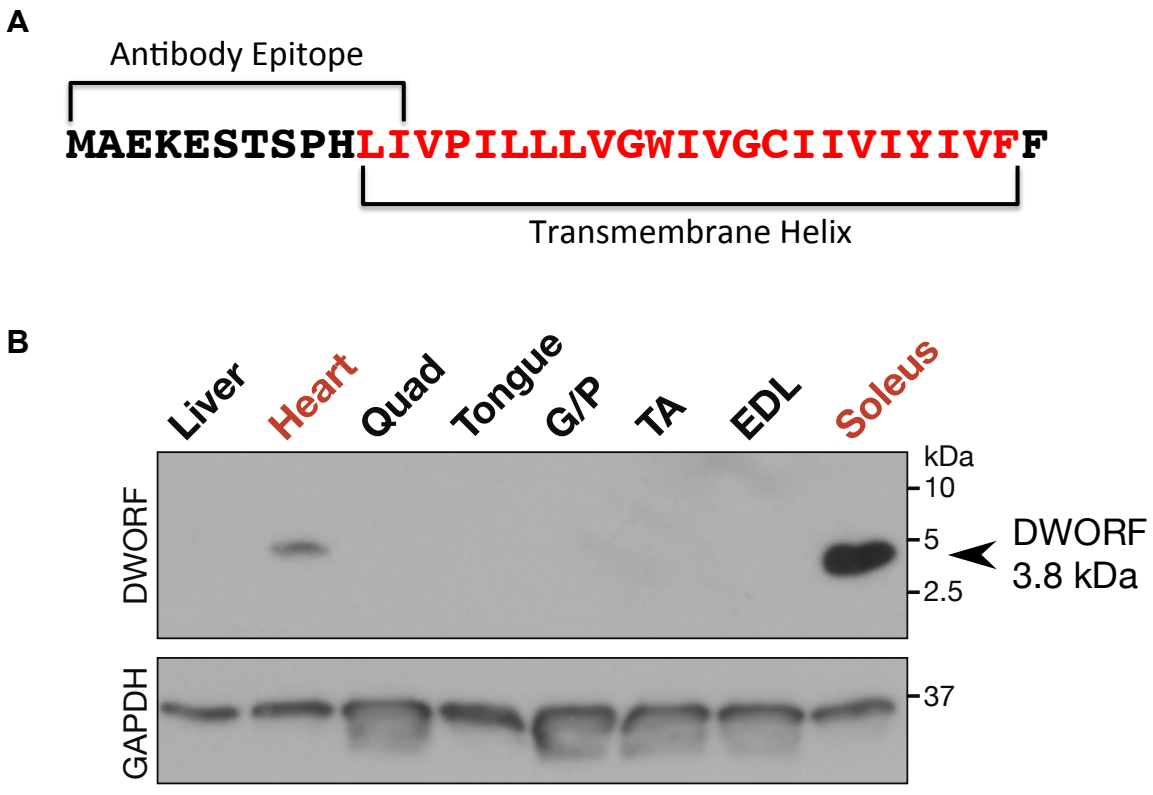

Figure 3-11. DWORF protein expression using a custom antibody.

(*A*) A custom antibody was derived against the N-terminus of the predicted DWORF protein. (*B*) Western blotting of adult mouse tissues with the DWORF antibody revealed a single low-molecular weight band at the predicted size of 3.8 kDa. The band was only observed in the soleus muscle and heart. Liver and other muscle groups, which are composed primarily of fast-twitch muscle, did not produce a detectable signal in this range.

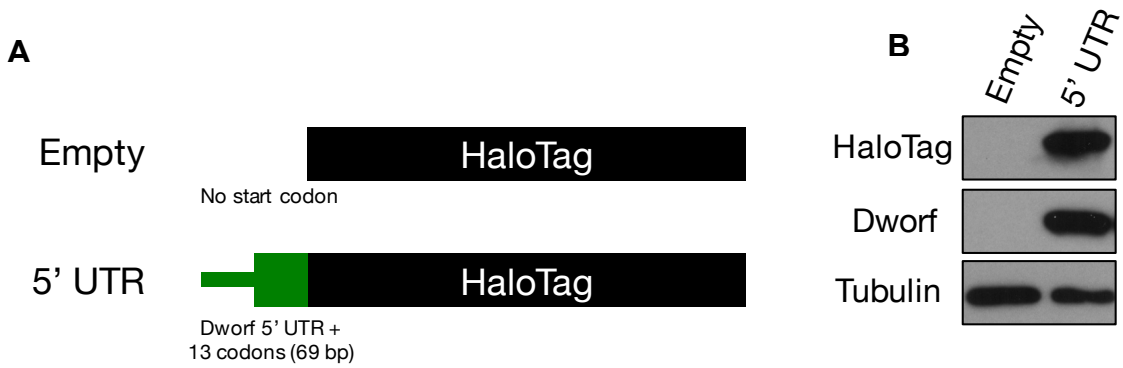

Figure 3-12. Protein-coding capacity of the *Dworf* 5' UTR.

(*A*) The 5' UTR and the first thirteen codons of *Dworf* was cloned as an in-frame fusion with the HaloTag protein. The empty HaloTag vector lacks an initiation codon and is not translated. (*B*) A HaloTag-specific antibody only yields a signal with the *Dworf* 5' UTR present by western blot. The custom DWORF antibody also recognizes the fusion protein.

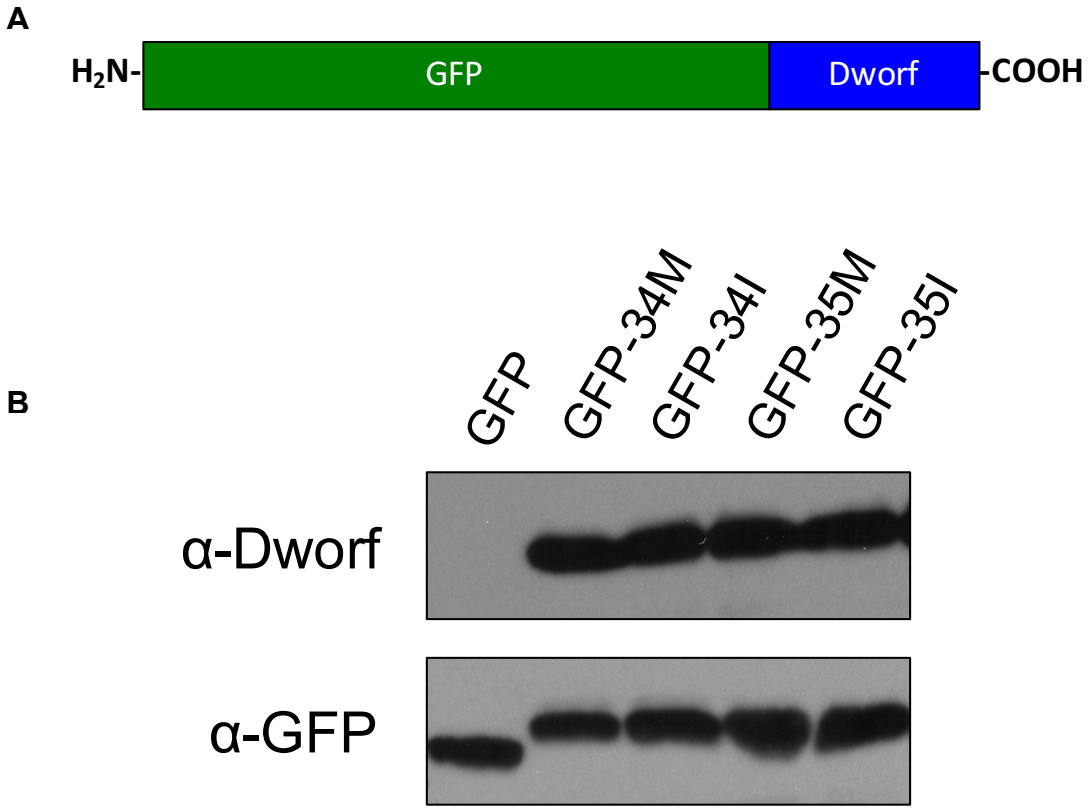

Figure 3-13. Recognition of DWORF variants by the DWORF polyclonal antibody.

(*A*) N-terminal GFP fusion proteins of the four DWORF variants were cloned and expressed in COS7 cells. (*B*) Western blotting of the DWORF expressing lysates reveals that the custom antibody is insensitive to the presence of these sequence variations.

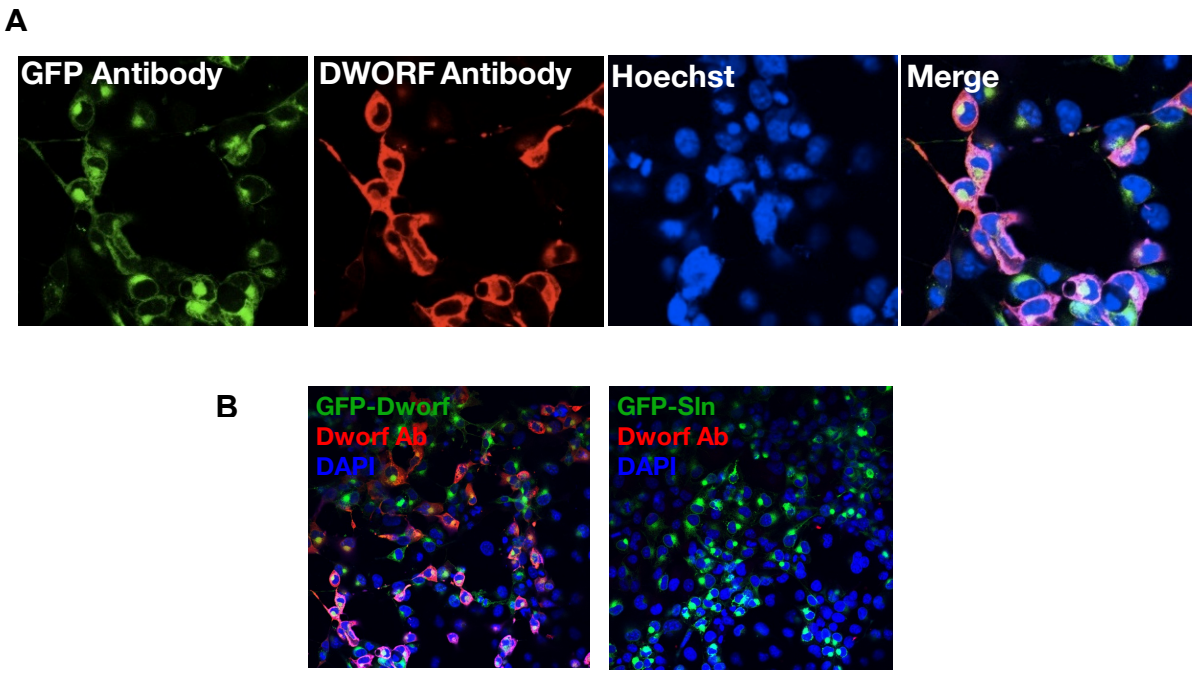

Figure 3-14. Immunofluorescent labeling of DWORF expressing COS7 cells.

(*A*) COS7 cells were transfected with a GFP-DWORF fusion construct (as shown in Figure 3-13A). The custom DWORF antibody only reacts with cells that have been transfected. (*B*) GFP-DWORF and GFP-Sarcolipin (Sln) were transfected separately into COS7 cells and stained with the DWORF antibody. The antibody is not cross-reactive with COS7 cells or the small transmembrane peptide sarcolipin.

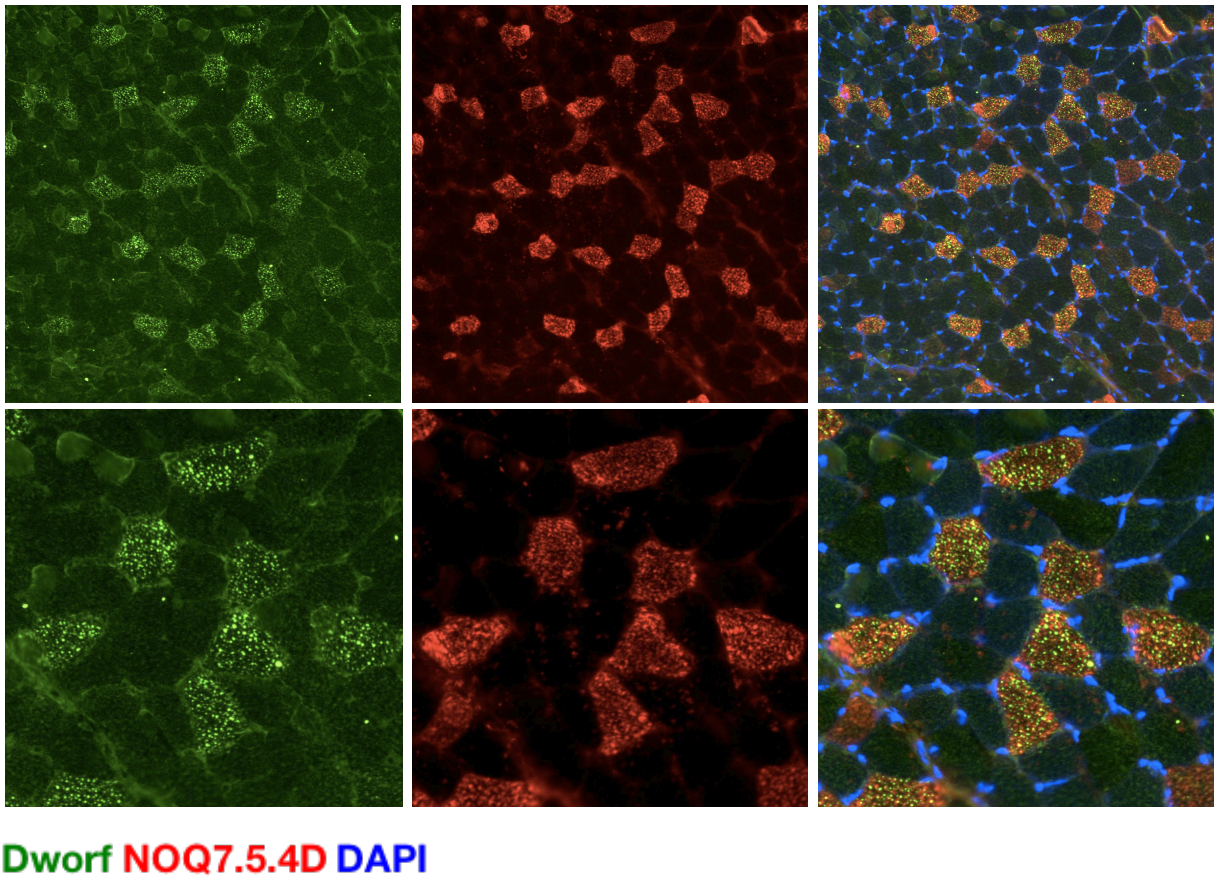

Figure 3-15. Immunofluorescent labeling of plantaris muscle with the Dworf antibody.

The gastrocnemius and plantaris muscles were excised, cryosectioned, and immunolabeled using the DWORF antibody and the slow-twitch myosin specific monoclonal antibody NOQ7.5.4D. A subset of fibers was noted to label with the DWORF antibody in a punctate pattern. These same fibers also labeled with the NOQ7.5.4D antibody indicating that Dworf is expressed in the slow-twitch fibers of the plantaris muscle. *Upper* wide view, *Lower* close view.

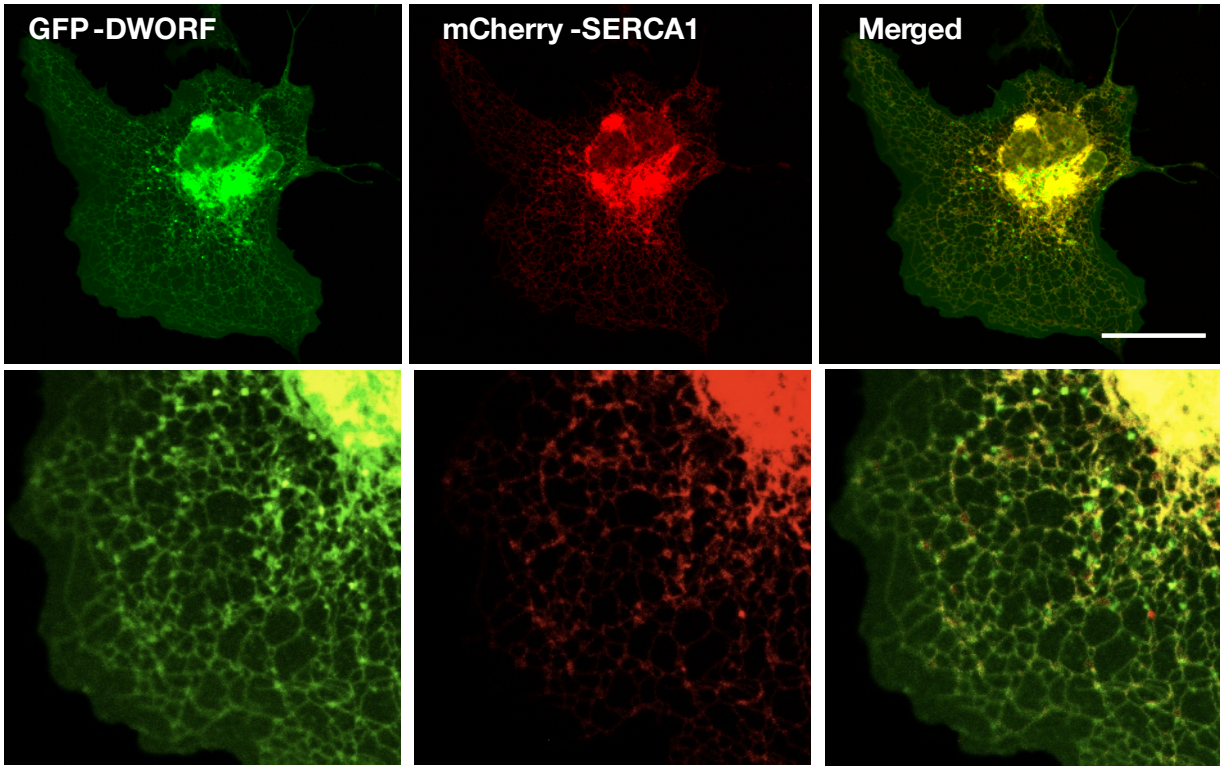

Figure 3-16. Co-localization of GFP-DWORF and mCherry-SERCA1.

COS7 cells were co-transfected with GFP-DWORF and mCherry-SERCA1a constructs. Cells were imaged by live confocal microscopy and reveal co-localization of DWORF and SERCA1a in the endoplasmic reticulum. GFP-DWORF also appears to have an additional faint signal which may be cytoplasmic.

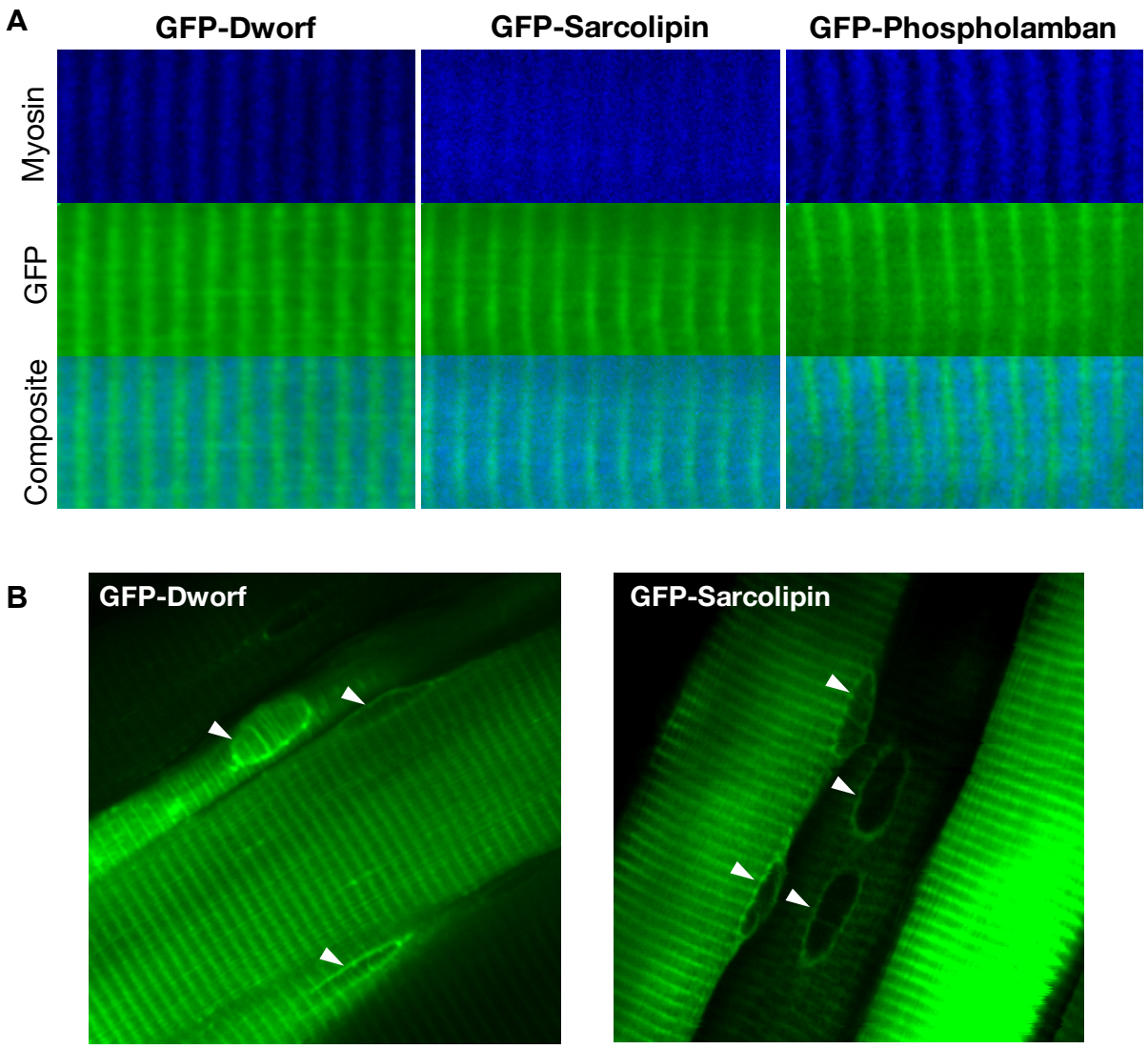

Figure 3-17. Localization of GFP-DWORF in skeletal muscle.

(*A*) Expression constructs for GFP-Dworf, GFP-Sarcolipin, and GFP-Phospholamban were electroporated into the flexor digitorum brevis muscle of adult mice. After one week, the muscles were harvested and imaged live by two-photon microscopy. Myosin was visualized by second harmonic generation. DWORF and the other two small transmembrane peptides, localize in an alternating pattern with myosin consistent with the SR, the expected localization site of sarcolipin and phospholamban. (*B*) Wider view of GFP-Dworf and GFP-Sarcolipin expressing myofibers. The DWORF localization pattern is nearly indistinguishable from sarcolipin. Arrows indicate similarity in peri-nuclear regions.

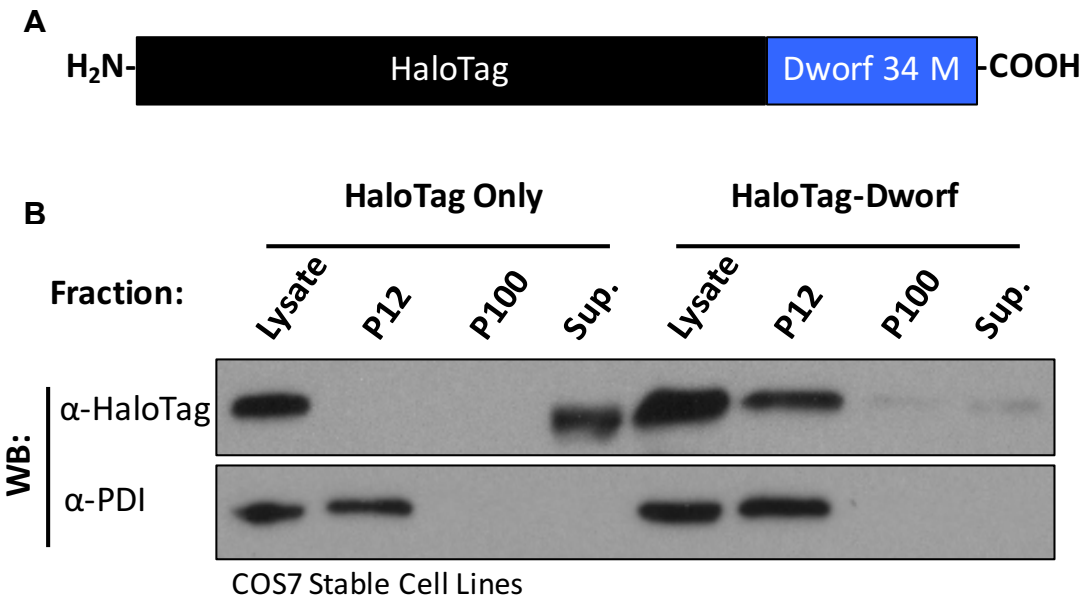

Figure 3-18. Subcellular fractionation of a DWORF fusion protein.

(*A*) A fusion construct of HaloTag-Dworf and HaloTag alone were stably expressed in COS7 cells. (*B*) The cells were fractionated by differential centrifugation and examined by western blot. The HaloTag protein alone remained in the supernatant, while HaloTag-Dworf was found mostly in the P12 fraction which corresponds to heavy vesicles, as shown by co-localization with the ER protein PDI.

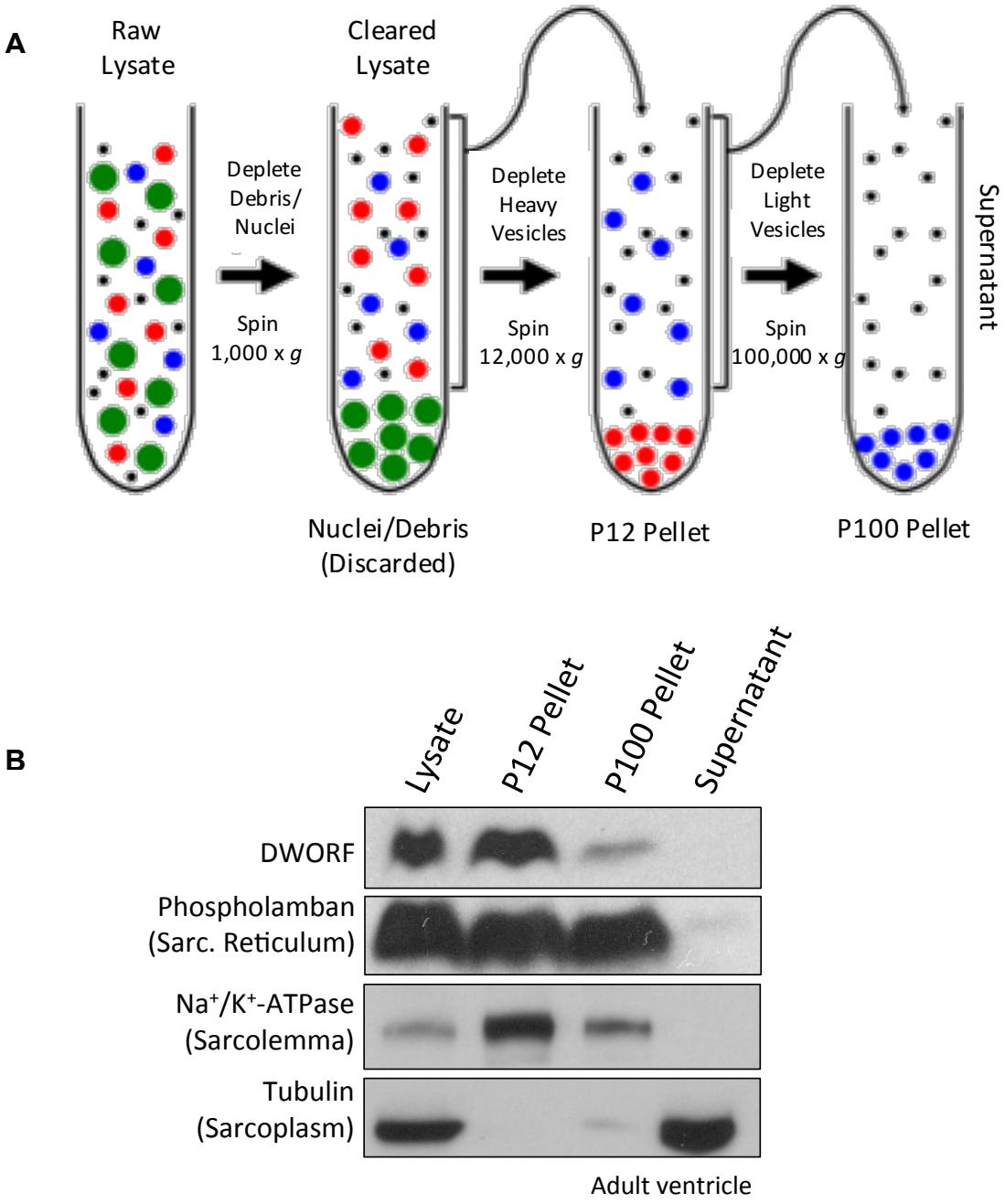

Figure 3-19. Sub-cellular fractionation of adult ventricle.

(A) Schematic representation of sub-cellular fractionation by differential centrifugation. (B) DWORF protein is retained in the insoluble pellet fractions that correspond to cellular membranes. DWORF is enriched in the plasma membrane fraction, but is also present in the SR fraction.

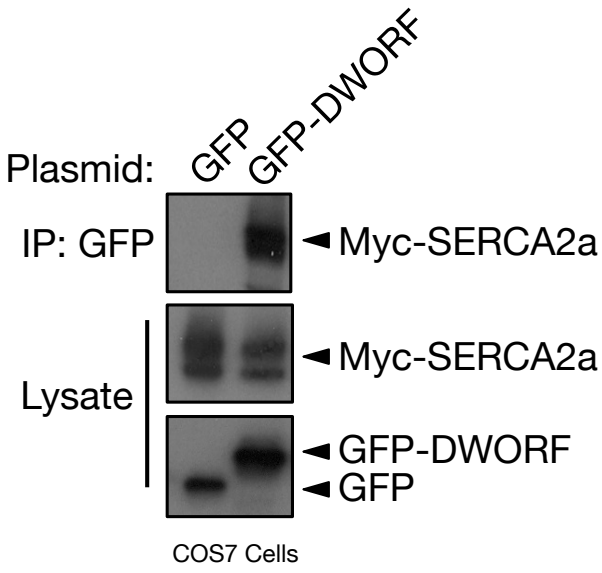

Figure 3-20. Myc-SERCA2a co-immunoprecipitates with GFP-DWORF.

COS7 cells were co-transfected with Myc-tagged SERCA2a and either GFP-tagged DWORF or GFP alone. Western blots reveal that Myc-SERCA2a co-immunoprecipitates with GFP-DWORF, indicating a physical interaction between the two proteins.

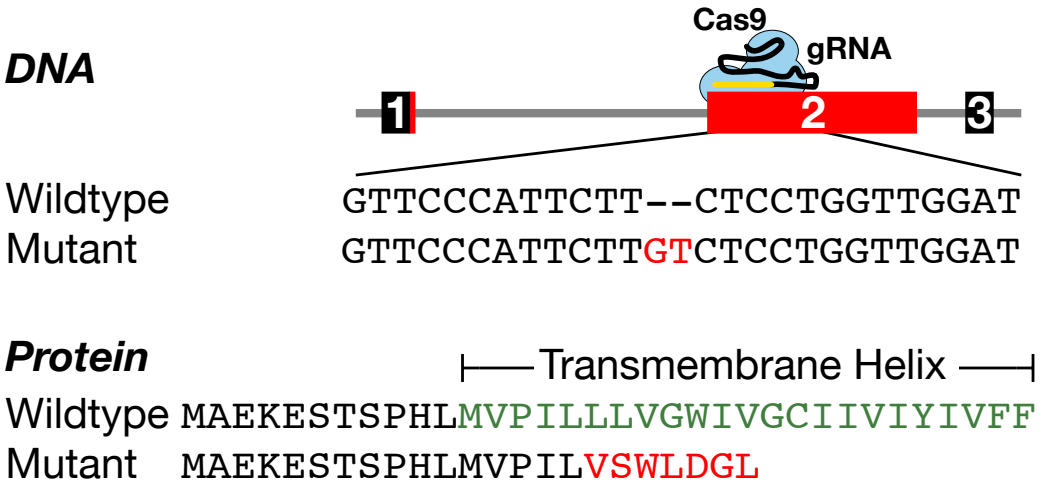

Figure 3-21. CRISPR/Cas9 knockout strategy.

A CRISPR gRNA was generated to target the coding sequence of exon two. An allele containing a 2 bp insertion was chosen for further experiments. The mutation is expected to produce a truncated protein lacking the transmembrane domain.

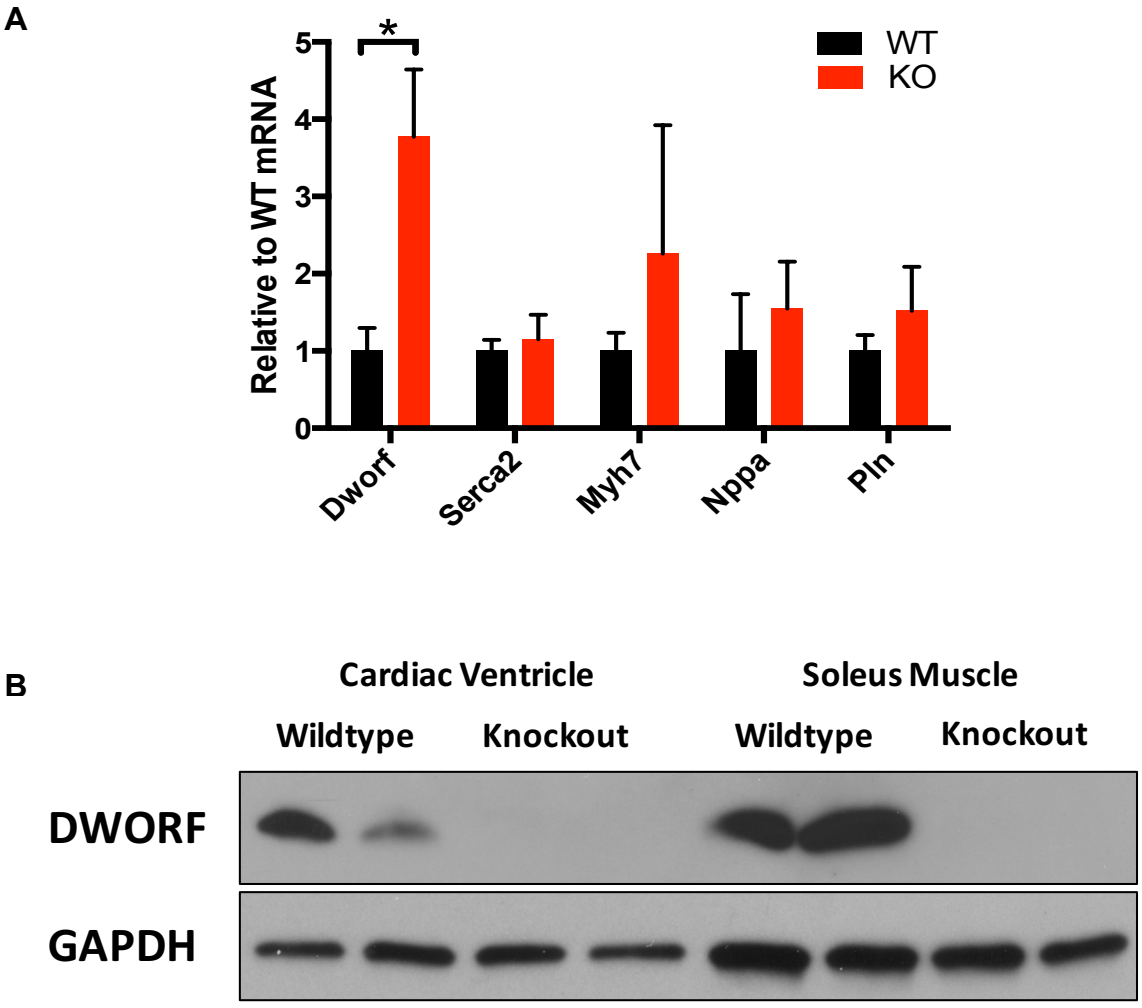

Figure 3-22. Confirmation of *Dworf* knockout.

(*A*) *Dworf* mRNA is increased approximately four fold in the hearts of adult knockout mice, but other notable genes are not altered. (*B*) DWORF protein is absent in the cardiac ventricle and soleus muscle of knockout mice. $^{*}P$-value = 0.006

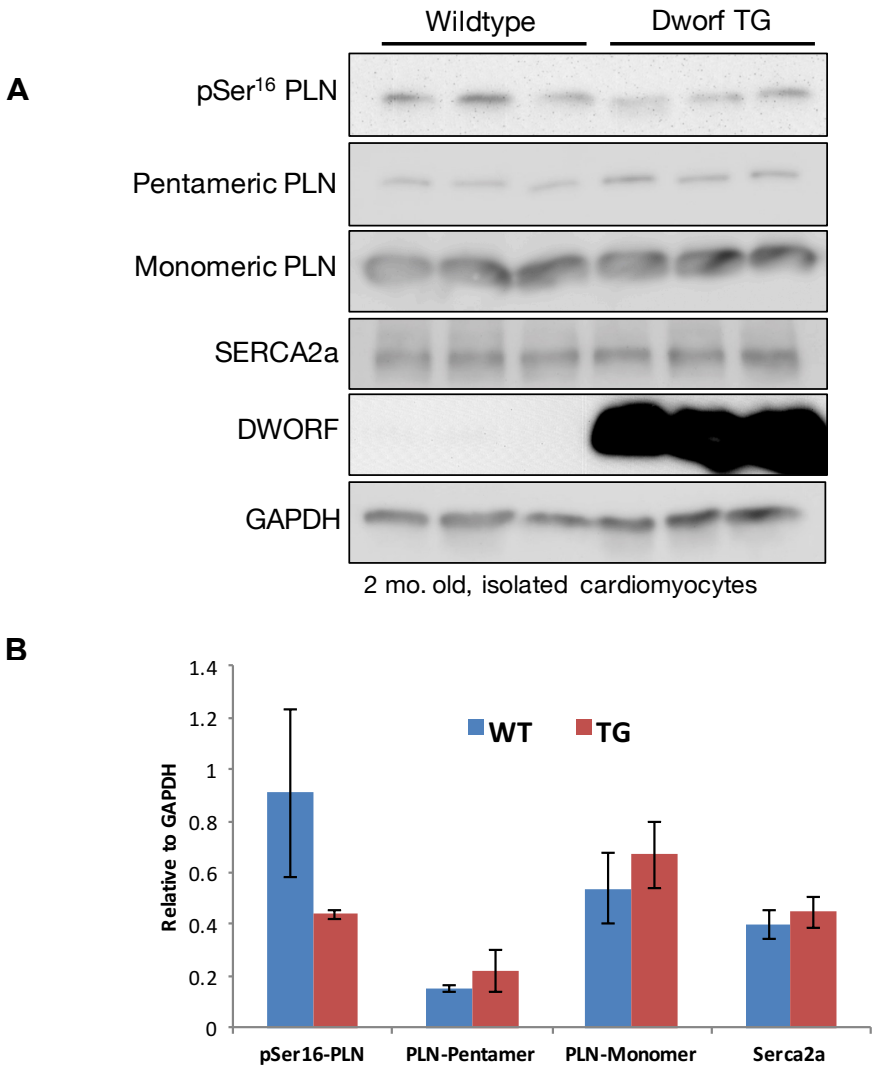

Figure 3-23. Calcium handling proteins in DWORF overexpressing cardiac myocytes.

(*A*) Expression of calcium handling proteins in cardiac myocytes of αMHC-DWORF transgenic mice. (*B*) Quantification of the blots in panel A, normalized to GAPDH.

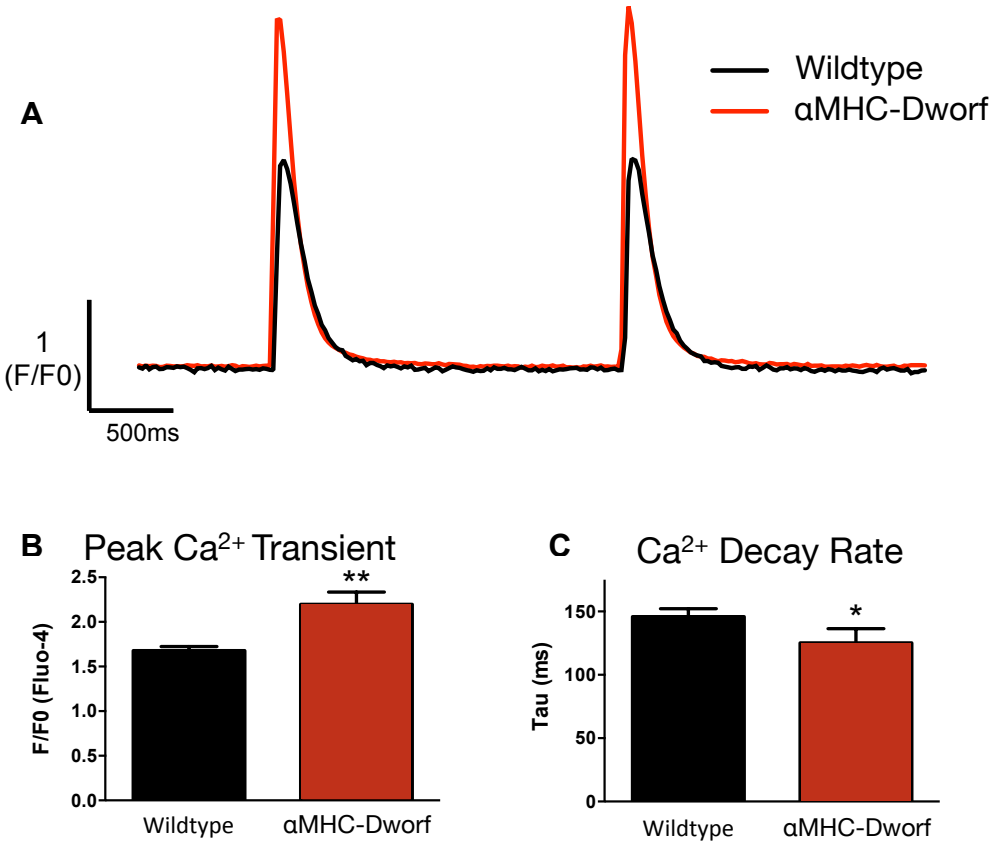

Figure 3-24. Calcium handling is enhanced in *Dworf* overexpressing cardiomyocytes.

A transgenic mouse line was generated to overexpress *Dworf* under the control of the cardiomyocyte-specific αMHC promoter. Myocytes were isolated from transgenic hearts and loaded with the fluorescent calcium indicator fluo-4 and paced at 0.5 Hz. Representative traces are shown in panel *A*. Overexpression of DWORF in cardiac myocytes resulted in an increased peak calcium release following stimulation (*B*) and an increased rate of clearance (*C*) following contraction. $^{*}P$-value = 0.0166, $^{**}P$-value = 0.0067.

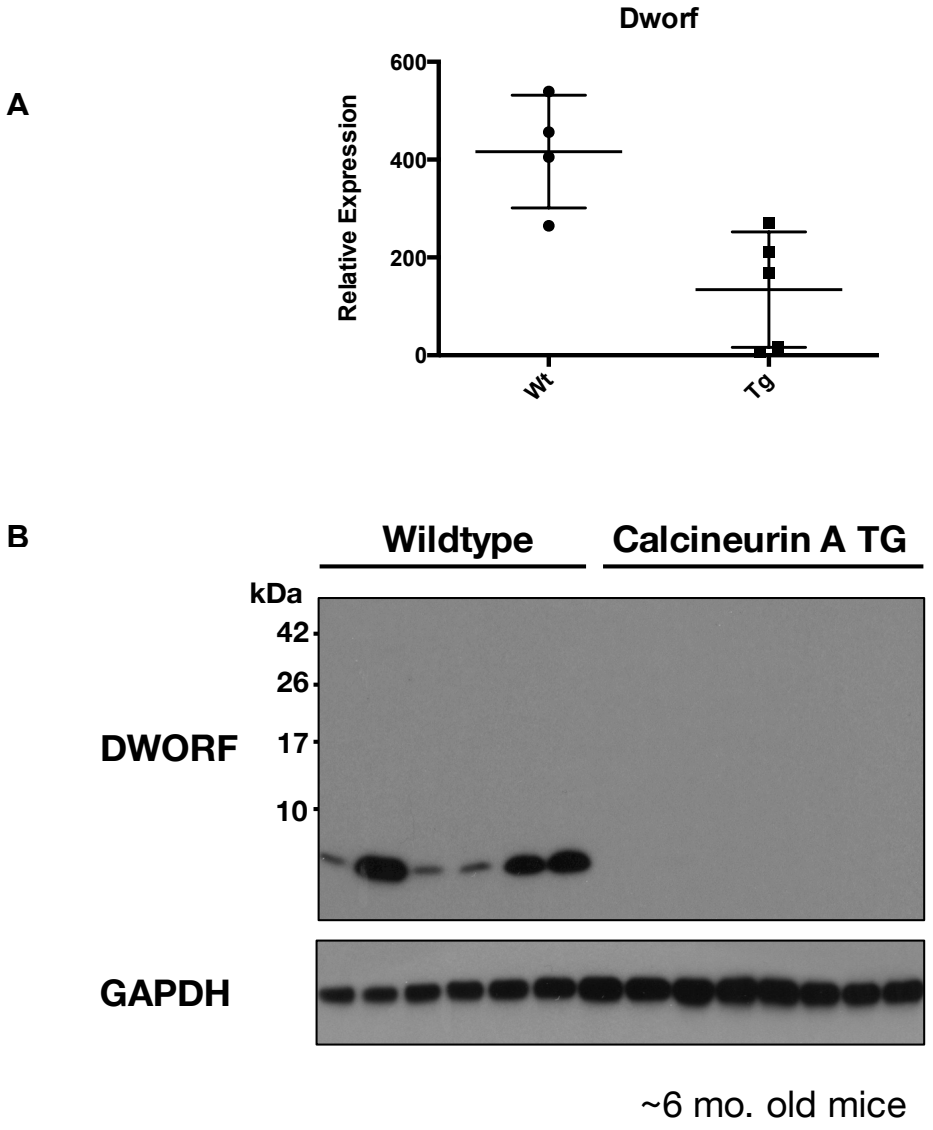

Figure 3-25. *Dworf* is decreased in calcineurin A transgenic hearts.

In calcineurin A transgenic hearts, *Dworf* mRNA (*A*) is significantly reduced, and the protein expression (*B*) is not detectable by western blot. Some variability in wildtype expression levels is notable, but the cause is currently unclear.

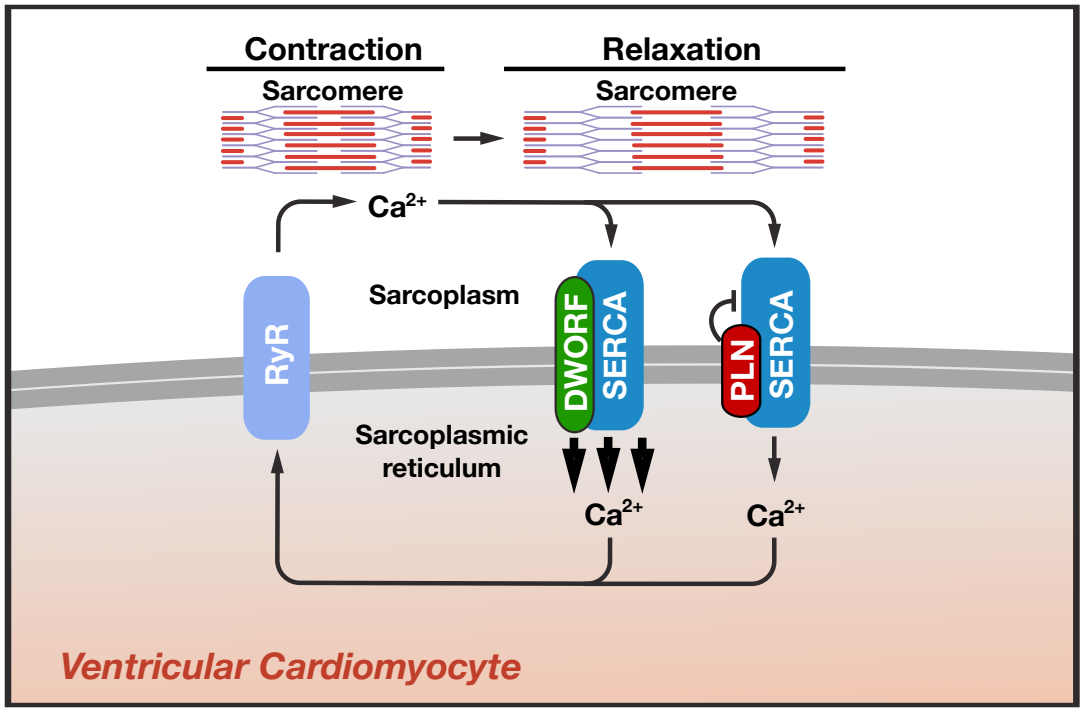

Figure 3-26. Summary of muscle calcium handling, including DWORF.

Upon electrical stimulation, myocytes release calcium from the sarcoplasmic reticulum through the ryanodine receptor (RyR), which causes the sarcomere to contract. In order for the muscle to relax, calcium must be shuttled out of the sarcoplasm, most of which is transported back to the sarcoplasmic reticulum by the SERCA pump. In cardiac myocytes, SERCA is inhibited by the small transmembrane protein, phospholamban (PLN). Phospholamban inhibition is opposed by the small transmembrane peptide, DWORF, which increases apparent pumping action of SERCA.

3.7 TABLES

Table 3-1. Smallest annotated open reading frames in mouse

Gene Name	ORF Length
Rpl41	25
Sarcolipin	31
Dworf	**34**
Mrps33	34
Ost4	37
Gm20494	37
Bre	43
Tmsb10	45
Aym1	45
Tmsb15a	45

*Based on data downloaded from the UCSC mm9 annotation

Table 3-2. List of oligonucleotides used

Name	Type	Use	Modification	Sequence (5' → 3')
Dworf-Endogenous	F	Q		TTCTTCTCCTGGTTGGATGG
Dworf-Endogenous	R	Q		TCTTCTAAATGGTGTCAGATTGAAGT
Dworf-Endogenous	P	Q	6FAM/ZEN/IBFQ	TTTACATTGTCTTCTTCTAGAAAAGGAAGAAG
αMHC-Dworf	F	Q		ATAAGAGTTTGAGTCGACCGC
αMHC-Dworf	R	Q		ACTGGGGAGGGGTCACAG
αMHC-Dworf	P	Q	6FAM/ZEN/IBFQ	TTGTCTTCTTCTAATAGAAGCTTGATGGGTG
Dworf-Geno	F	G		TCATTGCTTCTAAGCAGAGTCAACA
Dworf-Geno	R	G		ATGCAGCCTACAATCCATCCAA
Dworf-Geno WT	P	G	FAM/NFQ/MGB	CCAGGAGAAGAATG
Dworf-Geno KO	P	G	FAM/NFQ/MGB	CAGGAGACAAGAATG
hGH	F	G		GTCTGACTAGGTGTCCTTCT
hGH	R	G		CGTCCTCCTGCTGGTATAG
Myog-Geno	F	G		TTACGTCCATCGTGGACAGC
Myog-Geno	R	G		TGGGCTGGGTGTTAGCCTTA
Human-Dworf	F	Q		CCACCCACCAACAGGAATA
Human-Dworf	R	Q		TTATGATGCAGCCCACAATC

Legend: F = Forward; R = Reverse; P = Probe; C = Cloning; G = Genotyping; Q = qPCR

3.8 REFERENCES

1. Bers, D.M., *Cardiac excitation-contraction coupling.* Nature, 2002. **415**(6868): p. 198-205.

2. Kent, W.J., et al., *The human genome browser at UCSC.* Genome Res, 2002. **12**(6): p. 996-1006.

3. Trapnell, C., L. Pachter, and S.L. Salzberg, *TopHat: discovering splice junctions with RNA-Seq.* Bioinformatics, 2009. **25**(9): p. 1105-11.

4. Trapnell, C., et al., *Differential gene and transcript expression analysis of RNA-seq experiments with TopHat and Cufflinks.* Nat Protoc, 2012. **7**(3): p. 562-78.

5. Blankenberg, D., et al., *Making whole genome multiple alignments usable for biologists.* Bioinformatics, 2011. **27**(17): p. 2426-8.

6. Giardine, B., et al., *Galaxy: a platform for interactive large-scale genome analysis.* Genome Res, 2005. **15**(10): p. 1451-5.

7. Blankenberg, D., et al., *Galaxy: a web-based genome analysis tool for experimentalists.* Curr Protoc Mol Biol, 2010. **Chapter 19**: p. Unit 19 10 1-21.

8. Goecks, J., et al., *Galaxy: a comprehensive approach for supporting accessible, reproducible, and transparent computational research in the life sciences.* Genome Biol, 2010. **11**(8): p. R86.

9. Lin, M.F., I. Jungreis, and M. Kellis, *PhyloCSF: a comparative genomics method to distinguish protein coding and non-coding regions.* Bioinformatics, 2011. **27**(13): p. i275-82.

10. Long, C., et al., *Prevention of muscular dystrophy in mice by CRISPR/Cas9-mediated editing of germline DNA.* Science, 2014. **345**(6201): p. 1184-8.

11. Schweingruber, C., et al., *Nonsense-mediated mRNA decay - mechanisms of substrate mRNA recognition and degradation in mammalian cells.* Biochim Biophys Acta, 2013. **1829**(6-7): p. 612-23.

12. Sonnhammer, E.L., G. von Heijne, and A. Krogh, *A hidden Markov model for predicting transmembrane helices in protein sequences.* Proc Int Conf Intell Syst Mol Biol, 1998. **6**: p. 175-82.

13. Krogh, A., et al., *Predicting transmembrane protein topology with a hidden Markov model: application to complete genomes.* J Mol Biol, 2001. **305**(3): p. 567-80.

14. Goujon, M., et al., *A new bioinformatics analysis tools framework at EMBL-EBI.* Nucleic Acids Res, 2010. **38**(Web Server issue): p. W695-9.

15. Guido, A.N., et al., *Fiber type composition of the sternomastoid and diaphragm muscles of dystrophin-deficient mdx mice.* Anat Rec (Hoboken), 2010. **293**(10): p. 1722-8.

16. Schiaffino, S. and C. Reggiani, *Fiber types in mammalian skeletal muscles.* Physiol Rev, 2011. **91**(4): p. 1447-531.

17. Wang, F., et al., *The mechanism of tail-anchored protein insertion into the ER membrane.* Mol Cell, 2011. **43**(5): p. 738-50.

18. Mariappan, M., et al., *The mechanism of membrane-associated steps in tail-anchored protein insertion.* Nature, 2011. **477**(7362): p. 61-6.

19. Denic, V., V. Dotsch, and I. Sinning, *Endoplasmic reticulum targeting and insertion of tail-anchored membrane proteins by the GET pathway.* Cold Spring Harb Perspect Biol, 2013. **5**(8): p. a013334.

20. Lander, E.S., et al., *Initial sequencing and analysis of the human genome.* Nature, 2001. **409**(6822): p. 860-921.

21. Venter, J.C., et al., *The sequence of the human genome.* Science, 2001. **291**(5507): p. 1304-51.

22. Anderson, D.M., et al., *A micropeptide encoded by a putative long noncoding RNA regulates muscle performance.* Cell, 2015. **160**(4): p. 595-606.

23. Periasamy, M. and A. Kalyanasundaram, *SERCA pump isoforms: their role in calcium transport and disease.* Muscle Nerve, 2007. **35**(4): p. 430-42.